

Spring 2004

## Bio-Optical Properties of the Arctic Waters: Empirical and Theoretical Observations

Jian Wang  
*Old Dominion University*

Follow this and additional works at: [https://digitalcommons.odu.edu/oeas\\_etds](https://digitalcommons.odu.edu/oeas_etds)



Part of the [Oceanography Commons](#), and the [Remote Sensing Commons](#)

---

### Recommended Citation

Wang, Jian. "Bio-Optical Properties of the Arctic Waters: Empirical and Theoretical Observations" (2004). Doctor of Philosophy (PhD), Dissertation, Ocean & Earth Sciences, Old Dominion University, DOI: 10.25777/01jr-f671  
[https://digitalcommons.odu.edu/oeas\\_etds/167](https://digitalcommons.odu.edu/oeas_etds/167)

This Dissertation is brought to you for free and open access by the Ocean & Earth Sciences at ODU Digital Commons. It has been accepted for inclusion in OES Theses and Dissertations by an authorized administrator of ODU Digital Commons. For more information, please contact [digitalcommons@odu.edu](mailto:digitalcommons@odu.edu).

**BIO-OPTICAL PROPERTIES OF THE ARCTIC WATERS:  
EMPIRICAL AND THEORETICAL OBSERVATIONS**

by

Jian Wang  
B.S. July 1995, Nanjing University

A Thesis Submitted to the Faculty of  
Old Dominion University in Partial Fulfillment of the  
Requirement for the Degree of

DOCTOR OF PHILOSOPHY

OCEANOGRAPHY

OLD DOMINION UNIVERSITY  
May 2004

Approved by:

 \_\_\_\_\_  
Glenn Cota (Director)

 \_\_\_\_\_  
Larry Atkinson (Member)

 \_\_\_\_\_  
Zhonghai Jin (Member)

## ABSTRACT

### **BIO-OPTICAL PROPERTIES OF THE ARCTIC WATERS: EMPIRICAL AND THEORETICAL OBSERVATIONS**

Jian Wang  
Old Dominion University, 2004  
Director: Dr. Glenn F. Cota

Bio-optical observations were made during August 2000 in the Beaufort and Chukchi Seas. Chlorophyll *a* concentration (Chl) ranged from 0.068 to 18.51 mg chl m<sup>-3</sup>. Both total particulate and phytoplankton absorption at 443 nm were closely correlated with chlorophyll concentration. There is no strong correlation between chlorophyll concentration and absorption by soluble materials or nonpigmented particulates. Absorption, scattering, and attenuation all show strong first-order spectral relationships. Two semianalytical remote sensing reflectance models were evaluated and validated using bio-optical data collected in this region. Both models were proficient at retrieving chlorophyll concentration, phytoplankton absorption coefficients, and particulate backscattering coefficients. A chlorophyll-dependent reflectance model was also assessed, and proved to be highly successful in reproducing measured reflectance spectra. A four-component, Case 2 model with mean absorption spectra for phytoplankton, soluble materials, and nonpigmented particulates was employed in HYDROLIGHT simulations. The remote sensing reflectance spectra simulated in the radiative transfer model were in excellent agreement with field data. Regionally tuned algorithms explained >93% of the variability in the surface chlorophyll concentration. Time-series of remotely sensed distributions of sea ice, surface temperature, albedo, clouds, and phytoplankton were examined to evaluate variability of environmental conditions and

physical forcing of phytoplankton in the Beaufort and Chukchi Seas. Large-scale distributions of these parameters were studied for the first time using weekly and monthly composites from April 1998 through September 2002. Seasonal variations of ice cover dominated environmental conditions, and ice edge blooms followed retreating marginal ice zones northward. Blooms were most prominent in the southwestern Chukchi Sea, and were especially persistent immediately north of the Bering Strait in nutrient-rich Anadyr water and in some fronts. Chlorophyll concentrations increased from April to reach a maximum value in spring or summer depending on location. Large interannual variability of ice cover and phytoplankton distributions were observed. Phytoplankton responded rapidly to environmental changes with increases in biomass to large accumulations during 1998 in the Beaufort Sea when sea ice retreated early. Annual variations of mean surface temperature were also evident with 1998 being the warmest year. Correlation analyses between chlorophyll and a single environmental parameter showed relatively high negative correlation with ice concentration but a positive correlation with surface temperature.

Copyright, 2004, by Jian Wang, All Rights Reserved.

This thesis is dedicated to Lei Chen, my wife,  
the fountain of my inspiration and wisdom.

## ACKNOWLEDGMENTS

There are many people who have contributed to the successful completion of this dissertation. I extend many thanks to my committee members, Larry Atkinson and Zhonghai Jin for providing me with insight into their respective area of expertise. The untiring efforts of my major advisor, Dr. Glenn Cota, deserve special recognition. To me, he is a mentor and a close friend. I truly appreciate his guidance and help for all these years. His continuous support and encouragement are greatly acknowledged.

Special thanks to David Ruble for his assistance in every aspect. Without his effort, this work would have been much more difficult. I'd also like to thank Zhongping Lee, Ken Carder, Stephane Maritorena, David Siegel, Rick Reynolds, and Greg Mitchell for providing their models. I want to thank Dr. Joey Comiso for assistance in processing ocean color data.

This research was funded by NASA's SIMBIOS (Sensor Intercomparison and Merger for Biological and Interdisciplinary Oceanic Studies) and SeaWiFS projects, and the NSF Arctic System Science's Shelf-Basin Interactions program. I thank these agencies for their financial support. I am grateful to the officers, crew, and science liaison team of the US Coast Guard's Polar Star for their logistical support.

## TABLE OF CONTENTS

	Page
LIST OF TABLES .....	viii
LIST OF FIGURES .....	ix
 Chapter	
I. INTRODUCTION .....	1
II. ABSORPTION AND BACKSCATTERING IN THE BEAUFORT AND CHUKCHI SEAS.....	3
INTRODUCTION.....	3
MATERIALS AND METHODS .....	6
RESULTS AND DISCUSSION.....	11
CONCLUSIONS .....	39
III. REMOTE SENSING REFLECTANCE IN THE BEAUFORT AND CHUKCHI SEAS: OBSERVATIONS AND MODELS .....	42
INTRODUCTION.....	42
MATERIALS AND METHODS .....	44
RESULTS AND DISCUSSION.....	50
CONCLUSIONS .....	70
IV. PHYTOPLANKTON IN THE BEAUFORT AND CHUKCHI SEAS: DISTRIBUTIONS, DYNAMICS, AND ENVIRONMENT FORCING .....	72
INTRODUCTION.....	72
MATERIALS AND METHODS .....	74
RESULTS AND DISCUSSION.....	77
CONCLUSIONS .....	97
REFERENCES .....	99
VITA.....	110

## LIST OF TABLES

Table	Page
1. Notation .....	5
2. Results of linear correlations of total absorption coefficient minus water $a_{t-w}$ at the surface (0m) measured by spectrophotometric analyses and by ac-9 meters at eight wavelengths.....	22
3. Results of linear regression of remote sensing reflectance $R_{rs}$ versus ratio of backscattering to the sum of backscattering and absorption $b_b/(b_b+a)$ .....	31
4. Results of linear regression of phytoplankton absorption at seven wavelength versus $a_a(443 \text{ nm})$ .....	35
5. Results of linear regression of total absorption without water $a_{t-w}$ at seven wavelengths versus $a_{t-w}(488 \text{ nm})$ .....	37
6. Results of linear regression of particulate scattering coefficient $b_p$ at seven wavelengths versus $b_p(488 \text{ nm})$ .....	37
7. Results of linear regression of beam attenuation $c$ at seven wavelengths versus $c(488 \text{ nm})$ .....	38
8. Chlorophyll algorithm coefficients for SeaWiFS OC4V4, Arc00 OC4L, and Arc00 OC4P (n = 50) .....	68
9. Results of correlation analyses between two variables for each month from April to September.....	95

## LIST OF FIGURES

Figure	Page
1.	Station locations for the Arctic 2000 cruise in the Beaufort and Chukchi Seas. There are a total of 29 optical stations in this cruise..... 7
2.	Mean spectra of total absorption minus water $a_{t-w}$ , total particulate absorption $a_p$ , phytoplankton absorption $a_a$ , nonpigmented particulate absorption $a_n$ , and soluble absorption $a_s$ (n = 157 spectra)..... 12
3.	Ratios of absorption by nonpigmented particulates (A) and soluble materials (B) to total particulates at 443 nm versus chlorophyll concentration..... 14
4.	Power functions for total and nonpigmented particulates (A), phytoplankton (B), and soluble (C) absorption at 443nm versus chlorophyll concentration ..... 16
5.	Comparison of total absorption coefficient minus water $a_{t-w}$ at the surface (0m) measured by spectrophotometric analyses and by ac-9 meters (A) and correlation for $a_{t-w}(488)$ by the two methods (B)..... 21
6.	Ratio of particulate backscattering coefficient to total particulate scattering coefficient as a function of chlorophyll concentration ..... 25
7.	Relationships between backscattering coefficients of particles at 555 nm and chlorophyll concentrations (A) for Arc00, Ross Sea, and APFZ. Parameter describing backscattering spectral dependency $\gamma$ as a function of backscattering coefficients at 555nm for Arc00 (B, solid), is compared with <i>Reynolds et al.</i> 's [2001] model (B, dashed) ..... 27
8.	Relationships between backscattering coefficients of particles at 555 nm and remote sensing reflectance at 555 nm (A), and index of backscattering spectral dependency $\gamma$ versus ratios of reflectance at 443 nm to 488 nm (B)..... 29
9.	Relationships between remote sensing reflectance and the ratio of backscattering to the sum of absorption and backscattering for 555 nm..... 32
10.	Spectral relationships between phytoplankton absorption at seven wavelengths and phytoplankton absorption at 443 nm..... 34
11.	Total absorption coefficient minus water $a_{t-w}$ at seven wavelengths versus $a_{t-w}$ at 488 nm (A), the same relationships for light scattering

	coefficient $b_p$ (B) and beam attenuation coefficient $c$ (C) .....	36
12.	Remote sensing reflectance spectra (A, solid lines) for four biomass classes of Chl < 0.3, 0.3-1, 1-3, and > 3 mg m <sup>-3</sup> , respectively. Reflectance spectra of stations rich in nonpigmented particulates are shown as dashed lines (B).....	51
13.	Comparison of above-water and in-water maximum reflectance ratios. Data from 19 stations are shown as filled circles .....	54
14.	Comparisons of absorption coefficient of phytoplankton (A), absorption coefficient of colored dissolved organic matters plus nonpigmented particulates (B), and backscattering coefficient for total particulates (C) retrieved from tuned Lee <i>et al.</i> model and field measurements.....	56
15.	Comparisons of chlorophyll (A), absorption coefficient of colored dissolved organic matters plus nonpigmented particulates (B), and backscattering coefficient of total particulates (C) retrieved from Maritorena <i>et al.</i> model and field measurements.....	59
16.	Comparison of remote sensing reflectance predicted by Reynolds <i>et al.</i> model (solid line) and measured reflectance (dashed line, with standard deviation shown) for four biomass classes of Chl < 0.3, 0.3-1, 1-3, and > 3 mg m <sup>-3</sup> , respectively.....	62
17.	Comparison of remote sensing reflectance generated by HYDROLIGHT radiative transfer model (solid line) and measured reflectance (dashed line, with standard deviation shown) for four biomass classes of Chl < 0.3, 0.3-1, 1-3, and >3 mg m <sup>-3</sup> , respectively .....	65
18.	Regionally tuned linear (OC4L) and polynomial (OC4P) maximum band-ratio chlorophyll-retrieval algorithms for the Beaufort and Chukchi Seas and the OC4V4 SeaWiFS algorithms (A). Chlorophyll concentrations predicted by SeaWiFS OC4V4 and Arc00 OC4P are compared with Arc00 OC4L in panel B. SeaWiFS OC4V4 overestimates chlorophyll < 1.5× (B).....	69
19.	Geographic location of the Beaufort and Chukchi Seas. Two transects of 150°W and 170°W are shown as solid lines.....	75
20.	Monthly maps of chlorophyll concentration in April, May, June, July, August, and September 1998 .....	78
21.	Chlorophyll concentration in August and September 1998 along the Beaufort Sea 150°W transect .....	80

22.	Chlorophyll concentration in June, July, August, and September 1998 along the Chukchi Sea 170°W transect.....	81
23.	Weekly averages of chlorophyll concentration (A), ice concentration (B), and surface temperature (C) for 1998, 1999, 2000, 2001, and 2002 for the Beaufort Sea.....	84
24.	Weekly averages of chlorophyll concentration (A), ice concentration (B), and surface temperature (C) for 1998, 1999, 2000, 2001, and 2002 for the Chukchi Sea .....	85
25.	Monthly maps of chlorophyll concentration in April, May, June, July, August, and September 2001 .....	88
26.	Comparison of weekly averages of chlorophyll concentration (A & B), open water area(C & D), surface temperature (E & F), cloud cover (G & H), and albedo (I & J) in 1998 and 2001 for the Beaufort Sea .....	89
27.	Comparison of weekly averages of chlorophyll concentration (A & B), open water area(C & D), surface temperature (E & F), cloud cover (G & H), and albedo (I & J) in 1998 and 2001 for the Chukchi Sea.....	90
28.	Ice concentration in August and September 1998 (filled circle) and 2001 (unfilled circle) along the Beaufort Sea 150°W transect .....	92
29.	Ice concentration in June, July, August, and September 1998 (filled circle) and 2001 (unfilled circle) along the Chukchi Sea 170°W transect.....	93

# CHAPTER I

## INTRODUCTION

The Arctic Ocean is very important to the world's ocean and climate. It regulates the deep water formation in the North Atlantic via ice export, which impacts the global ocean circulation. It has been suggested the climate change will be amplified in the Arctic due to a positive feedback mechanism. There is evidence that the Arctic environment is changing. Both the extent and thickness of the arctic ice pack have been decreasing and sea surface temperature showed a trend of increasing [Comiso *et al.*, 2003]. The annual river discharge to the Arctic Ocean has increased about 7% from 1936-1999 [Peterson *et al.*, 2002].

Approximately 30% of the surface area of the Arctic Ocean is occupied by its continental shelves. These shelves experience seasonal changes in ice cover and are heavily impacted by seasonal riverine discharges. They are the most dynamic regions in biogeochemical activities and have immense impact on the deeper basin regions.

Among the shelf seas, the Beaufort and Chukchi Seas are of particular interest. Nutrient-rich north Pacific waters flow through the Bering Strait and across the Chukchi Sea shelf. A variety of physical and biogeochemical processes occurring on the shelf profoundly influence the regional circulation, water mass formation, and nutrient distributions and their effects can be seen throughout much of the Arctic Ocean [Weingartner *et al.*, 1998]. The Chukchi is believed to be among the most productive of the Arctic shelf seas due to the large nutrient supply both from the rivers and through the

---

The model journal for this dissertation is the *Journal of Geophysical Research*.

Bering Strait. The Beaufort Sea is mostly ice-covered each year. In spring and summer, the Beaufort shelf receives a large influx of fresh water from the Mackenzie River. In the upper layer (~50m) of water column, currents flow westward under the influence of wind-driven clockwise Beaufort Gyre. Beneath this layer, the Beaufort Undercurrent persistently flows eastward.

Despite its pivotal role, the Arctic Ocean remains poorly known because of the adverse weather conditions and long periods of darkness. Recent advances in satellite remote sensing have provided the most effective way to study large-scale surface physical and biological characteristics of the Arctic Ocean. However, satellite retrieval of many geophysical parameters, including chlorophyll concentration, relies on accurate algorithms and bio-optical information. Many studies suggested that bio-optical properties in polar waters are markedly different from lower latitude ecosystems [Mitchell and Holm-Hansen, 1991; Mitchell, 1992; Arrigo *et al.*, 1998; Sathyendranath *et al.*, 2001]. Therefore, current global algorithms should be used with caution when applied to the Arctic.

Using to date the most comprehensive field measurements of optical properties in the Beaufort and Chukchi Seas, this study aims to study the bio-optical properties of this region with the following objectives: 1). Investigate the empirical relationships of inherent optical properties (IOPs) and apparent optical properties (AOPs); 2). Test the empirical relationships in several theoretical models and develop regional algorithms; 3). Study the large-scale spatial and temporal variability of phytoplankton distributions in the Beaufort and Chukchi Seas using ocean color data retrieved from regional algorithms.

## CHAPTER II

### ABSORPTION AND BACKSCATTERING IN THE BEAUFORT AND CHUKCHI SEAS

#### 1. Introduction

The Arctic Ocean and its adjacent seas play important roles in global biogeochemical cycles, such as regulating global oceanic circulation. It has been suggested that increased atmospheric temperatures, resulting from anthropogenic release of greenhouse gases, would have profound effects on the Arctic. Despite its pivotal role, the Arctic Ocean is poorly known relative to the other oceans because of long periods of ice-cover and darkness in the region. Advances in new technologies, including satellite remote sensing, have greatly enhanced our abilities to monitor and understand the physical, chemical, biological and geological processes occurring within the Arctic Ocean. However, application of satellite remote sensing of ocean relies on accurate and adequate bio-optical information for this region. Previous studies have suggested that bio-optical properties in polar waters are markedly different from lower latitude ecosystems [Mitchell and Holm-Hansen, 1991; Mitchell, 1992; Arrigo *et al.*, 1998; Sathyendranath *et al.*, 2001] with highly packaged cells and lower chlorophyll-specific absorption. Therefore, accurate chlorophyll retrieval, which is the primary goal of satellite remote sensing of ocean color, for these regions relies on region-specific algorithms and bio-optical models involving inherent optical properties (IOPs), apparent optical properties (AOPs) and chlorophyll.

The IOPs depend only upon the medium and are independent of the ambient light field [Mobley, 1994], but are fundamental to understand and predict light propagation

within a water body. Spectral light absorption and backscattering are two IOPs of primary importance, because they are directly related to remote sensing measurements of ocean color. Several recent studies have examined the spectral relationships for IOPs. These relationships can be used to predict IOPs from measured IOPs at a single wavelength. *Barnard et al.* [1998] discovered linear relationships in the IOPs spectra based on the measurements made at 488 nm from a “global” data set. Their data set included 1914 vertical profiles from open ocean to estuarine environments, spanning a broad range of environmental conditions. They pointed out that more specific regional models should be developed for more accurate prediction of IOPs on regional scales. *Gould et al.* [1999] described linear spectral relationships for the scattering coefficients for various environments, and developed a simplified model to estimate the scattering coefficient at any wavelength from a known scattering value at a single wavelength. In this study, we examine spectral relationships of absorption, scattering and beam attenuation based on bio-optical data collected in the Beaufort and Chukchi Seas during August 2000.

The remote sensing reflectance  $R_{rs}$  (see Table 1 for symbols and definitions), defined as the ratio of water-leaving radiance  $L_w$  to downwelling irradiance  $E_d$ , is an apparent optical property (AOP). AOPs depend on both the medium and the geometric structure of the ambient light field. Systematic variations of AOPs from one water body to another help characterize the differences of optical properties of the two water bodies. The blue to green spectral ratios of  $L_w$  or  $R_{rs}$  vary with chlorophyll concentration, and are the basis of empirical algorithms for chlorophyll-retrieval from satellite remote sensing. For example, the current Ocean Color 4-band (OC4) algorithms [*O'Reilly et al.*, 2000] for

Table 1. Notation

Symbol	Definition	Unit
$R_{rs}$	Remote sensing reflectance ( $= L_w/E_d$ )	$\text{sr}^{-1}$
$L_w$	Water-leaving radiance	$\text{W m}^{-2} \text{sr}^{-1}$
$L_{wn}$	Normalized water-leaving radiance	$\text{sr}^{-1}$
$L_u$	In-water upwelling radiance	$\text{W m}^{-2} \text{sr}^{-1}$
$E_d$	Downwelling irradiance	$\text{W m}^{-2}$
$E_u$	Upwelling irradiance	$\text{W m}^{-2}$
$E_s$	Above-water incident irradiance	$\text{W m}^{-2}$
Chl	Chlorophyll concentration	$\text{mg m}^{-3}$
$a$	Total absorption coefficient	$\text{m}^{-1}$
$a_p$	Total particulate absorption coefficient	$\text{m}^{-1}$
$a_a$	Phytoplankton absorption coefficient	$\text{m}^{-1}$
$a_n$	Nonpigmented particles absorption coefficient	$\text{m}^{-1}$
$a_s$	Soluble materials absorption coefficient	$\text{m}^{-1}$
$a_{cdm}$	Nonpigmented plus soluble materials absorption coefficient ( $= a_n + a_s$ )	$\text{m}^{-1}$
$a_a^*$	Chlorophyll-specific absorption coefficient for phytoplankton	$\text{m}^2 \text{mg}^{-1}$
$b_b$	Total backscattering coefficient	$\text{m}^{-1}$
$b_{bw}$	Water backscattering coefficient	$\text{m}^{-1}$
$b_{bp}$	Particulate backscattering coefficient	$\text{m}^{-1}$
$b_{bc}$	Phytoplankton backscattering coefficient	$\text{m}^{-1}$
$b_{bn}$	Nonpigmented particulate backscattering coefficient	$\text{m}^{-1}$
$b_p$	Particulate scattering coefficient	$\text{m}^{-1}$
$b_c$	Phytoplankton scattering coefficient	$\text{m}^{-1}$
$b_n$	Nonpigmented particulate scattering coefficient	$\text{m}^{-1}$
$\lambda$	Wavelength	nm
$\gamma$	Parameter describing backscattering spectral dependency	
$S$	Spectral decay constant for soluble materials absorption	$\text{nm}^{-1}$
$F$	Proportionality factor between $R_{rs}$ and $b_b/a$	
$Q$	Ratio of upwelling irradiance to upwelling radiance	sr

NASA Sea-viewing Wide Field-of-View Sensor (SeaWiFS) use the maximum band ratio of  $R_{rs}$  for the band combinations of 443/555, 490/555, or 510/555.

Apparent optical properties such as  $R_{rs}$  and  $L_w$  are very important to remote sensing application, but they depend upon inherent optical properties, such as absorption and backscattering. In this paper, the variability of absorption and backscattering are investigated to develop region-specific models to link  $R_{rs}$  with chlorophyll and inherent optical properties. Spectral dependencies of absorption, scattering, and attenuation are studied to gain more insight into fundamental relationships of individual IOPs. Our primary objective is to obtain sound relationships of IOPs for future bio-optical modeling and chlorophyll-retrieval algorithm developing for the Arctic Ocean.

## **2. Materials and Methods**

Bio-optical observations were made on board USCGC Polar Star from August 7<sup>th</sup> to August 31<sup>st</sup>, 2000 in the Beaufort and Chukchi Seas. This cruise to the Arctic Ocean in 2000 is hereafter referred to as “Arc00”. Figure 1 shows the station map of the cruise. There were 29 optical stations spanning the area from about 168° to 144°W and 70° to 75°N, covering parts of the shelf, slope, and basin regions of the Beaufort and Chukchi Seas. Most of the stations were on the shelves, which were largely ice-free or < 50% ice-covered by August. Discrete water samples were collected for chlorophyll and spectral absorption analyses. Passive optical profiles determined spectral reflectance (Satlantic profiler). An active instrument package was deployed to measure spectral absorption, beam attenuation (WET Labs ac-9), and backscattering (HOBI Labs HydroScat-6) within the water column. Our data set from Arc00 represents to date the most comprehensive field measurements of optical properties in the Beaufort and Chukchi Seas.

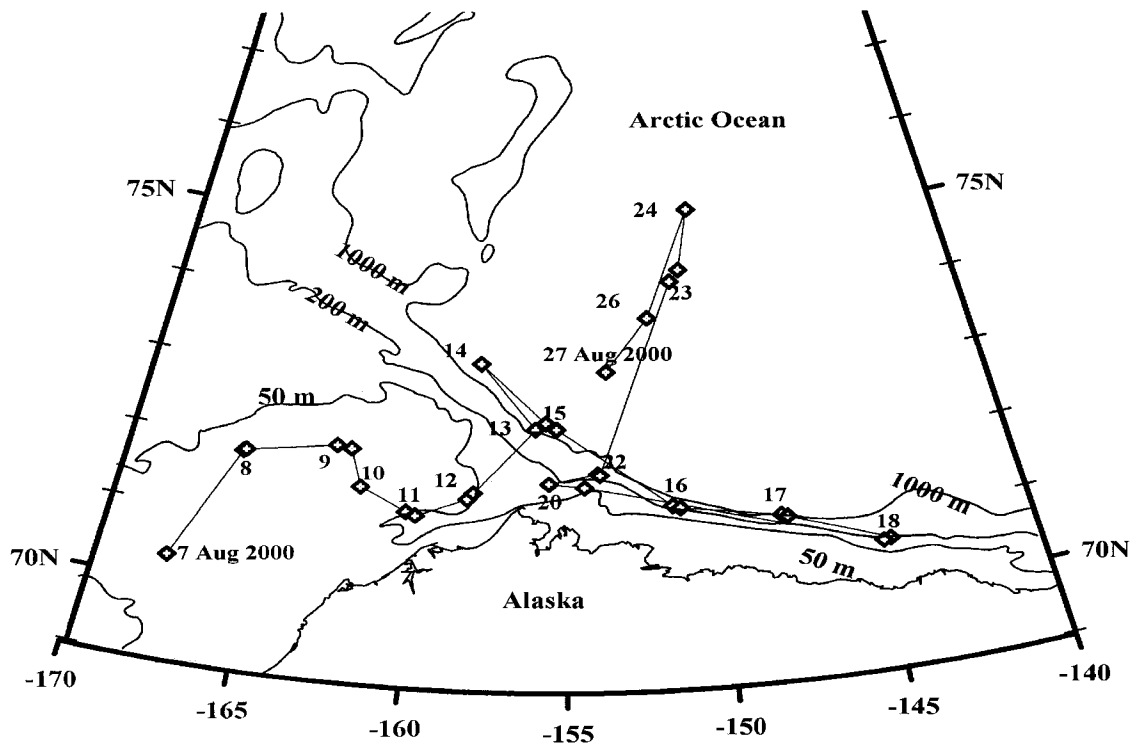


Figure 1. Station locations for the Arctic 2000 cruise in the Beaufort and Chukchi Seas.

There are a total of 29 optical stations in this cruise.

## 2.1 Discrete Water Samples

Discrete water samples for chlorophyll and absorption were collected with Niskin bottles at six light depths corresponding to 100%, 50%, 30%, 15%, 5% and 1% of surface irradiance at most stations. Triplicate samples were collected at the surface (100% light level). Water samples were filtered onto 25 mm Whatman glass fiber filters (GF/F). The filters were extracted in 90% acetone at  $-20^{\circ}\text{C}$  in the dark for 24 hours, and chlorophyll *a* concentrations (Chl) of the extract were measured with a Turner Design fluorometer using standard fluorometric methodology [Strickland and Parsons, 1972].

Spectral absorption was determined on particulate and filter-passing or soluble fractions with discrete samples. Total particulate absorption coefficients were measured according to the filter pad technique of Mitchell [1990] after concentration on Whatman GF/F filters with a nominal pore size of  $0.7\ \mu\text{m}$ . All samples were analyzed within one hour of filtration. The absorption coefficients of total particulate matter,  $a_p(\lambda)$ , were measured on a Shimadzu 2401 dual beam scanning spectrometer from 280 nm to 850 nm at 1-nm spectral resolution using a moist GF/F filter as a blank. Absorption spectra were normalized to the mean absorption coefficient from 750 nm to 850 nm. Absorption coefficients of nonpigmented particulates  $a_n(\lambda)$  were determined after cold methanol extraction [Kishino *et al.*, 1985]. The phytoplankton absorption coefficients,  $a_a(\lambda)$ , were obtained by subtracting  $a_n(\lambda)$  from  $a_p(\lambda)$ . The absorption coefficients of phytoplankton  $a_a(\lambda)$  were then normalized to chlorophyll concentration to obtain chlorophyll-specific absorption coefficients  $a_a^*(\lambda)$ .

Filtrate from GF/F filter was collected and filtered through  $0.2\ \mu\text{m}$  Nucleopore membrane for analysis of absorption by soluble substances [Bricaud *et al.*, 1981]. A

deionized water blank was employed in a 10 cm quartz cuvette. The measured optical densities (ODs) were fitted to a power function ( $Y = a + b X^c$ ), and baseline adjustment was made to the spectra by normalizing the OD values to OD(750 nm). The fitted ODs were converted to absorption coefficients of soluble materials  $a_s(\lambda)$ . The total absorption coefficient minus water  $a_{t-w}$  was considered as the sum of the particulate and soluble absorption coefficients.

## 2.2 Continuous Profile Observations

### 2.2.1 Active Optical Measurements

Vertical profiles of absorption and beam attenuation coefficients were measured *in situ* by an ac-9 meter (WET Labs, Inc.) at nine wavelengths: 412, 440, 488, 510, 555, 630, 650, 676, and 715 nm. A 0.2  $\mu\text{m}$  pore-size cartridge filter was placed at the inlet of the absorption meter of another ac-9 meter for measuring absorption by soluble materials. Temperature and salinity corrections were applied to absorption and beam attenuation coefficients as described by *Pegau et al.* [1997], and absorption coefficients were further corrected for scattering by subtraction of absorption at 715 nm (ac-9 protocol, WET Labs, Inc.).

The ac-9 meters measure total absorption coefficient minus water  $a_{t-w}$ , and beam attenuation coefficient  $c$ . The scattering coefficient of particles  $b_p(\lambda)$  was calculated by subtracting the absorption coefficient from the beam attenuation coefficient:

$$b_p(\lambda) = c(\lambda) - a_{t-w}(\lambda) \quad (1)$$

Here particulate scattering coefficient  $b_p$  is considered equivalent to total scattering coefficient  $b$  because molecular scattering by water and soluble materials are small, and normally are negligible compared with that of particulate matter.

Due to the lack of instrumentation, there have been few *in situ* measurements of backscattering coefficients in the Arctic. During Arc00, the backscattering coefficient  $b_b$  was measured with a HydroScat-6 backscattering meter (HOBI Labs) at six wavelengths: 443, 488, 510, 555, 676, and 852 nm in the Beaufort and Chukchi Seas. Data from the ac-9 and HydroScat-6 were integrated and acquired by using Modular Ocean Data And Power System (MODAPS, WET Labs).

### 2.2.2 Passive Optical Measurements

Measurements of downwelling spectral irradiance  $E_d(\lambda)$  and upwelling radiance  $L_u(\lambda)$  were made with a Satlantic free-fall profiling spectral radiometer and a surface reference at 13 channels: 400, 412, 443, 490, 510, 520, 532, 555, 565, 620, 665, 683, and 700 nm. The instrument includes tilt and roll sensors, a pressure sensor, and a conductivity-temperature sensor. Optical casts were normally made to the depth of 70-100 m, and profiler tilt  $< 5^\circ$  was considered acceptable. All radiometric sensors were deployed more than 10 m away from the ship to minimize the effects of ship shadow.

Optical data acquisition and analyses were done as described by *Cota et al.* [2003], and were in accordance with current SeaWiFS protocols [*Muller and Austin*, 1995]. After correction for attenuation, reflection and refraction, radiance profiles were extrapolated to and through the air-water interface to estimate water-leaving radiance  $L_u(\lambda, \theta^+)$ . Normalized water-leaving radiance  $L_{wn}(\lambda)$  were obtained by normalizing  $L_u(\lambda, \theta^+)$  to incident solar radiation at the top of the atmosphere. Remote sensing reflectance  $R_{rs}(\lambda)$  was computed as the ratio of  $L_u(\lambda, \theta^+)$  to incident irradiance  $E_s((\lambda, \theta^+)$  just above the surface. Regional bio-optical algorithm for chlorophyll retrieval [*Wang and Cota*, 2003] was established by regression of ratios of remote sensing reflectance

from 2 or more bands against surface chlorophyll concentrations [*O'Reilly et al.*, 1998, 2000].

### 3. Results and Discussion

#### 3.1 Absorption

##### 3.1.1 Mean Absorption Spectra

In oceanic “case 1” waters [*Morel and Prieur*, 1977], the total absorption  $a_t$ , is the sum of absorption by water  $a_w$ , total particulates  $a_p$ , and soluble materials  $a_s$ .

$$a_t = a_w + a_p + a_s \quad (2)$$

Particulate absorption  $a_p$  can be further partitioned into algal or phytoplankton absorption  $a_a$  and absorption by nonpigmented particulates  $a_n$ :

$$a_p = a_a + a_n \quad (3)$$

Our data set from Arc00 includes 157 individual absorption spectra measured in the euphotic zone of the Beaufort and Chukchi Seas. The mean spectra of absorption by total particulates, phytoplankton, nonpigmented particulates, and soluble materials as well as total absorption coefficient minus water are shown in Figure 2. The effects of chlorophyll absorption on the particulate absorption spectrum are evident from the peaks around 440 and 675 nm (see Figure 2). The mean  $a_a(440)$  for the 157 spectra is  $0.0397 \text{ m}^{-1}$  with a standard deviation of 0.0517, while  $a_a(675)$  has a mean value of  $0.0233 \pm 0.0372 \text{ m}^{-1}$ . The mean values for  $a_p$  at 440 and 675 nm are  $0.0725 \pm 0.0707 \text{ m}^{-1}$  and  $0.0288 \pm 0.0411 \text{ m}^{-1}$ , respectively. Absorption by nonpigmented particulates in the blue partially masks the chlorophyll absorption peak around 440 nm in total particulate absorption spectrum. Absorption by soluble materials decreases exponentially with increasing wavelength (Figure 2).

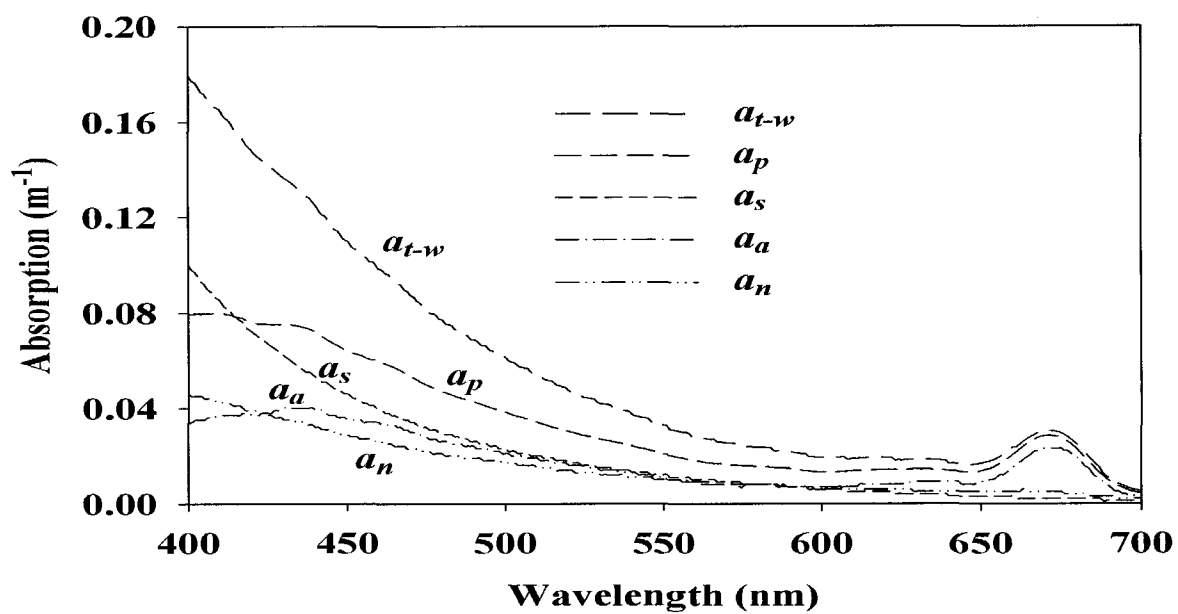


Figure 2. Mean spectra of total absorption minus water  $a_{t-w}$ , total particulate absorption  $a_p$ , phytoplankton absorption  $a_a$ , nonpigmented particulate absorption  $a_n$ , and soluble absorption  $a_s$  ( $n = 157$  spectra).

The mean ratio of absorption by phytoplankton to total particulates at 443 nm is  $0.51 \pm 0.19$ , which suggests phytoplankton contributes to about 51% of particulate absorption around the blue peak. *Bricaud et al.* [1998] found that absorption by nonpigmented particulates is a relatively constant portion of total particulate absorption around 25 - 30% throughout the chlorophyll concentration range from 0.02 to 25  $\text{mg m}^{-3}$ . While their data set ( $n = 1166$ ) included much larger and diverse observations from various areas of the world ocean, our data from Arc00 ( $n = 157$ ) showed larger variability. Absorption by nonpigmented particulates accounts for 10 - 90% of total particulate absorption at 443 nm for chlorophyll concentrations less than 0.3  $\text{mg m}^{-3}$ , which implies that nonpigmented particulates are often more abundant but variable in low biomass waters (Figure 3A). The contribution of absorption by nonpigmented particulates to total particulate absorption is about 20 - 40% for chlorophyll concentrations higher than 5  $\text{mg m}^{-3}$ . Consistent with the results of *Cleveland* [1995] for subpolar region, the proportion of total particulate absorption due to nonpigmented particulates does not exhibit a clear trend with chlorophyll concentration for Arc00, but is higher for lower biomass overall (Figure 3A). Similarly, no simple trend was observed for ratio of soluble absorption to particulate absorption as a function of chlorophyll concentration (Figure 3B). The ratio of soluble absorption to total particulate absorption at 443 nm has an average value of  $1.16 \pm 1.08$ . The standard deviation is comparable to the mean ratio in magnitude, showing soluble materials are extremely variable, especially for the low chlorophyll concentration where soluble absorption can be as high as five times of particulate absorption. *Pegau* [2002] reported that soluble materials increase total absorption from 350 to 700 nm by over 30% in the Arctic surface waters. Therefore,

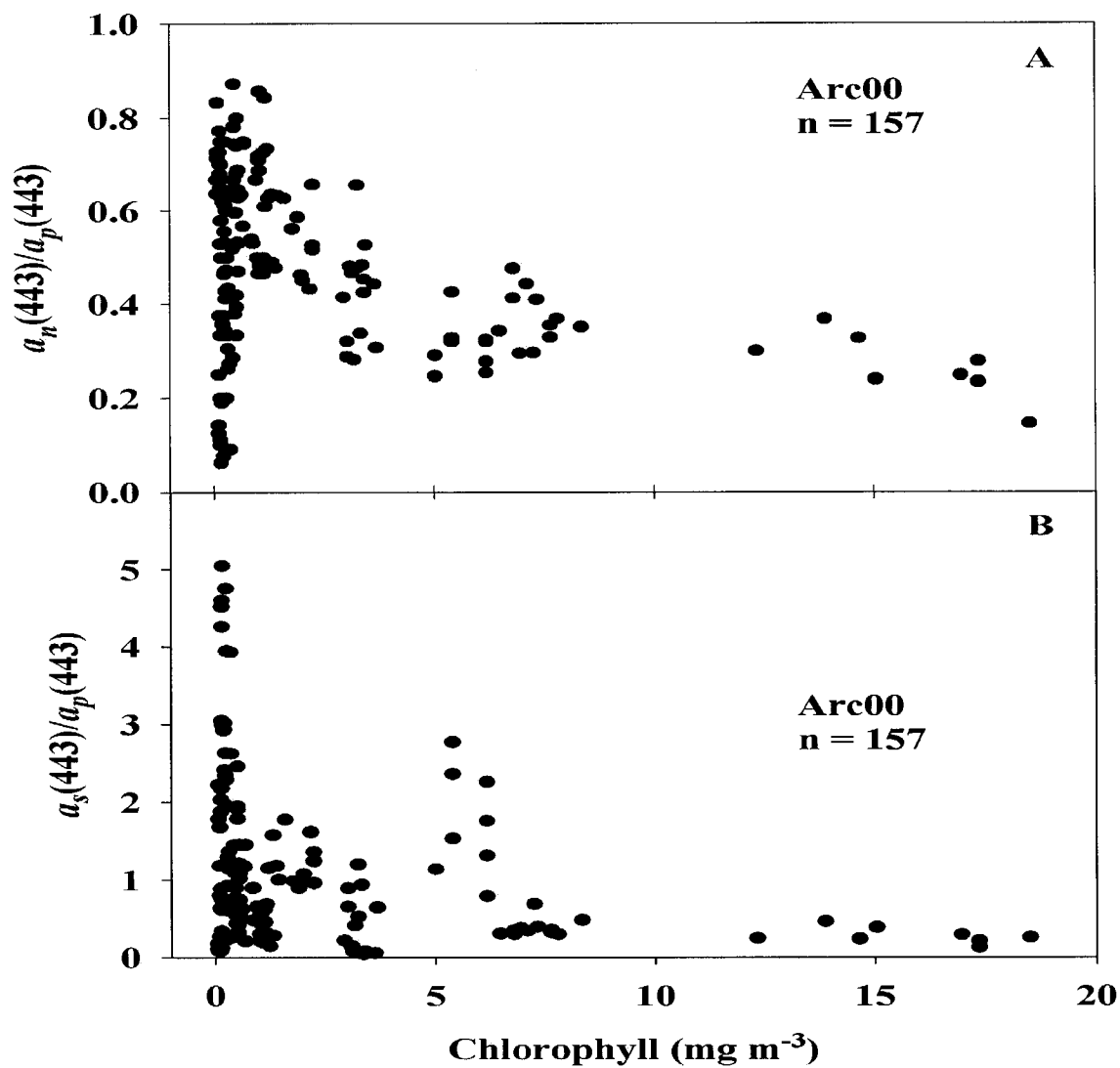


Figure 3. Ratios of absorption by nonpigmented particulates (A) and soluble materials (B) to total particulates at 443 nm versus chlorophyll concentration.

absorption by soluble materials is important in determining the total absorption in the Arctic waters.

### 3.1.2 Relationships between Absorption and Chlorophyll

A power function [Bricaud *et al.*, 1995, 1998] has been suggested to describe the nonlinearity between absorption coefficients and chlorophyll concentrations:

$$a(\lambda) = A(\lambda) [chl]^{B(\lambda)} \quad (4)$$

where  $A$  and  $B$  are two wavelength-dependent constants. The chlorophyll concentration measured in Arc00 ranged from 0.066 to 18.51 mg m<sup>-3</sup>, spanning three orders of magnitude. Nonlinear fits of absorption coefficients at 443 nm of total particulates, nonpigmented particulates, phytoplankton, and soluble materials versus chlorophyll concentration to the power function provided highly significant description of the data ( $p < 0.00001$  for all cases):

$$a_p(443) = 0.0511 [chl]^{0.585}, \quad r^2 = 0.79, \quad n=157 \quad (5)$$

$$a_a(443) = 0.0151 [chl]^{0.957}, \quad r^2 = 0.89, \quad n=157 \quad (6)$$

$$a_n(443) = 0.0306 [chl]^{0.296}, \quad r^2 = 0.41, \quad n=157 \quad (7)$$

$$a_s(443) = 0.0509 [chl]^{0.197}, \quad r^2 = 0.18, \quad n=157 \quad (8)$$

where  $r^2$  is the coefficient of determination and  $n$  is the sample size.

The relationships between absorption coefficients and chlorophyll concentration are illustrated in Figure 4. In this nonlinear model, chlorophyll explains about 80% and 90% of the variability of particulate and phytoplankton absorption, respectively, as indicated by  $r^2$  values. Cota *et al.* [2003] previously reported  $r^2$  of 0.80 and 0.70 for absorption by total particulates and phytoplankton for Labrador Sea, and corresponding  $r^2$  of 0.89 and 0.93 for Resolute Bay [Cota *et al.*, unpublished data]. Bricaud *et al.* [1998]

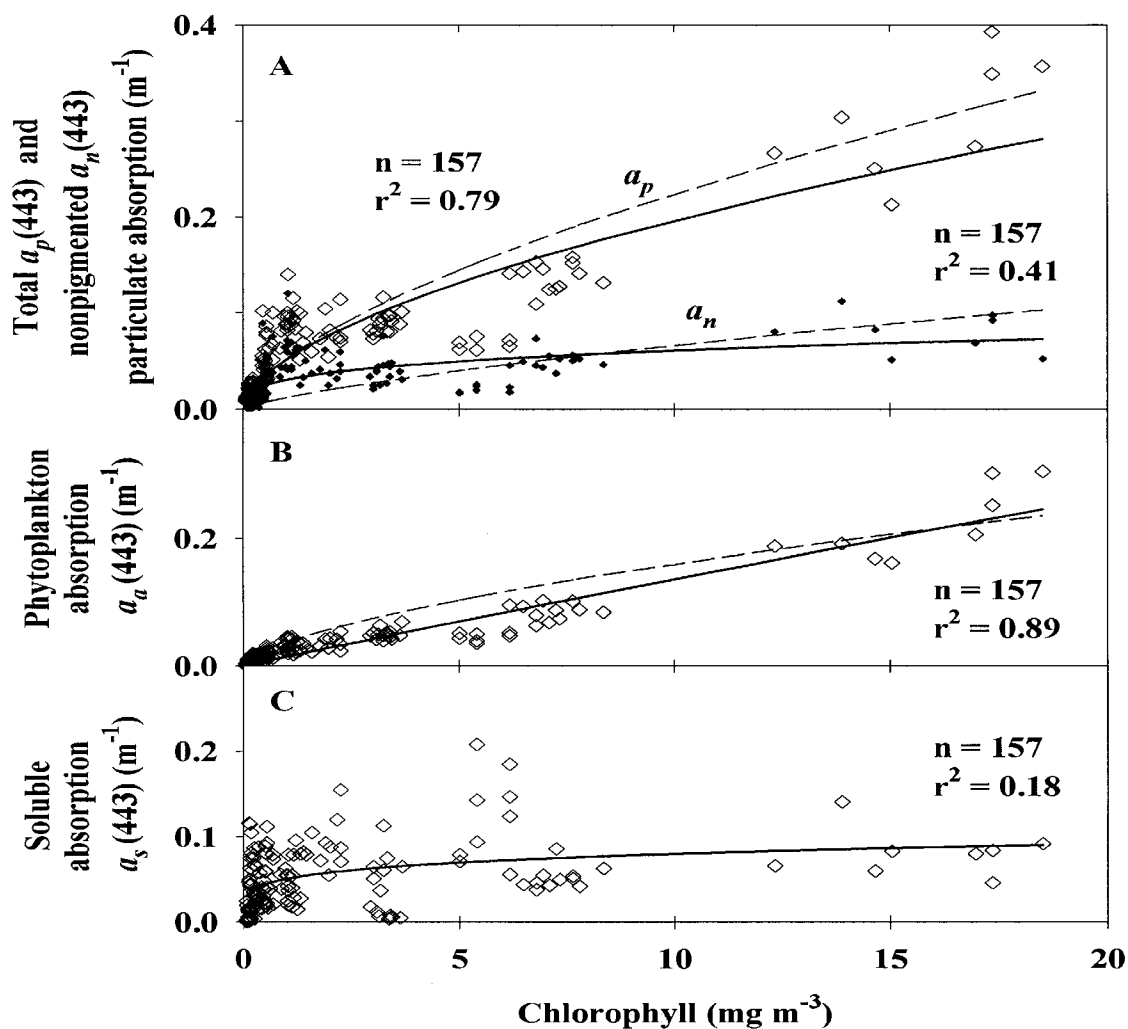


Figure 4. Power functions for total and nonpigmented particulates (A), phytoplankton (B), and soluble (C) absorption at 443nm versus chlorophyll concentration. Filled diamonds refer to nonpigmented particulates. Dashed lines are the relationships of *Bricaud et al.* [1998].

observed determination coefficients  $r^2$  of 0.90 and 0.91 for particulate and phytoplankton absorption, respectively, with a much larger data set ( $n = 1166$ ). Their relationships would overestimate particulate and phytoplankton absorption across the observed biomass range of Arc00 (Figure 4A, B). While coefficient of determination is statistically derived, and is data and site specific, the high  $r^2$  for all these regions suggest that the relationships between absorption by total particulates or phytoplankton and chlorophyll are fairly strong in the high northern latitude regions. Chlorophyll is a significant variable to predict absorption by total particulates and phytoplankton, which is important for building chlorophyll-dependent semianalytical models [Reynolds *et al.*, 2001]. Note that the relationships are only valid within the chlorophyll range over which they were developed, and may not be applicable to other areas.

About 40% of the variability of the absorption by nonpigmented particulates at 443 nm is explained by this power function, which is similar to that observed in Labrador Sea, where about 50% of the variability is accounted for by this model [Cota *et al.*, 2003]. The relationship between absorption by soluble materials and chlorophyll concentration (Figure 4C) only explains 18% of the variability. Similar relationships [DeGrandpre *et al.*, 1996; Nelson *et al.*, 1998] suggest soluble materials often do not covary closely with chlorophyll. The composition and quantities of soluble materials in the water column are controlled by many processes, including grazing, sedimentation, photolysis, and bacterial degradation. Furthermore, shelf waters of the Beaufort and Chukchi Seas are influenced by river discharges and ice melting. The annual discharge to the Arctic Ocean has increased by 7% from 1936 – 1999 [Peterson, *et al.*, 2002]. The Beaufort Sea receives a total annual discharge of  $3.3 \times 10^{11} \text{ m}^3 \text{ y}^{-1}$  from the Mackenzie

River, the 5<sup>th</sup> highest in the Arctic and the total discharge into the Chukchi Sea is  $0.7 \times 10^{11} \text{ m}^3 \text{ y}^{-1}$  [Gordeev, *et al.*, 1996]. Hence, it is not surprising that most of the variability of soluble materials cannot be explained by chlorophyll alone. It is rather controlled by combined effects of many biological, chemical and physical processes. Since the absorption by soluble materials has to be taken into account for interpreting ocean color signatures, the lack of covariance between soluble materials and chlorophyll often complicates accurate chlorophyll retrievals from satellite remote sensing.

In equation (6), the exponent (0.957) is close to 1. In fact, strong linearity was observed between absorption by phytoplankton at 443 nm and chlorophyll concentration ( $r^2 = 0.91$ ,  $p < 0.0001$ ), and the linear regression slope of  $0.013 \text{ m}^2 (\text{mg chl})^{-1}$  was equivalent to the chlorophyll-specific phytoplankton absorption coefficient at 443 nm  $a_a^*(443)$ . The chlorophyll-specific absorption coefficients of phytoplankton  $a_a^*(\lambda)$  describe the in vivo absorption capacity of living algal cells. Phytoplankton cells can be less efficient at harvesting light because their pigments are packaged. The diminution of the pigment absorption in algal cells is known as pigment packaging [see Kirk, 1994]. Examining the red absorption band of chlorophyll *a* near 676 nm, where the influence of accessory pigments is minimal, provides a measure of the pigment packaging effects. The commonly accepted values of  $a_a^*(676)$  for unpackaged pigments have the range of 0.023-0.029  $\text{m}^2 (\text{mg chl})^{-1}$  [Johnsen *et al.*, 1994; Moisan and Mitchell, 1999]. The  $a_a^*(676)$  for Arc00 averaged  $0.014 \pm 0.006 \text{ m}^2 (\text{mg chl})^{-1}$ , which suggests moderate pigment packaging effects in the Beaufort and Chukchi Seas. Pigment packaging can be very significant at high latitudes as phytoplankton cells acclimate themselves to the low light and nutrient rich environment. Cota *et al.* [unpublished data] found highly

packaged red peak values of  $0.006 \pm 0.002 \text{ m}^2 (\text{mg chl})^{-1}$  for large diatoms near Resolute Bay and  $0.010 \pm 0.002 \text{ m}^2 (\text{mg chl})^{-1}$  for the Labrador Sea [Cota *et al.*, 2003]. Natural variability of  $a_a^*$  are normally associated with phytoplankton composition (species, cell size, and pigment composition), or photoacclimation within the local population. Results of pigment analysis using High Performance Liquid Chromatography (HPLC) and size fractionated chlorophyll from spring and summer cruises to the Beaufort and Chukchi Seas in 2002 help better understand the phytoplankton community structure. There appears to be a seasonal succession of phytoplankton in this region [Hill *et al.*, 2004]. Diatoms with cell size larger than  $5 \mu\text{m}$  dominated on the shelf with retreating ice and high nutrient conditions in spring. In summer, when nutrients were depleted in ice-free waters, smaller prasinophytes and chlorophytes dominated near surface, but diatoms were still abundant at depths down to 15% of surface irradiance level. The dominance of smaller cells with lower packaging effects in summer corroborates the observation of higher chlorophyll-specific absorption in the Beaufort and Chukchi Seas than some other Arctic regions.

### 3.1.3 Comparison of Spectrophotometer Analyses and ac-9 meter Measurements

The traditional discrete sample methods for spectral absorption with spectrophotometric analyses provide 1-nm spectral resolution for absorption coefficients, but are limited in vertical resolution. Often only a few discrete water samples from several depths are collected for analyses. In contrast, ac-9 absorption and beam attenuation meters provide high vertical resolution, but limited spectral resolution at only nine selected wavelengths. Profiles with ac-9 meters often have the vertical resolution of a few to tens of centimeters, and can observe fine water column structure. However, ac-9

data are often binned, and for Arc00 had a spatial resolution of 0.5 m.

The absorption coefficients obtained from *in situ* measurements by ac-9 meters and laboratory measurements using discrete water samples were compared to investigate the agreement between the two methods. Simultaneous measurements of absorption coefficients by both methods were taken at 18 stations during Arc00. The average values of the total absorption coefficient minus water  $a_{t-w}$  at the surface are presented in Figure 5A. Pegau *et al.* [1995] compared spectral absorption coefficients measured by six different techniques, including laboratory measurements using water samples and *in situ* measurements. They reported the overall agreement within 40% at 456 nm and 25% at 532 nm. Our results showed that the relative difference between absorption coefficients measured by a spectrophotometer and by ac-9 meters did not exceed 33% at 412, 440, 488, and 510 nm, but was larger than 60% for 555, 630, 650, and 676 nm, which can be attributed to the smaller relative magnitude of absorption coefficients at longer wavelength. Root-mean-square (rms) error between the two measurements is 0.017, and the normalized rms error is 28%.

It is clear that in most cases  $a_{t-w}$  measured by ac-9 meters is higher than  $a_{t-w}$  obtained from spectrophotometric analyses (see Figure 5A). The total absorption coefficient minus water  $a_{t-w}$  is directly measured by ac-9 meters, and is calculated as the sum of total particulate absorption  $a_p$  and soluble absorption  $a_s$  for spectrophotometric analyses. Particles concentrated on 0.7  $\mu\text{m}$  GF/F filters and filtrate passing through 0.2  $\mu\text{m}$  membrane were collected for determination of  $a_p$  and  $a_s$ , respectively. In our spectrophotometric techniques, materials of size between 0.2  $\mu\text{m}$  and 0.7  $\mu\text{m}$  were ignored. This may include nonattached bacterial and some colloidal materials. Therefore,

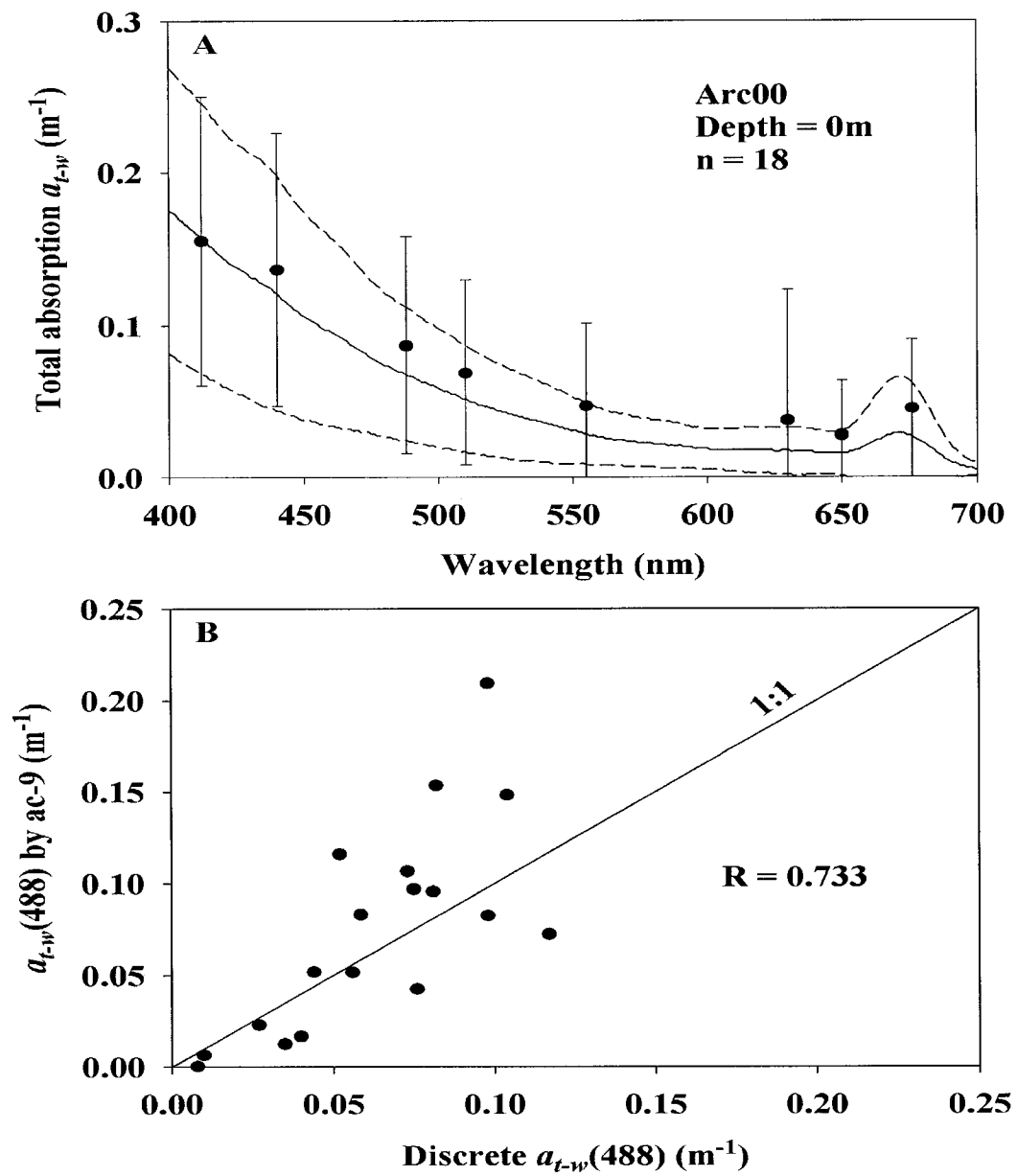


Figure 5. Comparison of total absorption coefficient minus water  $a_{t-w}$  at the surface (0m) measured by spectrophotometric analyses and by ac-9 meters (A) and correlation for  $a_{t-w}(488)$  by the two methods (B).

Table 2. Results of linear correlations of total absorption coefficient minus water  $a_{t-w}$  at the surface (0m) measured by spectrophotometric analyses and by ac-9 meters at eight wavelengths.

---

Wavelength (nm)	Correlation coefficient (R)
412	0.810
440	0.816
488	0.733
510	0.776
555	0.719
630	0.805
650	0.730
676	0.765

---

their contributions to total absorption are missing in discrete analyses, whereas they are represented in measurements by ac-9 meters. The discrepancy observed between total absorption coefficients measured by the two methods is, in part, attributed to this difference in the techniques.

To further compare  $a_{t-w}$  measured by the discrete (spectrophotometer) and continuous methods (ac-9), correlation of  $a_{t-w}$  at 488 nm measured by the two methods are plotted in Figure 5B. The correlation coefficient for  $a_{t-w}(488)$  is 0.733. Correlation coefficients for  $a_{t-w}$  at eight of ac-9's bands are listed in Table 2. They are higher than 0.70 for all cases showing  $a_{t-w}$  measured by the discrete and continuous methods are closely correlated. Overall, absorption coefficients measured by ac-9 meters are generally in reasonable agreement with those derived from spectrophotometric analyses. This is promising because simultaneously observations with a spectrophotometer and ac-9 meters can provide both high spectral and high spatial resolutions, and yield much more detailed information about the structure of underwater light fields.

## 3.2 Backscattering

### 3.2.1 Relationships between Backscattering and Chlorophyll

The total backscattering coefficient  $b_b$  can be partitioned into backscattering of pure seawater,  $b_{bw}$ , and backscattering of particles,  $b_{bp}$ :

$$b_b = b_{bw} + b_{bp} \quad (9)$$

Using a reference wavelength  $\lambda_0$ , the total backscattering coefficient can be formulated as [Reynolds *et al.*, 2001]:

$$b_b(\lambda) = [b_{bw}(\lambda_0) + b_{bp}(\lambda_0)] \left(\frac{\lambda_0}{\lambda}\right)^\gamma \quad (10)$$

where  $\gamma$  is a parameter describing the spectral dependency of backscattering, and the reference wavelength is usually chosen to be 555 nm.

In case 1 waters phytoplankton and heterotrophic bacteria account for most of the scattering, while backscattering is mostly due to very small ( $< 1 \mu\text{m}$ ) and abundant nonpigmented particles [Morel and Ahn, 1991; Stramski and Kiefer, 1991]. Ulloa *et al.* [1994] pointed out that the particulate backscattering to scattering ratio ( $b_{bp}/b_p$ ) is sensitive to the presence of submicrometer particles and strongly dependent on the shape of particle-size distribution. Backscattering to scattering ratios at 443, 488, 510, 555, and 676 nm were calculated using surface values (0~10 m) from 19 optical stations. Linear regression of mean particulate backscattering to scattering ratio versus logarithm of chlorophyll concentration (Figure 6) gives the following results:

$$b_{bp}/b_p (\%) = 1.57 - 0.49 \log_{10}[\text{chl}] \quad (11)$$

with the  $r^2$  of 0.57 ( $p < 0.001$ ). This approach was based on the assumption that  $b_{bp}/b_p$  is wavelength independent, which is in accordance with the theoretical results of Ulloa *et al.* [1994]. The relationship between backscattering to scattering ratio and chlorophyll turns out crucial for selecting the phase function with correct backscattering fraction in HYDROLIGHT simulations of remote sensing reflectance [Wang *et al.*, 2003]. The regression slope (- 0.49) is not significantly different from the slope (- 0.42) suggested by Ulloa *et al.* [1994] ( $p > 0.05$ ,  $F$ -test), but our intercept is significantly higher ( $p < 0.0001$ ,  $F$ -test). The relatively higher backscattering ratios in our data set suggest larger amounts of nonpigmented particles present in the environment, since small particles has been reported to significantly contribute to the backscattering ratio [Risović, 2002]. Concentrations of nonpigmented particles were presumably high at some Arc00 stations

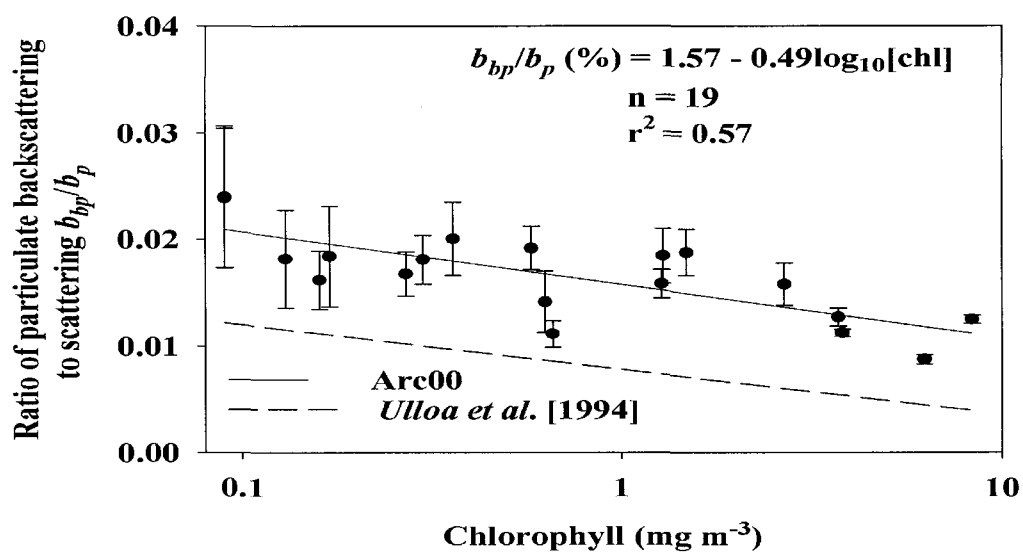


Figure 6. Ratio of particulate backscattering coefficient to total particulate scattering coefficient as a function of chlorophyll concentration.

further east past Barrow Canyon (Figure 1) that are subject to the influence of the Mackenzie River runoff. The larger standard deviation of backscattering to scattering ratios for lower chlorophyll concentration (Figure 6) implies higher spectral variability of backscattering to scattering ratios. This observation that backscattering by nonpigmented particles is spectrally more variable for low chlorophyll concentration is consistent with the high variability of particle concentrations at the low biomass range (Figure 3A). The effect becomes less prominent with increasing chlorophyll concentration because nonpigmented particles concentrations are less variable and absorption gradually dominates.

Backscattering coefficients of particulates at 555nm covary strongly with chlorophyll concentrations (Figure 7A):

$$b_{bp}(555) = 0.004 [chl]^{0.357}, \quad r^2 = 0.91, \quad n=15 \quad (12)$$

Previously reported relationships between  $b_{bp}(555)$  and chlorophyll concentration are also presented in Figure 7A. Our results are consistent with the model of *Morel* [1988]. Across the range of observed biomass, backscattering in the Beaufort and Chukchi Seas is significantly higher than in the Ross Sea. *Reynolds et al.* [2001] suggested that larger cell size or less abundant nonpigmented particulates in the Ross Sea led to the lowered backscattering. Compared with the Antarctic Polar Front Zone (APFZ), backscattering for low biomass ( $< 1.0 \text{ mg chl m}^{-3}$ ) waters in the Arctic Ocean is higher, while at higher biomass ( $> 1.0 \text{ mg chl m}^{-3}$ ) backscattering for Arc00 is lower, as illustrated in Figure 7A. The difference may be attributed to more abundant nonpigmented particulates in the low biomass arctic waters (Figure 3A).

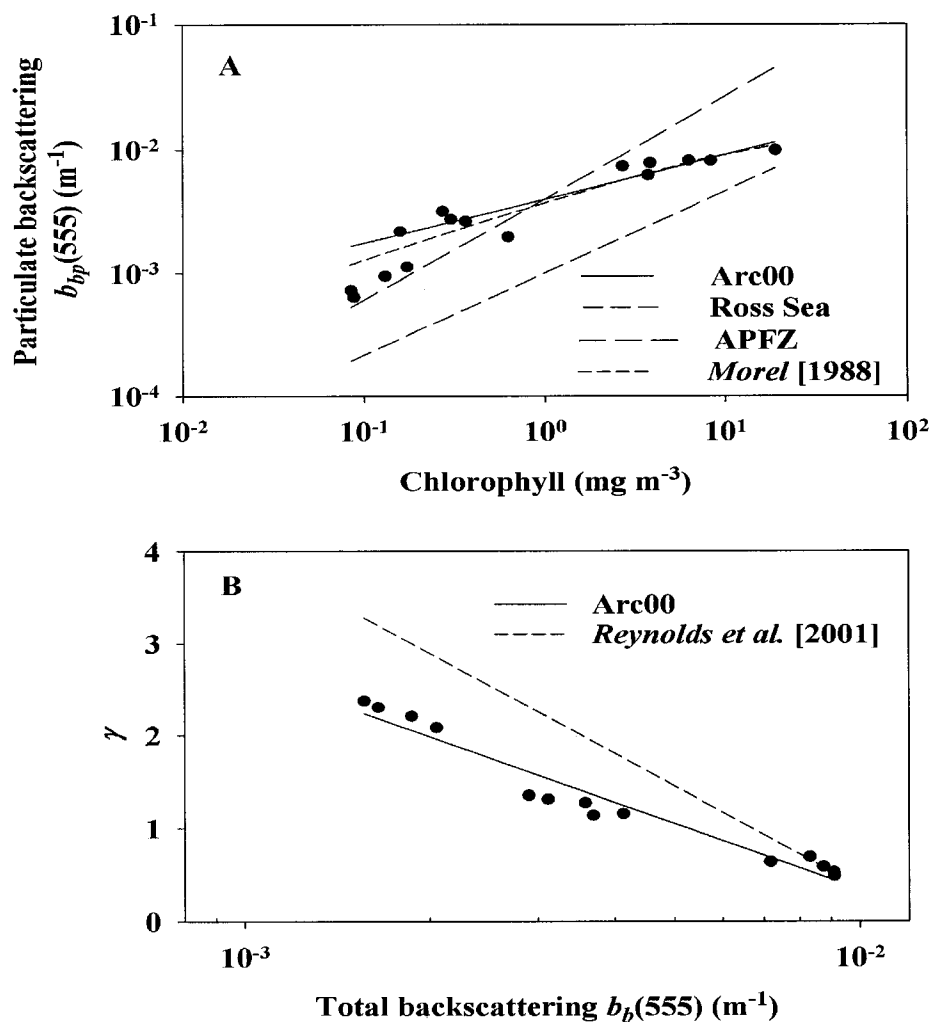


Figure 7. Relationships between backscattering coefficients of particles at 555 nm and chlorophyll concentrations (A) for Arc00, Ross Sea, and APFZ. The relationship predicted by *Morel* [1988] is shown for comparison. Parameter describing backscattering spectral dependency  $\gamma$  as a function of backscattering coefficients at 555nm for Arc00 (B, solid), is compared with *Reynolds et al.*'s [2001] model (B, dashed).

The index of backscattering spectral dependency  $\gamma$  [Reynolds *et al.*, 2001] shows strong correlation with backscattering at 555 nm (Figure 7B):

$$\gamma = -2.348 \log_{10}(b_b(555)) - 4.353 \quad (13)$$

with a determination coefficient of 0.95 ( $p < 0.00001$ ). Reynolds *et al.* [2001] reported a regression slope of  $-3.616$  for the same relationship. An  $F$ -test suggested that the regression slope and intercept for Arc00 were statistically different from those for the Ross Sea and the APFZ ( $p < 0.05$ ).

With the above formulation and the relationships between  $b_{bp}(555)$  and chlorophyll, total backscattering can be modeled based upon chlorophyll concentration and  $b_{bp}(555)$ , both of which can be obtained from field measurements. This approach provides the important backscattering component for constructing bio-optical models relating  $R_{rs}$  to chlorophyll and inherent optical properties (IOPs).

### 3.2.2 Relationships between Backscattering and Remote Sensing Reflectance

Carder *et al.* [1999] developed an inverse model for predicting chlorophyll and absorption by phytoplankton and soluble materials from remote sensing reflectance. The relationships between IOPs and  $R_{rs}$  are critical to construct such a model. Figure 8A demonstrates that relationship between particulate backscattering coefficients at 555nm and  $R_{rs}$  in Beaufort and Chukchi Seas is very close to that of Carder. The two relationships are not significantly different from each other ( $p > 0.05$ ,  $F$ -test). The spectral dependency  $\gamma$ , also correlates with the ratio of reflectance at 443 nm to 488 nm (Figure 8B), but has a slope different from that of Carder *et al.* [1999] ( $p < 0.05$ ,  $F$ -test). Note that Carder's model was developed for particulate backscattering, while in our relationship the parameter  $\gamma$  has a slightly different definition, describing the spectral

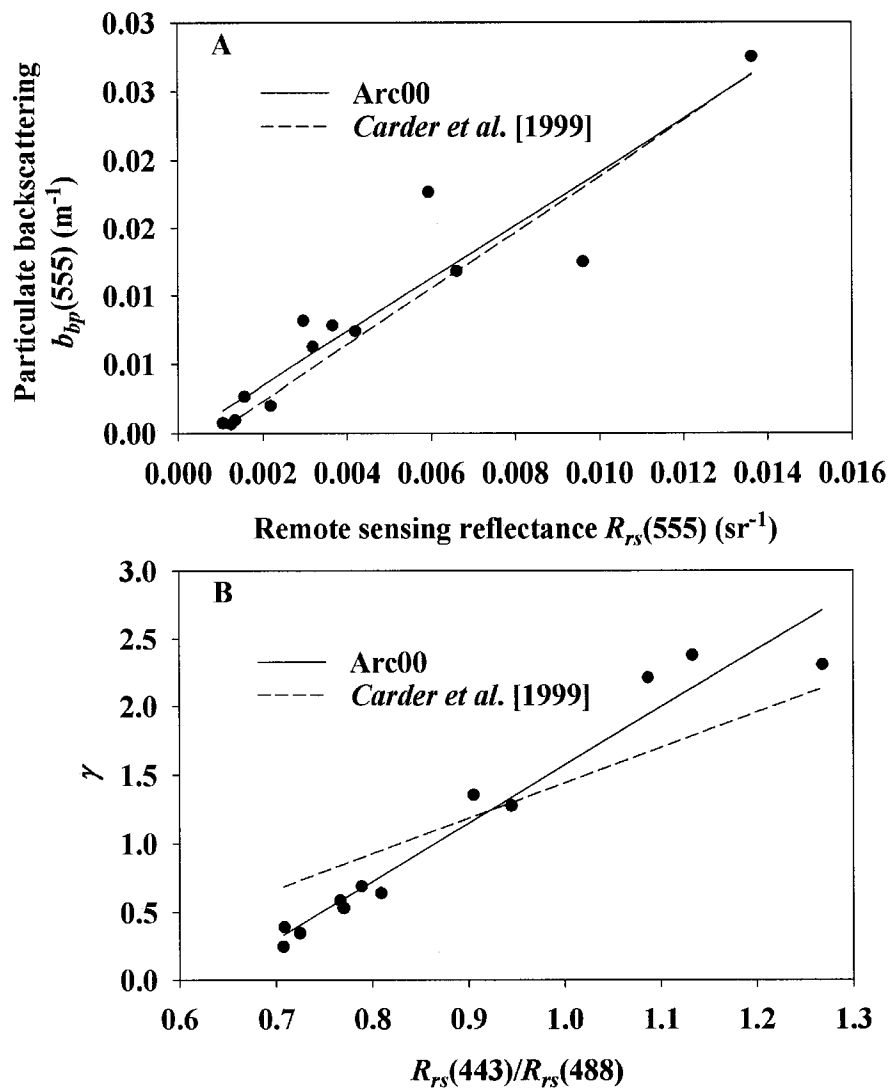


Figure 8. Relationships between backscattering coefficients of particles at 555 nm and remote sensing reflectance at 555 nm (A), and index of backscattering spectral dependency  $\gamma$  versus ratios of reflectance at 443 nm to 488 nm (B).

dependency of total backscattering including backscattering by water. Specific parameterizations for different regions are required to accurately retrieve bio-optical constituents using the model of *Carder et al.*

The remote-sensing reflectance  $R_{rs}$ , is linked to absorption and backscattering through the following formulation [*Lee et al.*, 1994]:

$$R_{rs}(\lambda) = \frac{ft^2}{Q(\lambda)n^2} \left( \frac{b_b(\lambda)}{a(\lambda) + b_b(\lambda)} \right) \quad (14)$$

where  $f$  is an empirical factor and is a function of the solar zenith angle [*Kirk*, 1984; *Morel and Gentili*, 1991],  $t$  is the transmittance of the air-sea interface,  $Q(\lambda)$  is the ratio of upwelling irradiance to radiance  $E_u(\lambda)/L_u(\lambda)$ , and  $n$  is the real part of the refraction index of seawater. Here  $t^2/n^2$  is found to be about 0.54, and relatively independent of wavelength [*Austin*, 1974]. Although individually  $f(\lambda)$  and  $Q(\lambda)$  may show high variability, the ratio of  $f(\lambda)/Q(\lambda)$  is less variable, and can be assumed to be constant [*Gordon et al.*, 1988; *Morel and Gentili*, 1993]. Linear regression of measured  $R_{rs}$  versus the ratio of backscattering to the sum of backscattering and absorption,  $b_b/(b_b+a)$ , at five wavelengths (Table 3) shows that values of  $f/Q$  are all within the range of 0.09 to 0.12 ( $p < 0.00001$ ). The values of  $f/Q$  are consistent with those empirically determined by *Reynolds et al.* [2001] and derived from Monte Carlo simulations [*Morel and Gentili*, 1993]. Figure 9 illustrates the linear relationships between  $R_{rs}$  and  $b_b/(b_b+a)$  at 555 nm for Arc00, with a determination coefficient of 0.88. Closure between  $R_{rs}$  and IOPs is achieved for all five spectral bands included in our measurements, lending credence to the accuracy of individual measurements. The closure between remote sensing reflectance and inherent optical properties is important for empirical formulations linking

Table 3. Results of linear regression of remote sensing reflectance  $R_{rs}$  versus ratio of backscattering to the sum of backscattering and absorption  $b_b/(b_b+a)$ . The value of  $f/Q$  was calculated by dividing the regression slope by 0.54.

$\lambda$ , nm	Slope	Intercept	$r^2$	$f(\lambda)/Q(\lambda)$
443	0.048	0.0004	0.44	0.089
488	0.067	-0.0017	0.74	0.124
510	0.064	-0.0009	0.83	0.119
555	0.057	-0.0006	0.88	0.106
665	0.053	-0.0001	0.89	0.098

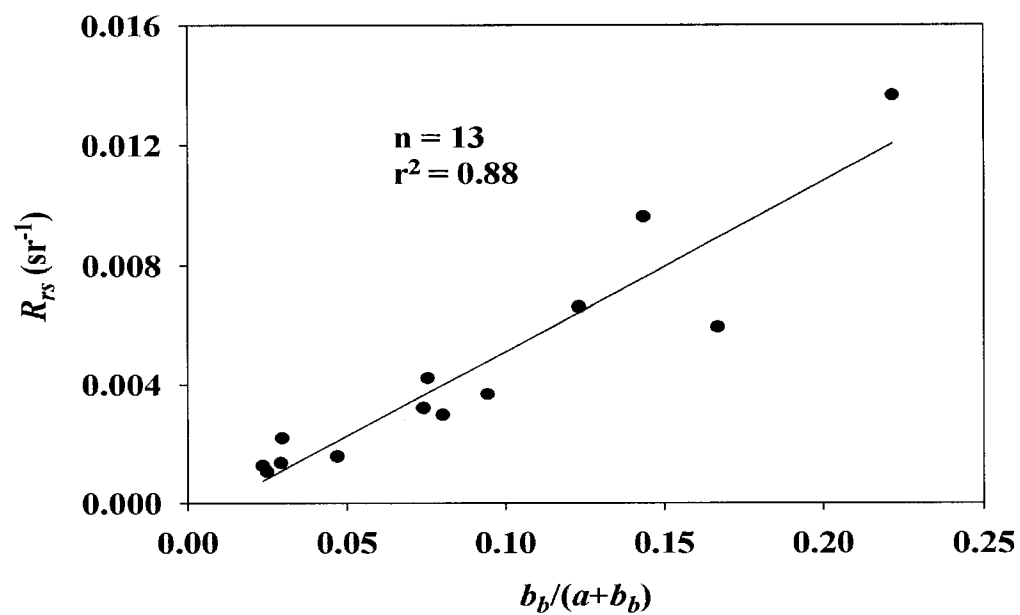


Figure 9. Relationships between remote sensing reflectance and the ratio of backscattering to the sum of absorption and backscattering for 555 nm.

$R_{rs}$  to IOPs and accurate modeling of  $R_{rs}$  or IOPs.

### 3.3 Spectral Dependencies of Inherent Optical Properties

Figure 10 shows the strong linear spectral dependencies of phytoplankton absorption observed in the Beaufort and Chukchi Seas. A reference wavelength of 443 nm was chosen because it is a SeaWiFS channel, and around the phytoplankton absorption peak in the blue. The slopes and intercepts for spectral dependencies of phytoplankton absorption are summarized in Table 4, and coefficients of determination  $r^2$  exceed 0.97 for all cases. Combining the spectral dependencies with chlorophyll-specific absorption coefficients for phytoplankton and other constituents, the absorption components of bio-optical models can be parameterized to chlorophyll and absorption at a single wavelength (e.g. 443 nm).

The total absorption coefficients minus water  $a_{t-w}$ , scattering coefficients  $b_p$ , and beam attenuation coefficients  $c$  also exhibited similar linear spectral dependencies. The spectral dependencies of these IOPs at 488 nm were determined using data from the ac-9 measurements in accordance with *Barnard et al.* [1998]. The spectral dependency of each IOP can be expressed as:

$$y(\lambda) = mx(488 \text{ nm}) + b \quad (15)$$

where  $m$  is the slope and  $b$  is the intercept.

The relationships between total absorption minus water  $a_{t-w}$  at 412, 440, 510, 555, 630, 650, or 676 nm and  $a_{t-w}$  at 488 nm are illustrated in Figure 11A. The slopes, intercepts, and coefficients of determination  $r^2$  are listed in Table 5. In the blue and green spectral domain, the linear relationships explain 80 to 93% of the variability. In the red, lower values of  $r^2$  are observed. The spectral shape of  $a_{t-w}$  is influenced by both soluble

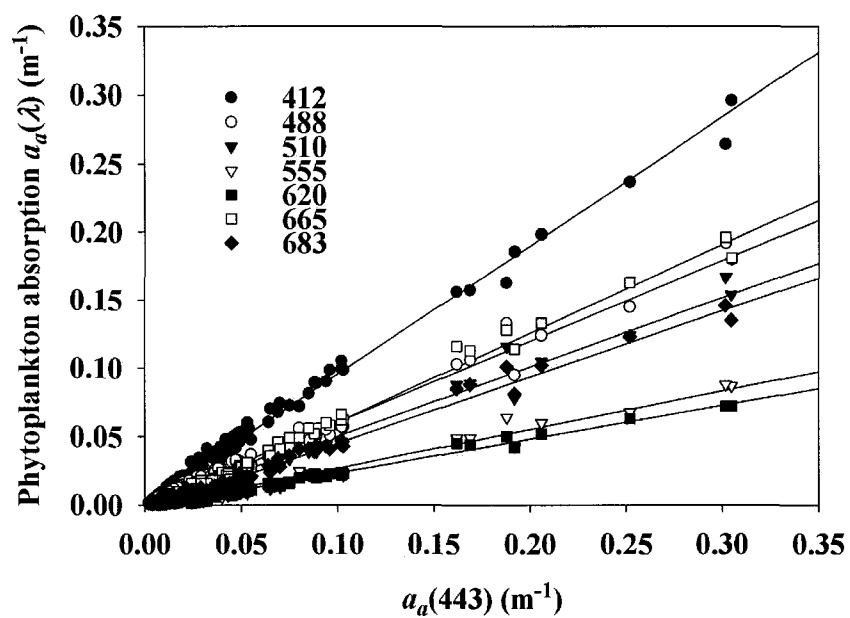


Figure 10. Spectral relationships between phytoplankton absorption at seven wavelengths and phytoplankton absorption at 443 nm. The linear regression fits are shown as lines.

Table 4. Results of linear regression of phytoplankton absorption at seven wavelength versus  $a_a(443 \text{ nm})$

$\lambda$ , nm	Slope	Intercept	$r^2$
412	0.94	0.014	0.99
488	0.59	0.001	0.99
510	0.51	-0.001	0.98
555	0.28	-0.001	0.97
620	0.25	-0.001	0.99
665	0.65	-0.005	0.99
683	0.49	-0.004	0.98

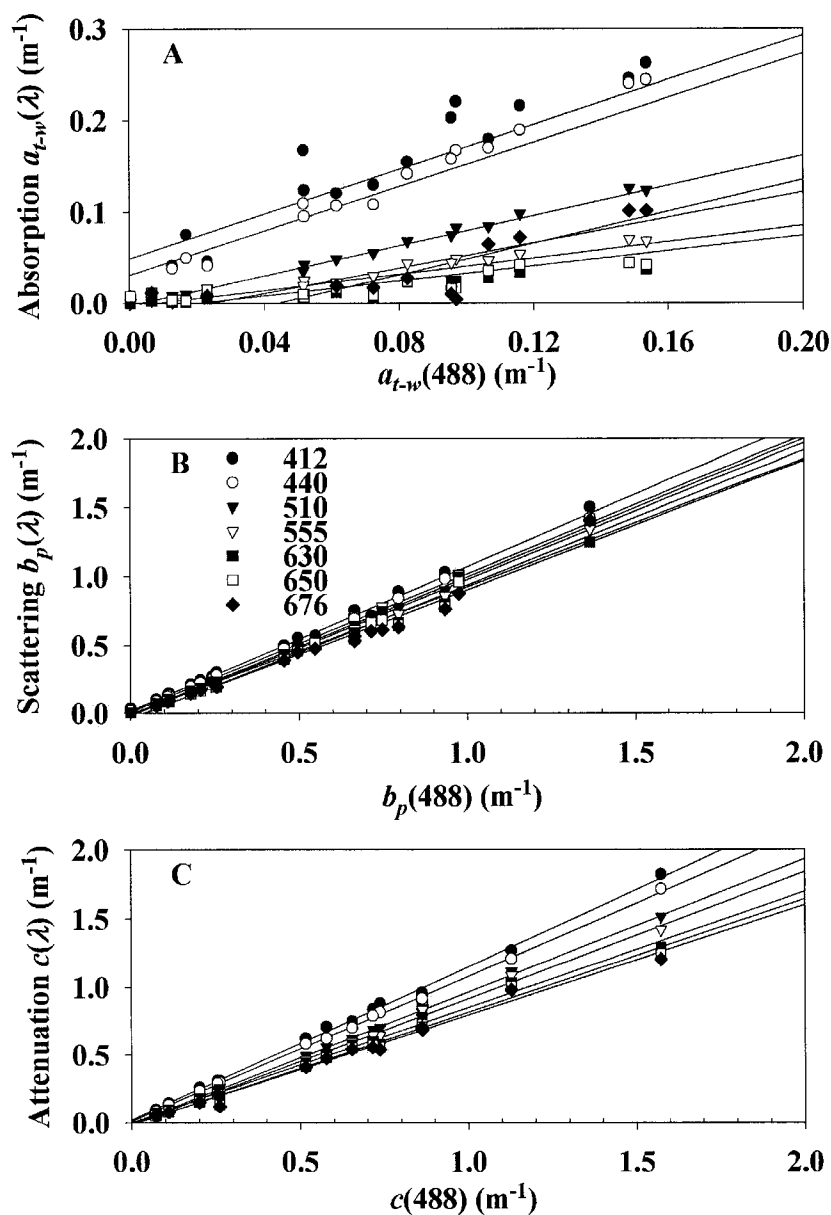


Figure 11. Total absorption coefficient minus water  $a_{t-w}$  at seven wavelengths versus  $a_{t-w}$  at 488 nm (A), the same relationships for light scattering coefficient  $b_p$  (B) and beam attenuation coefficient  $c$  (C).

Table 5. Results of linear regression of total absorption without water  $a_{t-w}$  at seven wavelengths versus  $a_{t-w}$  (488 nm)

$\lambda$ , nm	Slope	Intercept	$r^2$
412	1.216	0.050	0.843
440	1.208	0.032	0.930
510	0.820	-0.002	0.929
555	0.692	-0.016	0.802
630	0.868	-0.038	0.520
650	0.413	-0.008	0.667
676	0.444	-0.003	0.471

Table 6. Results of linear regression of particulate scattering coefficient  $b_p$  at seven wavelengths versus  $b_p$  (488 nm)

$\lambda$ , nm	Slope	Intercept	$r^2$
412	1.051	0.021	0.994
440	1.009	0.008	0.995
510	1.005	-0.009	0.998
555	0.993	-0.016	0.994
630	0.928	-0.004	0.988
650	0.980	-0.042	0.981
676	0.938	-0.035	0.978

Table 7. Results of linear regression of beam attenuation  $c$  at seven wavelengths versus  $c(488 \text{ nm})$

$\lambda$ , nm	Slope	Intercept	$r^2$
412	1.127	0.022	0.997
440	1.067	0.013	0.999
510	0.971	-0.005	0.999
555	0.927	-0.010	0.997
630	0.848	0.002	0.992
650	0.831	-0.014	0.990
676	0.807	-0.011	0.988

and particulate absorption fractions. Absorption by nonpigmented particulates and soluble materials decreases exponentially with increasing wavelength and both become very small in the red. They also do not covary with absorption by phytoplankton. As suggested by *Barnard et al.* [1998], this noncovariance and smaller magnitude range both contribute to the lower  $r^2$  values in the red.

The linear dependencies of light scattering  $b$  and beam attenuation  $c$  (Figure 11B and 11C) are robust at all the wavelengths examined. The coefficients of determination (Table 6 and 7) were higher than 0.97 for all cases, which demonstrates that the linear relationships discovered from a “global” data set [*Barnard et al.*, 1998] also exist in our arctic data. The linear spectral relationships of these IOPs make it possible to predict absorption, scattering, or attenuation from a single wavelength. This is of great importance in satellite remote sensing since bio-optical information is usually limited in most cases. It is crucial that more detailed models be developed and tuned with IOPs on regional scales for this purpose given the wide range of variability.

#### **4. Conclusions**

Bio-optical properties of Arctic waters have been found to be fundamentally different from low latitude waters [*Mitchell and Holm-Hansen*, 1991; *Cota et al.*, 2003]. Phytoplankton absorption and total particulate absorption at 443 nm both covary closely with chlorophyll concentration, which suggests that their underlying controlling mechanisms are dominated by the anabolic processes of phytoplankton. The nonpigmented portion of particulate absorption is highly variable at any single chlorophyll concentration, and the greatest variability is observed for low biomass ( $\text{Chl} < 0.3 \text{ mg chl m}^{-3}$ ). The explanation that the proportion of particulate absorption due to

nonpigmented particulates increases as chlorophyll concentration decreases is not supported by our data. River input to shelf waters and ice melting in summer contribute to the addition of soluble materials. No strong correlation exists between absorption by soluble materials and chlorophyll, which must be related to differences in the controlling catabolic and abiotic processes.

A comparison between spectrophotometric analyses and ac-9 measurements shows that absorption coefficients measured by both methods are generally in good agreement. The result indicates that ac-9 meters are reliable, precise, and highly complementary to discrete water sample methods. High spectral and spatial resolutions can be achieved by using both methods simultaneously, which provides more accurate and complete descriptions of the under water light field.

Strong spectral dependencies of phytoplankton absorption are observed. *Barnard et al.* [1998] suggested linear spectral dependencies for absorption, scattering, and attenuation, which are supported by our regional data. These first-order relationships can be used to predict absorption, scattering, and attenuation even when information is limited. The spectral dependency of backscattering and relationships between backscattering and chlorophyll are robust as shown by our data. The spectral relationships of IOPs are fundamental, and are very important for developing bio-optical models. Models linking chlorophyll and IOPs with remote sensing reflectance are more accurate with region-specific parameterizations. Understanding the variability of each inherent optical property is a prerequisite to develop such models. Parallel efforts include building bio-optical models based on the results presented in this paper, and further evaluating and tuning model performance [*Wang and Cota, 2003*]. These models are of immediate

interest in remote sensing applications, and critically important to better understand regional differences in bio-optical properties and remote sensing algorithms.

## CHAPTER III

### REMOTE SENSING REFLECTANCE IN THE BEAUFORT AND CHUKCHI SEAS: OBSERVATIONS AND MODELS

#### 1. Introduction

Satellite remote sensing provides unprecedented opportunities to study large-scale surface physical and biological characteristics of the oceans. Information about some of the optical constituents of the water can be derived from radiometric data such as remote sensing reflectance  $R_{rs}(\lambda)$  or normalized water-leaving radiance  $L_{wn}(\lambda)$  (see Table 1 for symbols and definitions). The remote-sensing reflectance,  $R_{rs}(\lambda)$ , is linked to absorption and backscattering through the following formulation [Lee *et al.*, 1994]:

$$R_{rs}(\lambda) \approx \frac{ft^2}{Q(\lambda)n^2} \left( \frac{b_b(\lambda)}{a(\lambda) + b_b(\lambda)} \right) \quad (16)$$

where  $\lambda$  denotes wavelength,  $b_b$  is the total backscattering coefficient,  $a$  is the total absorption coefficient,  $f$  is an empirical factor and is a function of the solar zenith angle [Kirk, 1984; Morel and Gentili, 1991],  $t$  is the transmittance of the air-sea interface,  $Q$  is the ratio of upwelling irradiance to radiance  $E_u/L_u$ , and  $n$  is the real part of the refraction index of seawater.

In case 1 waters absorption and backscattering are largely dependent on the chlorophyll concentration, which is the most important data product of ocean color, and is usually retrieved based on the empirical relationships between  $R_{rs}(\lambda)$  or  $L_{wn}(\lambda)$  and Chl [O'Reilly *et al.*, 1998, 2000]. Understanding the relationships between the inherent optical properties (IOPs) and  $R_{rs}$  is fundamental for remote sensing of ocean color. In recent years, several semi-analytical models have been developed to predict chlorophyll

concentration and key inherent optical properties, namely absorption and backscattering, from remote sensing reflectance. For example, *Carder et al.* [1999] developed an inversion model to retrieve chlorophyll *a* concentration and absorption coefficients for phytoplankton and colored dissolved organic matter (CDOM) from  $R_{rs}$  for the Moderate-Resolution Imaging Spectrometer (MODIS). A non-linear statistical model was constructed by *Garver and Siegel* [1997] to determine chlorophyll concentration, absorption coefficient for CDOM plus nonpigmented particulates, and the particulate backscattering coefficient for the Sargasso Sea. Based on the latter model, *Maritorena et al.* [2001] developed a more sophisticated model for the purpose of global scale application by adding an optimization scheme. Besides the inversion models, a “forward” semi-analytical model was developed by *Reynolds et al.* [2001] to predict the spectral remote sensing reflectance  $R_{rs}$  as a function of chlorophyll concentration. This model was based upon chlorophyll-dependent parameterizations of absorption and backscattering from field measurements in the Southern Ocean. All of these models were designed to investigate relationships between remote sensing reflectance, chlorophyll, and IOPs over limited spatial domains, and may be used reliably for other regions with *in situ* or satellite ocean color data when properly tuned and validated.

Due primarily to sampling difficulties, the Arctic Ocean and its marginal and surrounding seas remain under-represented in the global bio-optical data set. Previous studies [*Mitchell and Holm-Hansen*, 1991; *Mitchell*, 1992] suggested the bio-optical properties in polar waters are markedly different from low latitude ecosystems in that pigment package effects are important and low chlorophyll-specific absorption and scattering are common. These differences imply that site and season specific

parameterizations for all of the aforementioned models are required to obtain accurate chlorophyll and IOPs estimates for these locations. Our bio-optical observations in the Beaufort and Chukchi Seas make it possible to tune these models and evaluate their performances for the high northern latitude regions. After validation, these semi-analytical models should provide accurate retrievals of several IOPs and chlorophyll simultaneously. Observed bio-optical relationships were also employed in HYDROLIGHT radiative transfer modeling to study the variability of remote sensing reflectance. Furthermore, current global empirical algorithms for chlorophyll retrieval were compared to our regionally developed algorithms in this paper. These efforts will improve our understanding of ocean color in the Arctic.

## **2. Materials and Methods**

### **2.1 Bio-optical Field Measurements**

Bio-optical observations were made on board USCGC Polar Star from August 7<sup>th</sup> to August 31<sup>st</sup>, 2000 in the Beaufort and Chukchi Seas, which are marginal seas of the Arctic Ocean [Wang *et al.*, 2004]. This cruise to the Arctic Ocean in 2000 is hereafter referred to as “Arc00”. The shelf was mostly ice-free or < 50% ice-covered by August. There were a total of 29 optical stations spanning the area from about 168° to 144°W and 70° to 75°N (see Figure 1).

#### **2.1.1 Chlorophyll and IOPs**

Methodological details were described more fully in Wang *et al.* [2004]. Discrete water samples were collected for chlorophyll and absorption analyses over the euphotic zone (i.e., 1% of surface light level). All particulate collections were made on Whatman glass fiber filters (GF/F). Chlorophyll *a* concentrations (Chl) were measured with a

Turner Design fluorometer using standard fluorometric methodology [Strickland and Parsons, 1972]. Total particulate absorption coefficients  $a_p(\lambda)$  were measured according to Mitchell [1990]. Absorption coefficients of nonpigmented particles  $a_n(\lambda)$  were determined after cold methanol extraction [Kishino et al., 1985]. Soluble absorption coefficients  $a_s(\lambda)$  were determined in accordance with Bricaud et al. [1981]. The phytoplankton absorption coefficients  $a_a(\lambda)$ , were obtained by subtracting  $a_n(\lambda)$  from  $a_p(\lambda)$ . The phytoplankton absorption  $a_a(\lambda)$ , was then converted to chlorophyll-specific absorption coefficient  $a_a^*(\lambda)$  by normalizing to the chlorophyll concentration. Backscattering coefficients  $b_b$  were measured by a HydroScat-6 backscattering meter (HOBI Labs) at six wavelengths, namely, 443, 488, 510, 555, 676 and 852 nm.

### 2.1.2 In-water Reflectance Measurements

Downwelling spectral irradiance  $E_d(\lambda)$  and upwelling radiance  $L_u(\lambda)$  measurements were made with a Satlantic free-fall profiling spectral radiometer and a surface reference at 13 channels: 400, 412, 443, 490, 510, 520, 532, 555, 565, 620, 665, 683 and 700 nm. The instrument includes tilt and roll sensors, a pressure sensor, and a conductivity-temperature sensor. Optical casts were normally made over the top 70-100 m; a profiler tilt  $< 5^\circ$  was considered acceptable. All radiometric sensors were  $\sim 20$  m or more away from the ship to minimize ship shadow.

Optical data acquisition and analyses were made according to current SeaWiFS protocols [Mueller and Austin, 1995] as described in Cota et al. [2003]. Water-leaving radiance  $L_u(\lambda, 0^+)$  were estimated by extrapolating radiance profiles to and through air-water interface correcting for attenuation, reflection, and refraction. Normalized water-leaving radiance  $L_{wn}(\lambda)$  were obtained by normalizing  $L_u(\lambda, 0^+)$  to incident radiation at the

top of the atmosphere. Remote sensing reflectance  $R_{rs}(\lambda)$  was computed as the ratio of  $L_u(\lambda, 0^+)$  to incident irradiance  $E_s(\lambda, 0^+)$  just above surface.

### 2.1.3 Above-water Reflectance Measurements

During our cruise to the Beaufort and Chukchi Seas, a Satlantic Surface Acquisition System III (SAS) was mounted on the flying bridge to measure downwelling irradiance, downwelling sky radiance, and upwelling water-leaving radiance at 13 wavelengths: 380, 400, 412, 443, 490, 510, 532, 555, 665, 683, 700, 780 and 865 nm. The solar azimuth angle was adjusted to  $90^\circ$  for each above water measurement. This permitted near-simultaneous in-water and above-water observations.

## 2.2 Formulation of Reflectance Models

### 2.2.1 Model of *Lee et al.*

The model of *Lee et al.* [2001] is based on the model of *Carder et al.* [1999] with some modifications. In the former model, phytoplankton absorption  $a_a(\lambda)$  is simulated as:

$$a_a(\lambda) = \{a_0(\lambda) + a_1(\lambda) \ln[a_a(440)]\} a_a(440) \quad (17)$$

where  $a_0$  and  $a_1$  are two region-specific constants. Absorption coefficient for CDOM plus nonpigmented particulates  $a_{cdm}(\lambda)$  is expressed as:

$$a_{cdm}(\lambda) = a_{cdm}(440) \exp[-S(\lambda - 440)] \quad (18)$$

where  $S$  is the spectral slope. Particulate backscattering coefficient  $b_{bp}(\lambda)$  is formulated as:

$$b_{bp}(\lambda) = b_{bp}(555) \left(\frac{555}{\lambda}\right)^Y \quad (19)$$

where  $Y$  describes the spectral dependence of particulate backscattering.

Model computations were made in the Excel program with a function called “Solver”. Original parameters of Lee’s model were modified by fitting data from Arc00 to Eqs. (17) – (19) to tune the model for Beaufort and Chukchi Seas. The measured remote sensing reflectance spectrum was the model input, while outputs were absorption coefficient for phytoplankton at 440 nm, absorption coefficient for CDOM plus nonpigmented particulates at 440 nm, and the particulate backscattering coefficient at 555 nm. Chlorophyll concentration could then be calculated for a given chlorophyll-specific absorption based on field measurements [*Wang et al.*, 2004].

### **2.2.2 Model of *Maritorena et al.***

A detailed model description can be found in the original reference [*Maritorena et al.*, 2001]. This model uses formulations of  $a_{cdm}(\lambda)$  and  $b_{bp}(\lambda)$  similar to *Lee et al.*’s model, but phytoplankton absorption is expressed as the product of chlorophyll concentration and chlorophyll-specific phytoplankton absorption. An array of  $R_{rs}$  data for the six visible SeaWiFS wavelengths (412, 443, 490, 510, 555, and 670 nm) is required to run the model. The model yields the chlorophyll concentration, absorption by CDOM plus nonpigmented particulates  $a_{cdm}(443)$ , and particulate backscattering  $b_{bp}(443)$ . Parameters in the original model were optimized from a “global”, non-polar data set. Variables retrieved from the model were obtained by minimizing the mean square difference (MSD) between modeled and measured reflectance. The model was run for Arc00 without changing any original coefficients.

### 2.2.3 Model of Reynolds et al.

Reynolds et al.'s model is a chlorophyll-dependent semianalytical reflectance model, which uses region-specific relationships between inherent optical properties and chlorophyll concentration to predict the reflectance spectra.

Particulate absorption  $a_p(\lambda)$  is fitted to the power function:

$$a_p(\lambda) = A(\lambda) [\text{Chl}]^{B(\lambda)} \quad (20)$$

where  $A$  and  $B$  are two wavelength-dependent constants. Soluble absorption  $a_s$  at 400 nm is also fitted to Eq. (20) and soluble absorption spectrum is modeled as:

$$a_s(\lambda) = a_s(\lambda_0) \exp[-S(\lambda - \lambda_0)] \quad (21)$$

where  $S$  is the spectral decay constant with the value of  $0.018 \pm 0.004 \text{ nm}^{-1}$  for Arc00, and  $\lambda_0$  is the reference wavelength (i.e. 400 nm). The total absorption is computed as the sum of absorption by seawater, total particulates, and soluble materials.

The total backscattering coefficient  $b_b(\lambda)$  is partitioned into backscattering by water  $b_{bw}(\lambda)$  and backscattering by particles  $b_{bp}(\lambda)$ :

$$b_b(\lambda) = [b_{bw}(\lambda_0) + b_{bp}(\lambda_0)] \left(\frac{\lambda_0}{\lambda}\right)^\gamma \quad (22)$$

The reference wavelength  $\lambda_0$  is chosen to be 555 nm in this case. The backscattering coefficient for particulates  $b_{bp}(555)$  is fitted to the power function

$$b_{bp}(555) = A[\text{Chl}]^B \quad (23)$$

where  $A$  and  $B$  are two constants, with the values of 0.004 and 0.357, respectively. Superscript  $\gamma$  represents the spectral dependency of total backscattering relative to  $\lambda_0$ , and is strongly correlated with backscattering at 555 nm through the equation:

$$\gamma = -2.348 \log_{10}[b_b(555)] - 4.353 \quad (24)$$

The forward model of reflectance is formulated as:

$$R_{rs}(\lambda, 0^+, Chl) = 0.54 \left( \frac{f(\lambda)}{Q(\lambda)} \right) \left( \frac{b_b(\lambda, Chl)}{a(\lambda, Chl) + b_b(\lambda, Chl)} \right) \quad (25)$$

The ratio of  $f/Q$  was obtained by fitting measured  $R_{rs}$  versus  $b_b/(a+b_b)$  [Wang *et al.*, 2004].

With the above equations, reflectance spectrum can be generated for any given chlorophyll concentration. Parameters were specified to run the model for Arc00 as coefficients in Eqs. (20) – (25) were all empirically derived from field measurements [Wang *et al.*, 2004].

#### 2.2.4 HYDROLIGHT Simulation

Reflectance simulations of the Beaufort and Chukchi Seas were made with HYDROLIGHT 4.1 radiative transfer model [Mobley and Stramski, 1997]. A four-component (pure water, chlorophyll-bearing particles, CDOM, and nonpigmented particles) absorption and scattering routine was specified to run the model. Constant conditions in model runs included GMT20:00 on Julian day 229 (Aug. 16) at a position of 72.00°N, 156.50°W, no clouds, a wind speed of 5 m/s, no bioluminescence, inelastic scattering for chlorophyll, and the observed mean chlorophyll-specific absorption spectra for phytoplankton, nonpigmented particulates, and soluble materials. The water was taken to be homogeneous and infinitely deep for simplicity of analysis. A series of runs were conducted from 350 to 800 nm using average chlorophyll concentrations for bins: < 0.3, 0.3-1, 1-3, and > 3 mg chl m<sup>-3</sup>. The ratio of total particulate backscattering to scattering ( $b_{bp}/b_p$ ) was calculated according to the following:

$$b_{bp}/b_p (\%) = 1.57 - 0.49 \log_{10}[\text{chl}] \quad (26)$$

which was developed using our field-measured data [Wang *et al.*, 2004]. The backscattering ratio of phytoplankton  $b_{bc}/b_c$  is assumed to be constant and equal to 0.5% [Ulloa *et al.*, 1994]. The backscattering ratio of nonpigmented particulates  $b_{bn}/b_n$  was solved from the following equation:

$$b_{bp}/b_p = (b_{bc}/b_c) (b_c/b_p) + (b_{bn}/b_n) (1 - b_c/b_p) \quad (27)$$

with the assumption of a  $b_c/b_p$  ratio of 0.3 for the two low biomass bins and of 0.5 for the two high biomass bins. A Fournier-Forand phase function was chosen for phytoplankton and another for nonpigmented particulates, to correspond to their respective backscattering fractions.

### 3. Results and Discussion

#### 3.1 Remote Sensing Reflectance Spectra

The means for observed remote sensing reflectance spectra are illustrated in Figure 12A (standard deviations are shown in Figure 16 below) for the chlorophyll range of less than  $0.3 \text{ mg m}^{-3}$  to  $10 \text{ mg m}^{-3}$ . Combined effects of absorption and backscattering determine the spectral shape of reflectance. There is no clear pattern for reflectance, as chlorophyll concentration increases (Figure 12A), in this limited data set. If increases in absorption are greater than increases in backscattering, reflectance may decrease. This observation, however, is complicated by pigment packaging effects and the variability of nonpigmented materials. Pigment packaging is usually caused by changes in pigment composition that are due to photoacclimation or nutrient limitation, or by changes in cell size [Sathyendranath *et al.*, 1987; Bricaud *et al.*, 1988]. Absorption by chlorophyll within algal cells is not always linearly correlated to chlorophyll concentration because of the effects of pigment packaging. Nonpigmented particles, including nonliving detrital

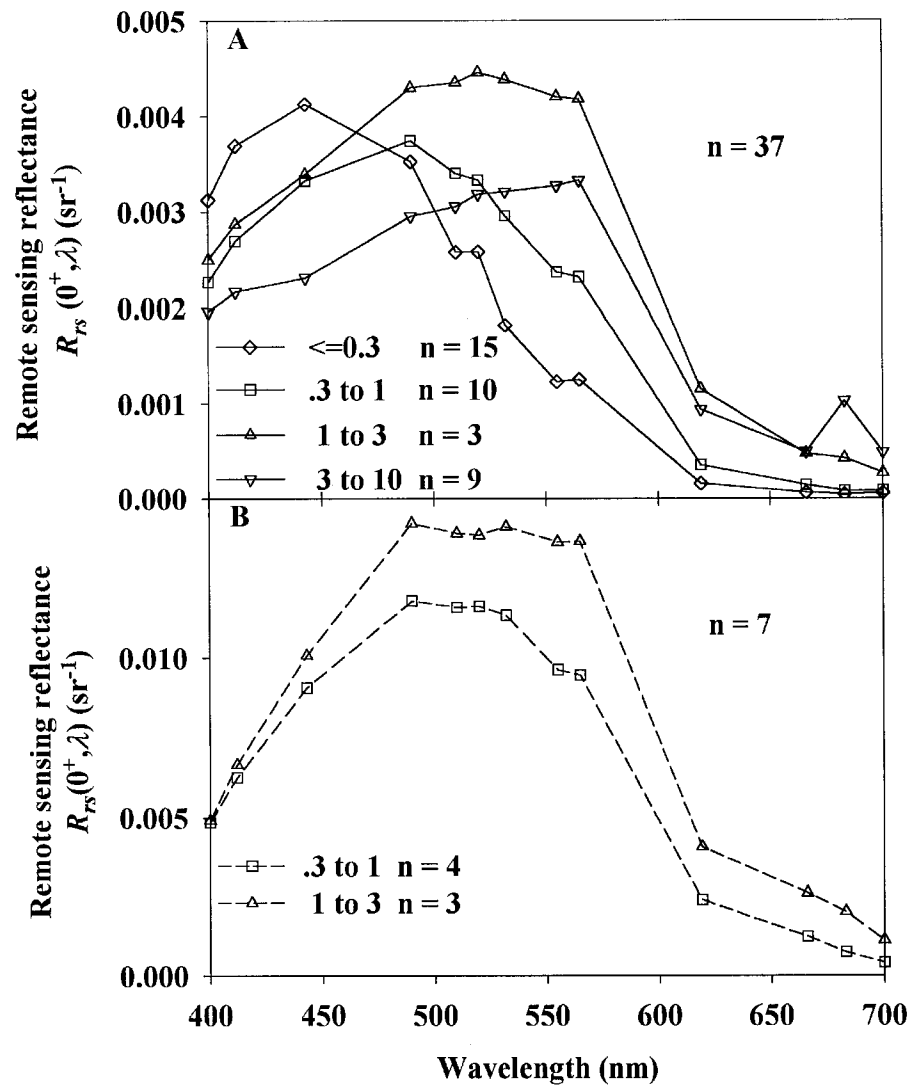


Figure 12. Remote sensing reflectance spectra (A, solid lines) for four biomass classes of Chl  $< 0.3$ ,  $0.3$ - $1$ ,  $1$ - $3$ , and  $> 3$   $\text{mg m}^{-3}$ , respectively. Reflectance spectra of stations rich in nonpigmented particulates are shown as dashed lines (B).

particles and bacteria, are smaller than most phytoplankton cells, and tend to be more effective at backscattering [Morel and Ahn, 1991; Stramski and Kiefer, 1991]. They did not covary with chlorophyll concentration, and were highly variable in concentration at lower biomass. Toole and Siegel [2001] found that in coastal regions affected by high river discharge the  $R_{rs}$  spectra were regulated almost entirely by backscattering under extreme conditions such as sediment plume. Higher backscattering by particles results in elevated remote sensing reflectance spectra (Figure 12B) observed at some stations rich in nonpigmented particulates.

### 3.2 Above-water and In-water Comparison

As illustrated in Figure 13, the maximum four-band-ratios of  $R_{rs}$  from above-water are highly correlated to in-water observations. Linear regression between these two ratios shows a slope of 0.87 and a determination coefficient of 0.95 ( $p < 0.0001$ ). Note that the remote sensing reflectance is not directly compared, and the comparison of reflectance ratios decrease the influence of systematic errors such as those caused by calibration uncertainties. Toole *et al.* [2000] compared the  $R_{rs}$  measurements by three optical instrumentations, namely an Analytical Spectral Devices (ASD) spectrometer, a Biospherical Instruments profiling reflectance radiometer (PRR), and a Satlantic Tethered Spectral Radiometer Buoy (TSRB). They reported an overall root-mean-square (rms) uncertainty in  $R_{rs}$  of 17-45% for above-water determinations and 12-24% for in-water determinations. Root-mean-square error for comparison between measurements by the SAS and the Satlantic profiler is 0.057, which suggests a rms uncertainty of 33%. The above-water measurements are sensitive to many environmental factors, including sky conditions (sun angle, cloud cover, etc.) and the sea state (wind speed) [Toole *et al.*,

2000]. The similarity between in-water and above-water results provides confidence in  $R_{rs}$  measurements by SAS III, which is easier to deploy in the field. Results from the SAS can augment or be merged with in-water measurements to reduce the errors in  $R_{rs}$  determinations.

### 3.3 Semianalytical Models of Remote Sensing Reflectance

The remote sensing reflectance  $R_{rs}$  is defined as the ratio of water-leaving radiance  $L_w$  to downwelling irradiance  $E_d$ . The relationship between  $R_{rs}$  and inherent optical properties can be expressed as:

$$R_{rs} \approx F \frac{b_b}{a} \quad (28)$$

where the constant  $F$  depends on the volume scattering function within water and on the geometric structure of the incident light field [Moblely and Stramski, 1997; Bricaud *et al.*, 1995]. The correlation between  $R_{rs}$  and  $b_b/a$  allows us to extract information about  $b_b/a$  from  $R_{rs}$  measurements. Furthermore, if assumptions about how  $b_b$  and  $a$  depend on individual bio-optical constituents in the water column are made, it may be possible to extract information about  $b_b$  and  $a$  individually. This inversion from  $R_{rs}$  to  $b_b$  and  $a$  relies on known or assumed relationships for inherent optical properties of various constituents. Conversely, if the constituent IOP models can be built by a simple parameterization, for example depending on one variable such as chlorophyll, forward predictions of remote sensing reflectance can be obtained from such parameters.

#### 3.3.1 Model of Lee *et al.*

Lee *et al.* [2001] developed an optimization technique to retrieve the optical properties of the water column. The model was originally built for shallow-water environments at temperate latitudes. After tuning model parameters with observed bio-

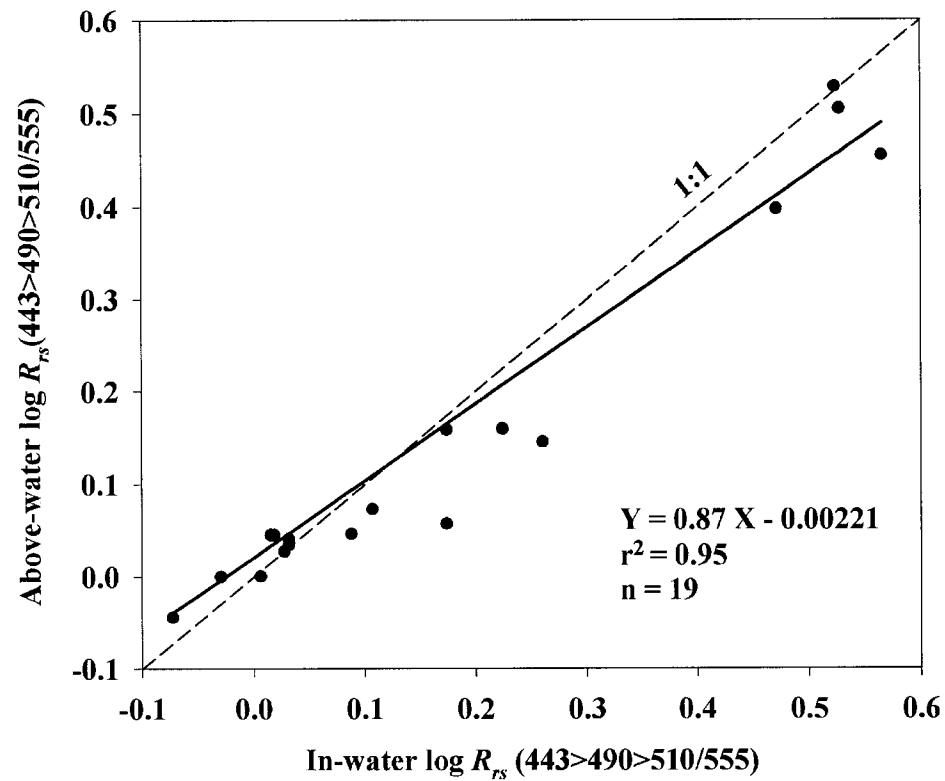


Figure 13. Comparison of above-water and in-water maximum reflectance ratios. Data from 19 stations are shown as filled circles. The solid line represents linear regression fit to the data points, and dashed line is the 1:1 relationship.

optical relationships from all 29 stations in the Beaufort and Chukchi Seas, the model was run for 13 cases with measured spectral remote sensing reflectance  $R_{rs}(\lambda)$  as input data. In this instance, the model was tested for each station using the tuned mean coefficient. Three IOPs, namely phytoplankton absorption at 440 nm  $a_a(440)$ , CDOM plus nonpigmented particulates absorption at 440 nm  $a_{cdm}(440)$ , and the particulate backscattering coefficient at 555 nm  $b_{bp}(555)$  were retrieved from the tuned model. These were compared to observed values.

The model variable of most interest is the absorption coefficient of phytoplankton at 440nm, from which chlorophyll concentration can be derived with measured chlorophyll-specific phytoplankton absorption coefficient. The modeled values of  $a_a(440)$  agree relatively well with our field measurements (Figure 14A), with the  $r^2$  of 0.71 ( $p < 0.0001$ ). There is one high value for both  $a_a(440)$  and  $a_{cdm}(440)$  predicted by the model (shown as triangle in Figure 14A and 14B). These two high values do not correspond to the same optical station. Because the model was run for each station, the variability of measured reflectance and the formulation of absorption using mean coefficients in the model both possibly contributed to generating the two high values. With the exclusion of these two points, the coefficient of determination for each linear regression increased significantly (Figure 14A and 14B). Without the outlier, the slope of linear regression between model predicted and measured  $a_a(440)$  is not significantly different from the value of 1 ( $p > 0.05$ ,  $t$ -test).

Excluding the outlier for  $a_{cdm}(440)$ , there is a strong correlation between modeled and observed absorption coefficient of CDOM plus nonpigmented particulates ( $r^2 = 0.86$ , Figure 14B), but the relationship between the modeled and measured values deviates

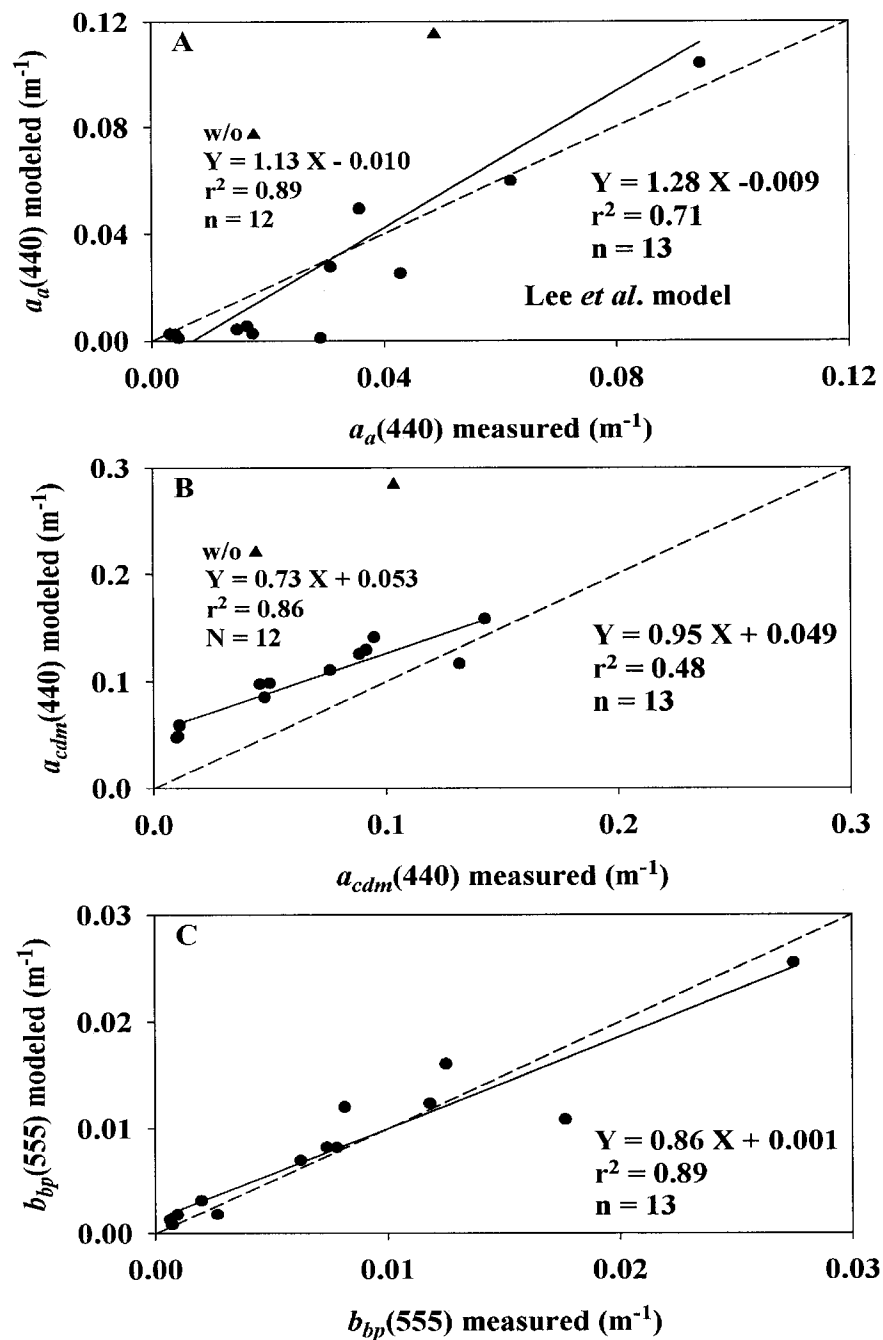


Figure 14. Comparisons of absorption coefficient of phytoplankton (A), absorption coefficient of colored dissolved organic matters plus nonpigmented particulates (B), and backscattering coefficient for total particulates (C) retrieved from tuned Lee *et al.* model and field measurements.

from the 1:1 relationship ( $p < 0.05$ ,  $t$ -test). Field data shown here were collected in different areas including offshore and near-shore waters off the coast of Alaska, covering a broad range of environmental conditions. *Wang et al.* [2004] showed that absorption coefficients of soluble materials and nonpigmented particulates do not vary closely with chlorophyll in the Beaufort and Chukchi Seas. Unless soluble and nonpigmented particulate materials vary coherently with other constituents, they will remain difficult to predict.

The model performed best in predicting the particulate backscattering coefficient. The linear regression of modeled versus measured  $b_{bp}(555)$  has a slope of 0.86 and  $r^2$  of 0.89. The slope is not significantly different from the 1:1 relationship ( $p > 0.05$ ,  $t$ -test), which represents the perfect match between the modeled and measured values. The results suggest that the formulation of backscattering in the model is accurate.

The small sample size limited our abilities to evaluate and tune the model for the Beaufort and Chukchi Seas. Whereas tuning and testing against the same small data set lack rigor, the tuned model will be tested with data from recent cruises. Currently there were only 13 stations with matching absorption, backscattering, and reflectance measurements. Model refinement will be better achieved with more bio-optical data from this region. Overall, the testing on limited data seems to indicate good agreements between measured and model predicted inherent optical properties.

### 3.3.2 Model of *Maritorena et al.*

*Maritorena et al.* [2001] improved the inverse model of *Garver and Siegel* [1997] by applying a global optimization scheme. The model returns chlorophyll concentration, absorption coefficient of CDOM plus nonpigmented particulates, and backscattering

coefficient of particulates. Our concurrent observations of the three variables in the Arctic Ocean allow for the comparison of model results and field measurements.

The predicted chlorophyll and measured chlorophyll deviate from a 1:1 relation ( $p < 0.05$ ,  $t$ -test), but show strong linearity ( $r^2 = 0.98$ , Figure 15A). The untuned model underestimates chlorophyll about 50% as shown by the linear regression slope of 0.49 ( $p < 0.0001$ ). One possible reason for the discrepancy is the pigment packaging effect observed in the Beaufort and Chukchi Seas relative to their “global” dataset dominated by low latitude observations. In the initial implementation of the model, a model [Morel, 1988] for chlorophyll-specific absorption coefficient for phytoplankton  $a_a^*(\lambda)$  was adopted. Specific absorption coefficients are not always constant due to the pigment packaging effects. The chlorophyll-specific phytoplankton absorption at the red peak  $a_a^*(676)$  for Arc00 averaged  $0.014 \pm 0.006 \text{ m}^2 (\text{mg chl})^{-1}$ . Compared with the commonly accepted values of  $a_a^*(676)$  for unpackaged pigments of 0.023 - 0.029  $\text{m}^2 (\text{mg chl})^{-1}$  [Johnsen *et al.*, 1994; Moisan and Mitchell, 1999], the value of  $a_a^*(676)$  for Arc00 suggests moderate pigment packaging effects of about 50% in the Beaufort and Chukchi Seas. This packaging effect for high northern latitude regions, if taken into account, would greatly improve the model performance for chlorophyll retrieval. Another possible reason for the offset between predicted and measured data is the variations of phytoplankton absorption associated with changes in the phytoplankton community structure. For example, Sathyendranath *et al.* [2001] found systematic differences between reflectance ratios modeled using low and mid latitude data and reflectance ratios observed in Labrador Sea. They further separated phytoplankton samples into two broad groups, namely diatoms and prymnesiophytes, and re-ran the model using absorption

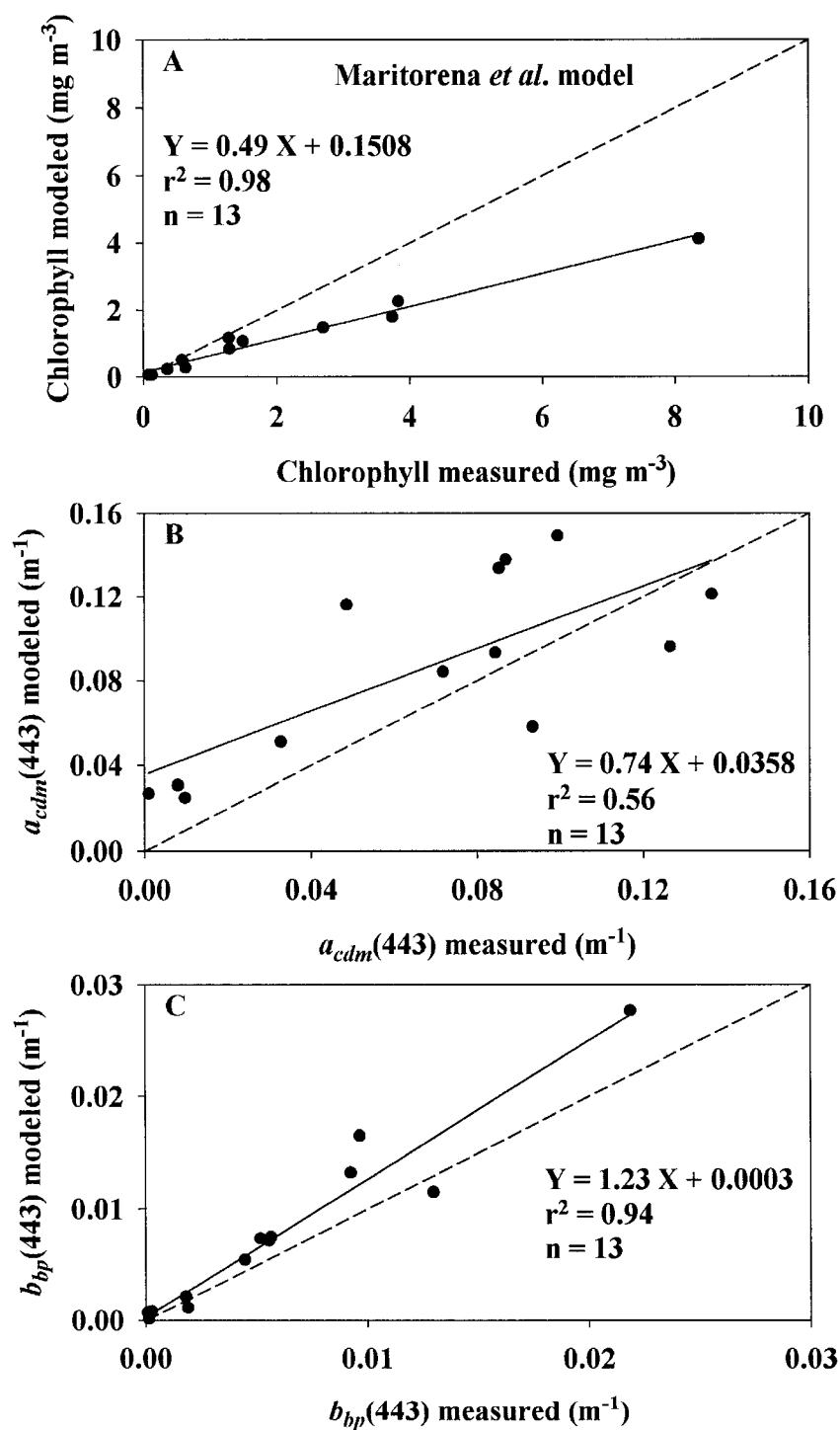


Figure 15. Comparisons of chlorophyll (A), absorption coefficient of colored dissolved organic matters plus nonpigmented particulates (B), and backscattering coefficient of total particulates (C) retrieved from Maritorena *et al.* model and field measurements.

parameters for diatoms and prymnesiophytes, respectively. The diatom model still showed larger differences, but the prymnesiophyte model behaved very much like the low-latitude model. Their empirical observations [Cota *et al.*, 2003] and model results [Sathyendranath *et al.*, 2001] imply that satellite retrievals and model performance may indeed be affected by species composition of the phytoplankton community.

Strong linearity is also discovered between modeled and measured particulate backscattering (Figure 15C), but the model slightly overestimates  $b_{bp}(443)$  with a slope of 1.23 deviating significantly from unity ( $p < 0.05$ ,  $t$ -test). In contrast to chlorophyll and  $b_{bp}(443)$ , the absorption coefficient by soluble and nonpigmented particulate materials is the worst predicted variable by the model (Figure 15B), as shown by the scatter around the 1:1 relationship.

The model of *Maritorena et al.* was developed and parameterized from a large non-polar data set. The results shown above for the polar waters were obtained without changing any coefficients in the original model. Despite that, the model performance is still encouraging. With the introduction of simulated annealing technique [Maritorena *et al.*, 2001], parameters could be optimized for the Beaufort and Chukchi Seas, and better performance of the model for high latitude regions is expected.

### 3.3.3 Model of *Reynolds et al.*

Our bio-optical data from Arc00 contains simultaneous observations of chlorophyll, inherent optical properties, and remote sensing reflectance. The relationships among various optical constituents were explored using this data set [Wang *et al.*, 2004]. Based on these relationships, the remote sensing reflectance can be

predicted by a single parameter such as chlorophyll concentration in a chlorophyll-dependent semianalytical model [Reynolds *et al.*, 2001].

In the model of Reynolds *et al.*, the absorption and scattering properties of each component were scaled to chlorophyll either directly or through time- and space-dependent regional relationships among inherent optical properties. The model was tuned with the IOP data from Arc00, and parameters were modified accordingly. Our measured remote sensing reflectance spectra for 13 wave bands were averaged into bins for chlorophyll concentration ranges of  $< 0.3$ ,  $0.3-1$ ,  $1-3$ , and  $> 3$  mg chl  $m^{-3}$ . The model predicted reflectance was computed using the average chlorophyll value of each bin.

Figure 16 shows the measured and model predicted reflectance spectra for Arc00. The model predicted reflectance spectra are generally in good agreement with the measured reflectance spectra. Criteria for fidelity of predictions were based on similar spectral shapes and predicted spectra lying within one standard deviation of observed values. A  $\chi^2$  test showed the model predicted and measured reflectance spectra were not significantly different ( $p > 0.05$ ). The largest discrepancy was found for the blue-green domain of the spectra of the lowest and highest biomass classes (Figure 16, panel A and D). High variability of nonpigmented particles at the lower chlorophyll concentrations probably is the main reason for the observed difference at low biomass. For the highest biomass bin, the discrepancy suggests that either backscattering is overestimated or absorption is underestimated. In general, the blue spectral region of  $R_{rs}$  is dominated by absorption properties and the green to red region by backscattering effects [Toole and Siegel, 2001]. The fraction of nonpigmented particles becomes smaller with increasing chlorophyll concentration [Mitchell and Holm-Hansen, 1991]. The diminishing

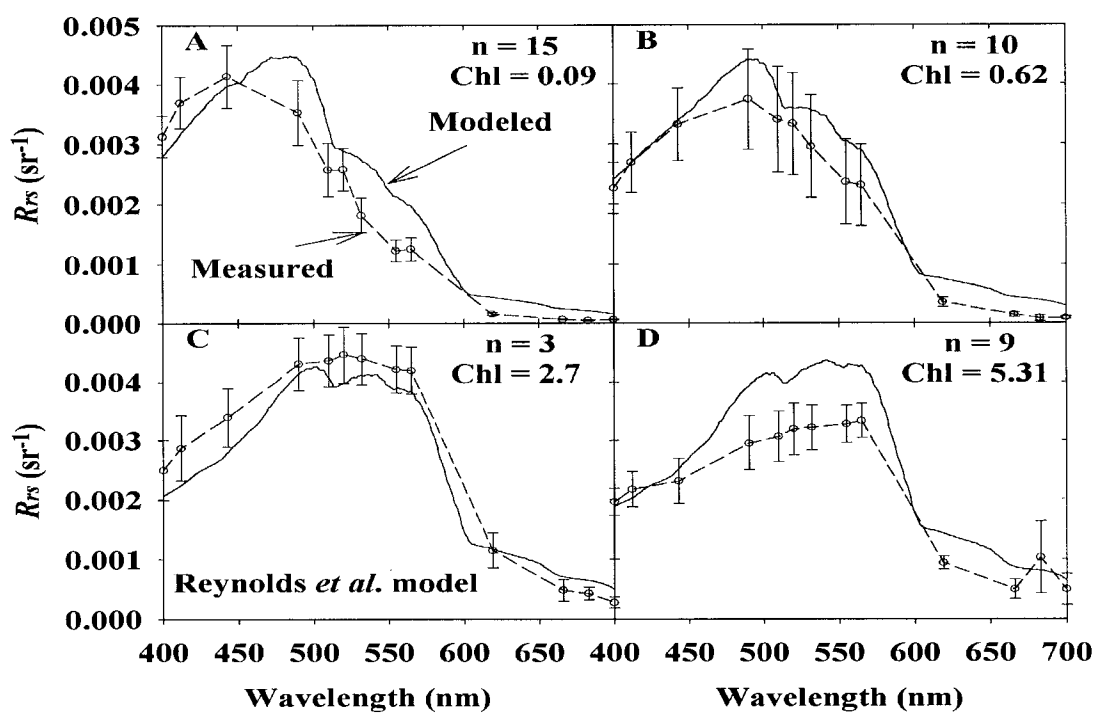


Figure 16. Comparison of remote sensing reflectance predicted by Reynolds *et al.* model (solid line) and measured reflectance (dashed line, with standard deviation shown) for four biomass classes of Chl  $< 0.3$ ,  $0.3-1$ ,  $1-3$ , and  $> 3 \text{ mg m}^{-3}$ , respectively.

contribution to backscattering from nonpigmented particles at higher biomass may not be adequately accounted for by the model since the chlorophyll dependent relationships of IOPs were developed over the entire biomass range. Therefore, the blue-green region of the modeled reflectance spectrum for the highest biomass bin is elevated.

The two inverse models [Maritorena *et al.*, 2001; Lee *et al.*, 2001] assessed above performed relatively well in predicting chlorophyll and backscattering coefficients, while both of them were less successful in predicting absorption by CDOM plus nonpigmented particulates. Natural variability of each model component is often not adequately reflected in semianalytical models. This is especially true for inverse models that try to predict independently varying IOPs from a dependent variable  $R_{rs}$ . In this case the high variability of concentrations of soluble and nonpigmented materials and their contribution to absorption make it a difficult task for inverse models to accurately predict them. The empirically derived relationships of IOPs from field measurements used in forward models already incorporate natural variability of each IOP. As a result, the forward model [Reynolds *et al.*, 2001] showed overall better performance than the two inverse models.

### **3.4 HYDROLIGHT Simulations of Remote Sensing Reflectance**

Constant environmental conditions were specified for a series of HYDROLIGHT runs. A four-component (pure water, chlorophyll-bearing particles, CDOM, and nonpigmented particles) Case 2 model was employed to simulate remote sensing reflectance in HYDROLIGHT 4.1. This approach was based on observed relationships of inherent optical properties in the Beaufort and Chukchi Seas [Wang *et al.*, 2004], and was chosen after sensitivity tests of model parameters. The measured mean chlorophyll-

specific absorption spectra for phytoplankton, nonpigmented particulates, and soluble materials were used as input to the HYDROLIGHT model.

The  $\chi^2$  goodness-of-fit tests indicated HYDROLIGHT provided accurate simulation of remote sensing reflectance ( $p > 0.05$ ). As illustrated in Figure 17, model predicted reflectance is very close to measured reflectance, except for the blue-green of the spectrum for the lowest biomass class (Figure 17, panel A). The concentrations of nonpigmented particles and their contribution to total particulate absorption showed highest variability in this low biomass range [Wang *et al.*, 2004]. For the 15 stations with chlorophyll concentration less than  $0.3 \text{ mg m}^{-3}$ , the contribution to total particulate absorption by nonpigmented particulates varied from 18% to 70%. The higher relative abundance of small particles presumably increases the backscattering throughout the blue and green regions of the spectrum. While the effects of all particles are already taken into account in measured reflectance, the discrepancy observed here suggest the high variability of nonpigmented particulates for the low chlorophyll concentration are not fully accounted for in our model reconstruction of reflectance in HYDROLIGHT.

If absorption, scattering, and the scattering phase function are known, the radiative transfer equation can be solved to obtain the radiance distribution within and leaving a water body [Mobley *et al.*, 2002]. While absorption and scattering can be obtained from field measurements, phase functions are rarely measured and often generated numerically. Mobley *et al.* [2002] considered the effects of phase function on oceanic light fields. Their results showed that the exact shape of the phase function in backscattering direction does not greatly affect the underwater light field, but the phase function must have the correct backscattering fraction. In our four-component model, the

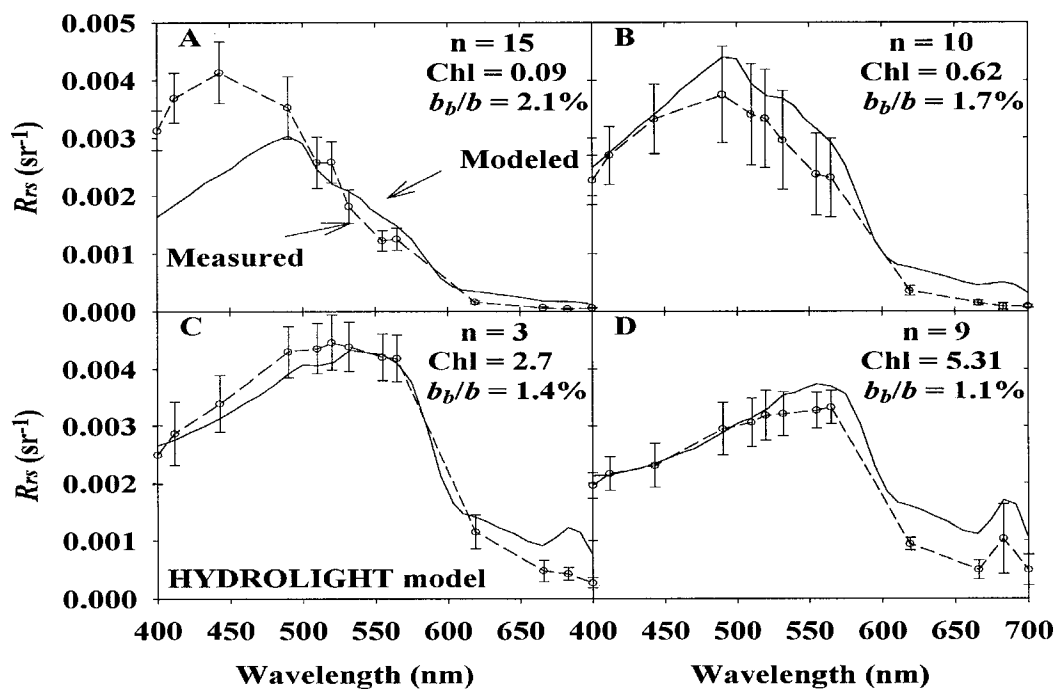


Figure 17. Comparison of remote sensing reflectance generated by HYDROLIGHT radiative transfer model (solid line) and measured reflectance (dashed line, with standard deviation shown) for four biomass classes of Chl  $< 0.3$ ,  $0.3-1$ ,  $1-3$ , and  $> 3 \text{ mg m}^{-3}$ , respectively.

backscattering fraction for nonpigmented particles was calculated based on two assumptions. Firstly, the backscattering fraction of phytoplankton is constant with the value of 0.5% [Ulloa *et al.*, 1994]. Secondly, the scattering portion due to phytoplankton is 30% for  $\text{Chl} < 1 \text{ mg m}^{-3}$  and 50% for  $\text{Chl} > 1 \text{ mg m}^{-3}$ . *Loisel and Morel* [1998] suggested the average contribution of phytoplankton to scattering is around 40%. The scattering portion due to phytoplankton would increase with increasing chlorophyll concentration. With the appropriate assumptions, the empirically developed relationship (e.g. Eq. (26)) from Arc00 provides a simplified way to obtain the correct phase function in numerical simulations.

The successful reproduction of reflectance spectra by HYDROLIGHT model suggests the input data are of high quality and the underlying relationships of IOPs are robust. The combination of HYDROLIGHT radiative transfer model with extensive and complete data sets containing inherent optical properties will be very useful for studying the variability of remote sensing reflectance in natural waters. The ability to produce precise reflectance spectrum makes HYDROLIGHT simulation a powerful tool for data validation, model development, and evaluation of accurate algorithms for remote sensing of ocean color.

### 3.5 Chlorophyll Algorithms Evaluations and Comparisons

Our tuned linear Arctic algorithm (Arc00 OC4L) can be expressed as:

$$\text{Chl (Arc)} = 10^{(a_1 + b_1 R)} \quad (29)$$

where  $\text{Chl (Arc)}$  is Arctic chlorophyll,  $R = \log (R_{rs443>490>510}/R_{rs555})$ , and  $a_1$  and  $b_1$  are tuned constants. Arc00 OC4P has the same formulation as SeaWiFS OC4V4

algorithm, which is a fourth order polynomial function with five coefficients. Coefficients for the three algorithms are listed in Table 8.

The OC2V2 algorithm [O'Reilly *et al.*, 1998] for SeaWiFS was developed with a data set ( $n = 1174$ ) including mostly oligotrophic data and some high latitude data from the Antarctic collected by Arrigo *et al.* [1998] and a few of our observations from the Arctic. The latest NASA's operational chlorophyll algorithm, OC4V4, as modified from O'Reilly *et al.* [2000], now includes more than 300 of our high latitude observations.

Operational chlorophyll algorithms for SeaWiFS are compared with our regional bio-optical algorithms tuned with limited data from the Beaufort and Chukchi Seas (Figure 18A). Tuned linear (Arc00 OC4L) and polynomial maximum band-ratio algorithms (Arc00 OC4P) explain >93% of the variance of surface chlorophyll concentrations. The linear model is preferred because of its simplicity and stable behavior near the range extremes. This algorithm data set from Arc00 has a limited biomass range ( $\sim 0.1$  to  $9 \text{ mg chl m}^{-3}$ ) and only fifty data points, but extends the minimum biomass values for existing polar algorithms.

Over most of the range of biomass, version 4 of ocean color 4 algorithm (OC4V4) overestimates chlorophyll concentrations almost by 1.5 fold at most stations (Figure 7B) in this region. As previously indicated by Cota *et al.* [2003], version 2 of the ocean color 2 algorithm (OC2V2) underestimated chlorophyll in the Labrador Sea by more than twofold over the range of biomass, and OC4V4 was still >1.5 fold low. The poor performance of "global" ocean color algorithm may be attributed to the distinctive bio-optical properties in the Arctic. The pigment package effects are relatively more important here than in low latitude regions, which often lead to low chlorophyll-specific

Table 8. Chlorophyll algorithm coefficients for SeaWiFS OC4V4, Arc00 OC4L, and Arc00 OC4P (n = 50). Arc00 OC4P has the same fourth order polynomial formulation as SeaWiFS OC4V4.

SeaWiFS OC4V4		Arc00 OC4L		Arc00 OC4P	
a	0.366	a <sub>1</sub>	-2.887	a <sub>2</sub>	0.271
b	-3.067	b <sub>1</sub>	0.298	b <sub>2</sub>	-6.278
c	1.93			c <sub>2</sub>	26.29
d	0.649			d <sub>2</sub>	-60.94
e	-1.532			e <sub>2</sub>	45.31

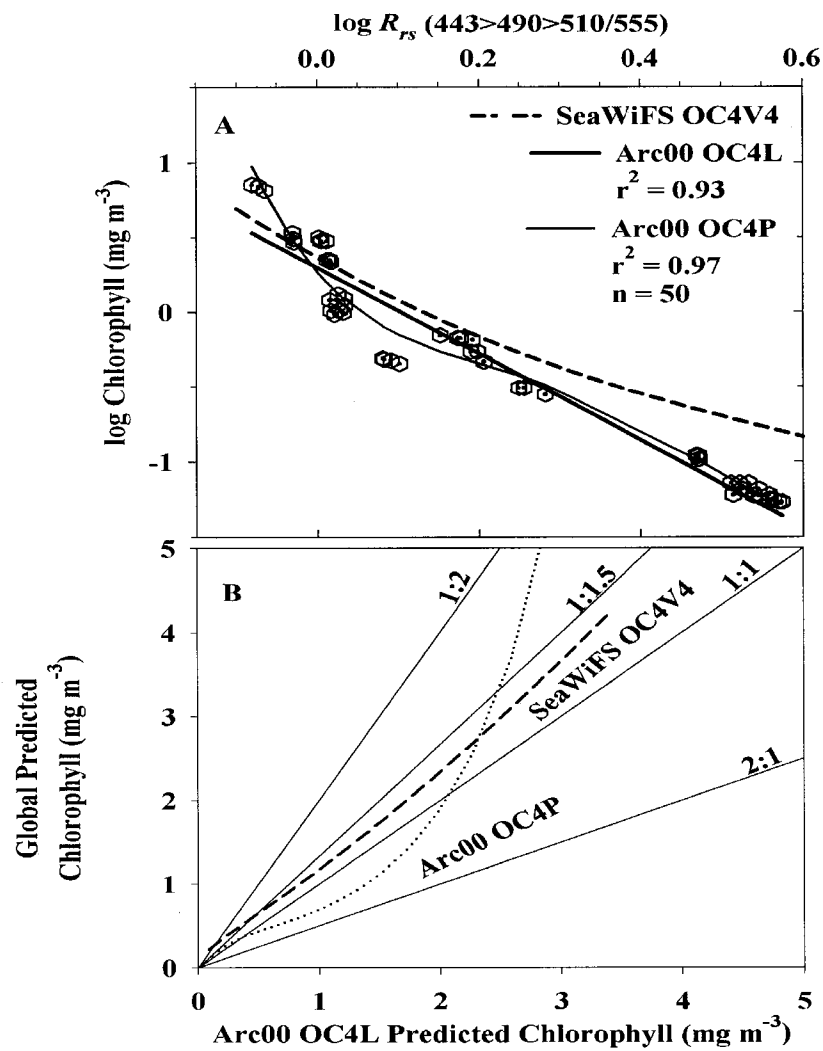


Figure 18. Regionally tuned linear (OC4L) and polynomial (OC4P) maximum band-ratio chlorophyll-retrieval algorithms for the Beaufort and Chukchi Seas and the OC4V4 SeaWiFS algorithms (A). Chlorophyll concentrations predicted by SeaWiFS OC4V4 and Arc00 OC4P are compared with Arc00 OC4L in panel B. SeaWiFS OC4V4 overestimates chlorophyll  $< 1.5 \times$  (B).

absorption and backscattering [Reynolds *et al.*, 2001; Mitchell and Holm-Hansen, 1991; Mitchell, 1992]. Chlorophyll retrievals from global algorithms can be misleading, and should be used with caution for high latitude regions. This problem can be solved by reprocessing with tuned regional algorithms or transformation of chlorophyll retrievals from “global” algorithms. Statistically an algorithm can be developed to bridge OC4V4 and our tuned linear algorithm. After this simple transformation, chlorophyll retrievals from OC4V4 for the Arctic will be more accurate.

#### **4. Conclusions**

Concurrent measurements of chlorophyll, absorption, backscattering, and remote sensing reflectance in the Beaufort and Chukchi Seas provide opportunities to investigate fundamental relationships among various optically important constituents in the environment. Two inversion models were assessed with these empirical relationships and compared. The model of *Lee et al.* [2001] was tuned with our data, and showed good overall behavior in predicting absorption coefficient for phytoplankton and backscattering coefficient of particulates. The chlorophyll concentration and particulate backscattering predicted by the original model of *Maritorena et al.* [2001] are highly correlated to measured values and relatively accurate. The model can be further tuned for regional applications with the eventual introduction of simulated annealing technique. Both models showed poor performance in providing the absorption coefficient for colored organic materials. Concentrations of soluble and nonpigmented materials and their contributions to total absorption are highly variable in our study region, which covered a broad range of environmental conditions [Wang *et al.*, 2004]. The dynamics of these constituents depend on heterotrophic and physical processes that are not necessarily

related closely with phytoplankton dynamics. A chlorophyll-dependent forward model [Reynolds *et al.*, 2001] produced reflectance spectra that are in very good agreement with measured reflectance spectra. These aforementioned models can be further refined with additional bio-optical data. They are of particular importance for interpreting the unique remote sensing signals for the Arctic.

Semianalytical models are capable of providing accurate retrievals of several parameters simultaneously, but some factors (e.g. fluorescence, Raman scattering, spectral dependency of scattering, etc.) contributing to ocean color are currently not incorporated in some models. The HYDROLIGHT radiative transfer model generated reflectance in close correspondence to the measured reflectance. The combination of HYDROLIGHT model and comprehensive bio-optical data sets is a very useful tool for understanding variability of ocean color.

The latest SeaWiFS algorithm (OC4V4) overestimates chlorophyll concentration by about 1.5-fold over most of the biomass range in this study, but generally underestimates chlorophyll in the Arctic [Cota *et al.*, 2003]. Our regionally developed algorithms improve the accuracy of chlorophyll retrievals significantly. Global algorithms should be used with caution for chlorophyll retrievals from the Arctic. Our future work will include algorithm transformation to improve the performance of global algorithms for the Arctic.

## CHAPTER IV

# PHYTOPLANKTON IN THE BEAUFORT AND CHUKCHI SEAS: DISTRIBUTIONS, DYNAMICS, AND ENVIRONMENT FORCING

### 1. Introduction

Studies of the spatial and temporal variability of phytoplankton in the ocean are important to evaluate the location and magnitude of marine primary productivity which is about half of that globally. Satellite remote sensing technology allows for accurate global retrievals of chlorophyll *a* concentration (Chl), a proxy for phytoplankton biomass, from space. Ocean color data from the Coastal Zone Color Scanner (CZCS) provided an unprecedented view of a large variety of biological processes in various regions of the world ocean [Gregg and Conkright, 2001; Yoder *et al.*, 1993]. However, data from the CZCS sensor are limited in spatial and temporal coverage. Since its launch in 1997, the Sea-viewing Wide Field-of-View Sensor (SeaWiFS) has provided synoptic and continuous ocean color observations, which allow studies of both seasonal and interannual variability of phytoplankton.

Large, shallow (< 100 m water depth) continental shelves occupy approximately 30% of total surface area of the Arctic Ocean. These shelf seas are seasonally ice free and are the most active parts of the Arctic in processes that control air-sea exchange, biological production, riverine discharges, and water mass transformation [Aagaard *et al.*, 1981, 1985; Jones and Anderson, 1986; Macdonald and Wong, 1987]. Among shelves, the Chukchi Sea is unique in that the northward transport of Pacific waters through Bering Strait profoundly influences the regional circulation, water mass properties, and nutrient distributions [Walsh *et al.*, 1989; Weingartner *et al.*, 1998]. The

Beaufort shelf is also important because it is relatively narrow and the most estuarine of the Arctic shelves, receiving a large influx of fresh water from the Mackenzie River. This discharge occurs mostly in spring with reduced flow during summer.

The impact of the Arctic and its peripheral seas on the world's oceans and climate is now widely recognized. Despite its importance, the Arctic is difficult to access and remains poorly known because of adverse weather conditions in the region. Recent studies [*Onstott and Shuchman*, 1990; *Comiso*, 1991) have shown that satellite remote sensing is the most effective way to investigate many physical and biological processes in the high latitude regions. *Comiso et al.* [1993] investigated spatial and seasonal variability of phytoplankton distributions in the Southern Ocean using the CZCS data versus a variety of environmental variables. A similar study in the Barents Sea by *Mitchell et al.* [1991] also used the CZCS data with more limited spatial and temporal coverage. Physical forcing of phytoplankton dynamics at large scale is best studied with satellite.

Seasonal changes in ice cover define many polar marine ecosystems. The breakup of sea ice in spring-summer is very important for phytoplankton in that it provides a stable surface layer and increased light becomes available for photosynthesis [*Sakshaug*, 1989]. The seasonal ice retreat can now be conveniently documented via remote sensing. In this paper, large scale spatial distributions of phytoplankton in the Beaufort and Chukchi Seas are studied with imagery from SeaWiFS and other satellites. Seasonal and interannual variability of phytoplankton are explored with five years of ocean color data from 1998 to 2002. In the ocean, biological activities are intimately linked to physical processes. Correlation results between chlorophyll concentration and

various geophysical parameters including ice concentration and surface temperature are presented to illustrate the impact of physical forcing on biological processes. The objective of this study is to improve our understanding of spatial and temporal variability of phytoplankton dynamics in this region.

## **2. Materials and Methods**

### **2.1 Study area**

Figure 19 shows the western Arctic including the Beaufort and Chukchi Seas. The study area is bordered by Wrangle Island (180°W) to the west, Banks Island (120°W) to the east, Bering Strait to the south (66°N), and 75°N latitude in the north to include all major areas of open water. In this study, the whole region was separated into the Beaufort Sea and the Chukchi Sea at Point Barrow using 156.5°W longitude. The wide shelf of the Chukchi Sea extends up to 300 km but is relatively shallow with depths of 30-50 m. Two bathymetric features, namely Herald Canyon and Barrow Canyon, are important for topographic steering of cross-shelf transport. The Beaufort Sea shelf is relatively narrow, extending only about 50-100 km off the coast and typically < 100 m deep.

### **2.2 Ocean color data**

Data delivered by SeaWiFS aboard SeaStar are the main source of remotely sensed chlorophyll concentration for the present work. SeaWiFS data provide good spatial and temporal coverage and have been widely used in ocean color studies. However, chlorophyll concentrations retrieved from the global SeaWiFS algorithm should be used with caution for regional analysis, especially for the high latitude regions where bio-optical properties are distinctively different [*Cota et al.*, 2003, 2004].

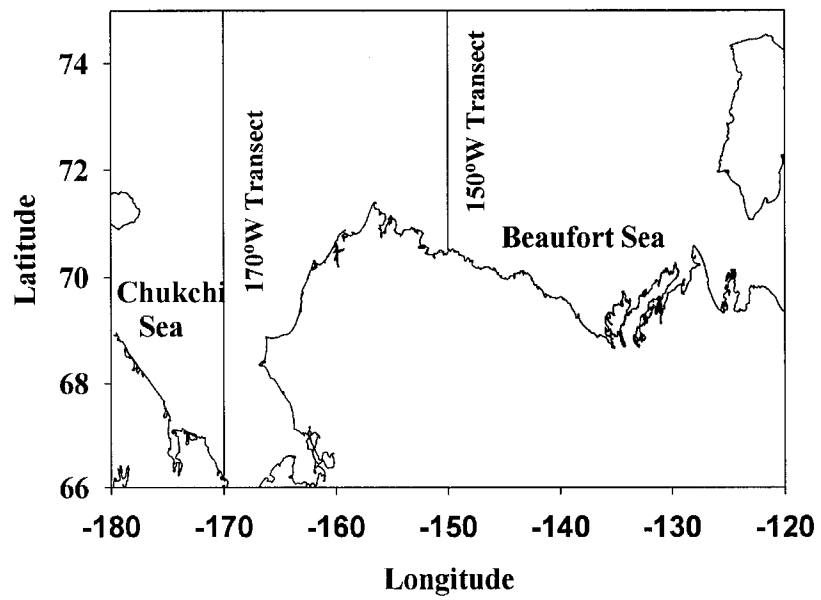


Figure 19. Geographic location of the Beaufort and Chukchi Seas. Two transects of 150°W and 170°W are shown as solid lines.

Weekly and monthly averages of SeaWiFS ocean color data (after the 4<sup>th</sup> reprocessing ) from April to September for five years (1998-2002) were transformed by linear interpolations to generate chlorophyll *a* concentrations for the Arctic. The linear interpolation scheme was developed by *Cota et al.* [2004]. The transformation produces more accurate chlorophyll values for the Beaufort and Chukchi Seas but preserves the spatial and temporal patterns in the original SeaWiFS images [*Comiso and Cota, 2004*].

### **2.3 Geophysical parameters**

Environmental factors regulate the spatial and temporal variability of phytoplankton distributions. Relationships between ocean color and key geophysical parameters were studied to better understand interactions between physical processes and biological activities. Among them, sea ice cover is of particular interest because the retreat of sea ice in spring promotes phytoplankton blooms [*Sakshaug, 1989*]. The passive microwave data from the Special Sensor Microwave Imager (SSM/I) provided the weekly mean sea ice concentrations [*Comiso et al., 1997*]. Surface temperature data were acquired from thermal infrared data from the Advanced Very High Resolution Radiometer (AVHRR). Clouds statistics and albedo were also derived from the AVHRR sensor [*Comiso, 2001*].

### **2.4 Data fusion**

Data from different sensors were processed and remapped onto the polar stereographic grid with a resolution of 12.5 by 12.5 km, which is sufficient for studies of regional variability. The uniform grid allows pixel-by-pixel comparisons for all parameters. There were frequently no data for ocean color observations because of ice and cloud cover. Time averaging was done using all data available within the week at

each pixel to produce weekly means. The spatially and temporally averaged data were used in correlation analyses for ocean color with various geophysical parameters.

### **3. Results and Discussion**

#### **3.1 Spatial variability**

During late summer, the extensive sea ice in the Arctic Ocean reaches its minimum. Phytoplankton in the Arctic can be observed by satellite ocean color in open water only after most sea ice melts. Figure 20 shows the monthly phytoplankton distributions derived from SeaWiFS for the Beaufort and Chukchi Seas for the growing season from April to September 1998.

As ice retreats in this region, the seasonal progression of phytoplankton biomass becomes evident. The spatial variability of phytoplankton over the growth season is apparent in Figure 20. High chlorophyll concentrations are observed in the southwestern Chukchi Sea and along the coast of the Beaufort Sea. It is well known that the Anadyr Current brings nutrient-rich water through the Bering Strait. The northward flow is sustained by the sea level difference between the Bering Sea and the Arctic Ocean. The flow field divides into at least two regimes north of Bering Strait. The low-salinity, nutrient-poor fraction on the east continues along the northeastern coast as the Alaska Coastal Current (ACC), and to the west the high-salinity, nutrient-rich portion flows to the north and through Hope Valley and Herald Canyon [Coachman *et al.*, 1975; Walsh *et al.*, 1989]. Primary production rates in the southwestern Chukchi Sea are among the highest ever recorded, but much lower values are found in the Alaskan coastal waters [Walsh *et al.*, 1989; Springer and McRoy, 1993]. On the outer Chukchi shelf, there is modest production decreasing into the basin [Cota *et al.*, 1996].

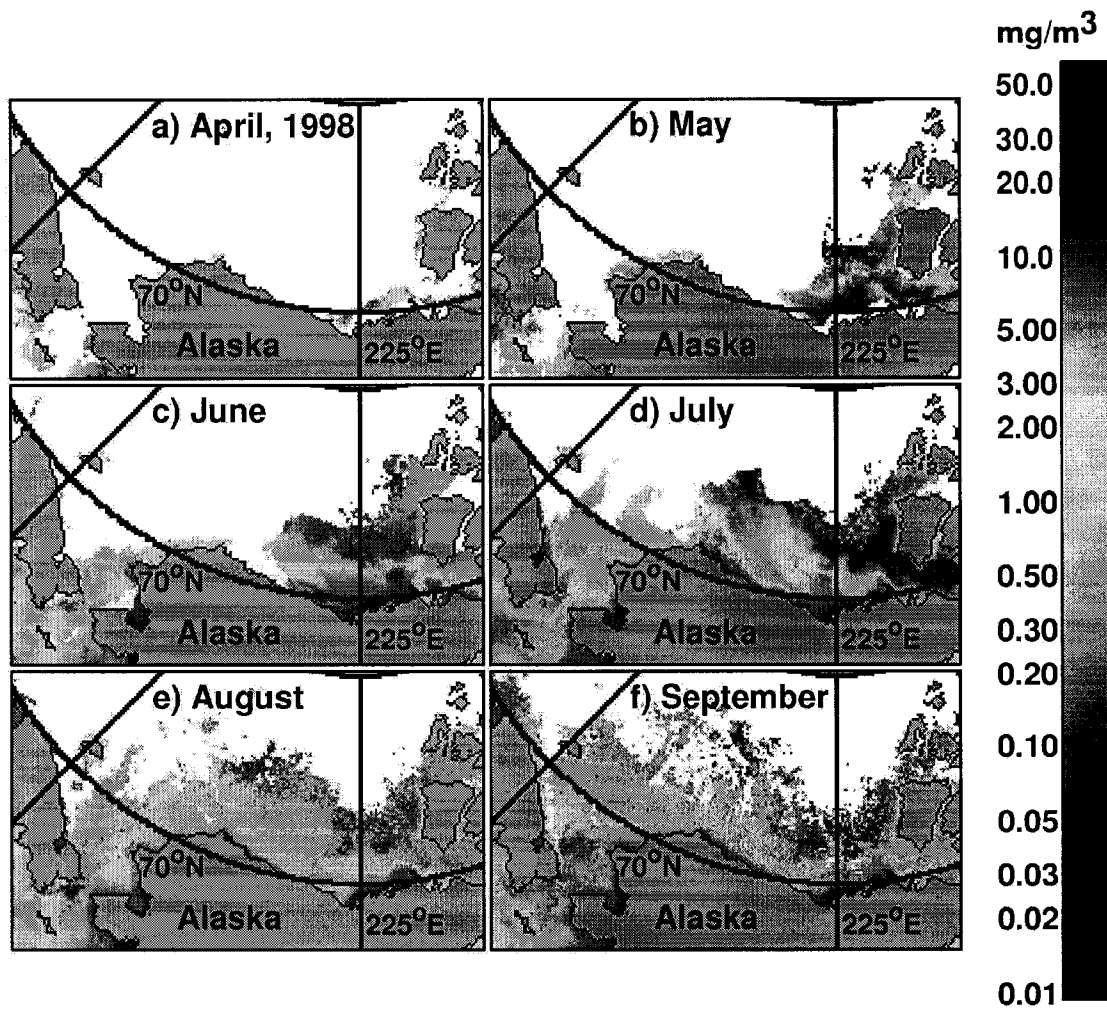


Figure 20. Monthly maps of chlorophyll concentration in April, May, June, July, August, and September 1998.

The Beaufort shelf is relatively narrow and ice covered most of the year, which results in relatively low production. However, new production based on nitrate drawdown has been estimated to  $20 \text{ g C m}^{-2} \text{ yr}^{-1}$  in the Mackenzie Shelf [Macdonald and Wong, 1987]. The interaction between river plume and seawater occurs on the open shelf due to the strong discharge of the Mackenzie River. Wind forcing and local circulation spread the river plume when little ice is present, as shown by high chlorophyll concentrations around the Mackenzie River mouth in Figure 20.

Two transects of longitude  $150^\circ\text{W}$  and  $170^\circ\text{W}$  (Figure 19) were chosen to illustrate the variations of phytoplankton biomass in the Beaufort and Chukchi Seas. The  $150^\circ\text{W}$  transect covers the shelf of Beaufort Sea but is removed from the mouth of Mackenzie river. The  $170^\circ\text{W}$  transect intersects the Bering Strait and widest part of the Chukchi shelf. Monthly mean chlorophyll concentrations along the two transects are plotted in Figure 21 and 22, respectively. For the  $150^\circ\text{W}$  transect, high chlorophyll values are observed in August and September close to the Beaufort Sea coast, which is indented with shallow bays and lagoons. The very shallow inner shelf is strongly wind-driven in summer, while the dominant feature of the outer shelf is the eastward Beaufort Undercurrent. Furthermore, there are frequent cross-shelf motions, which transport materials between the inner and outer shelf. Flows directed seaward are more common than landward ones [Aagaard, 1984]. The flow events serve as a dispersal mechanism and chlorophyll concentrations are lower northward of the coast (Figure 21). It should be noted that large amounts of colored dissolved organic matter (CDOM) are transported to the sea by river discharge. Ocean color observations are often complicated by high concentrations of CDOM and chlorophyll retrieval could be biased [Carder *et al.*, 1989].

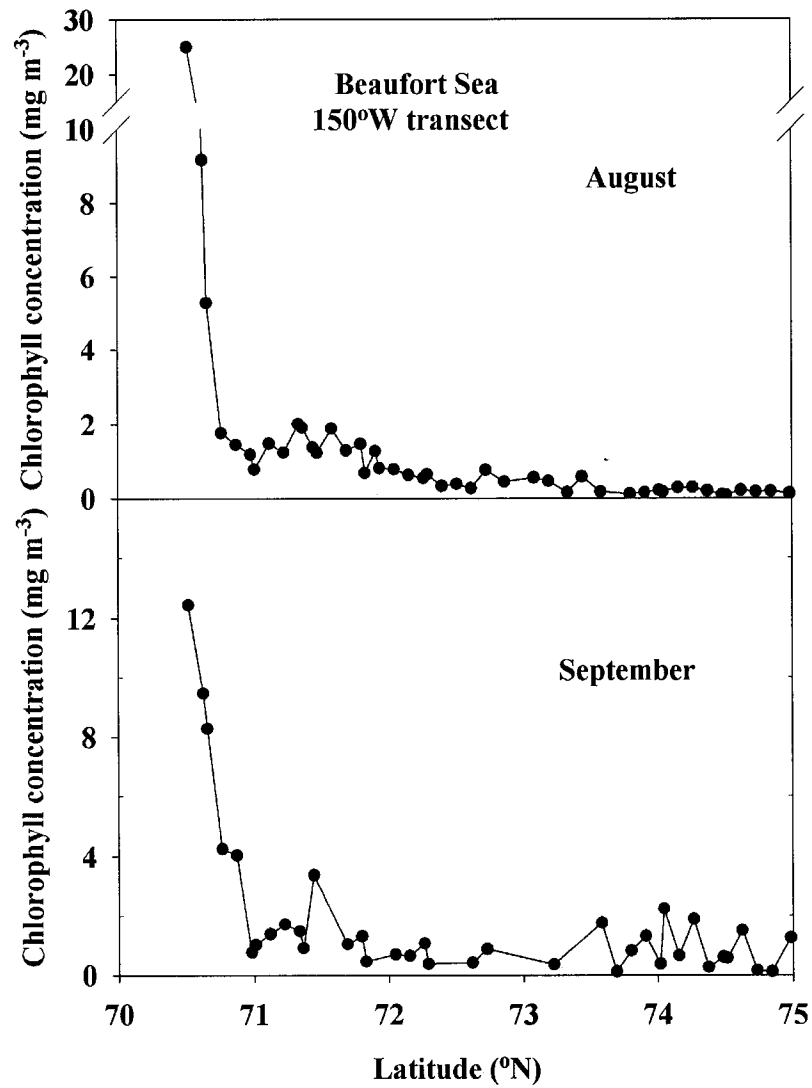


Figure 21. Chlorophyll concentration in August and September 1998 along the Beaufort Sea 150°W transect.

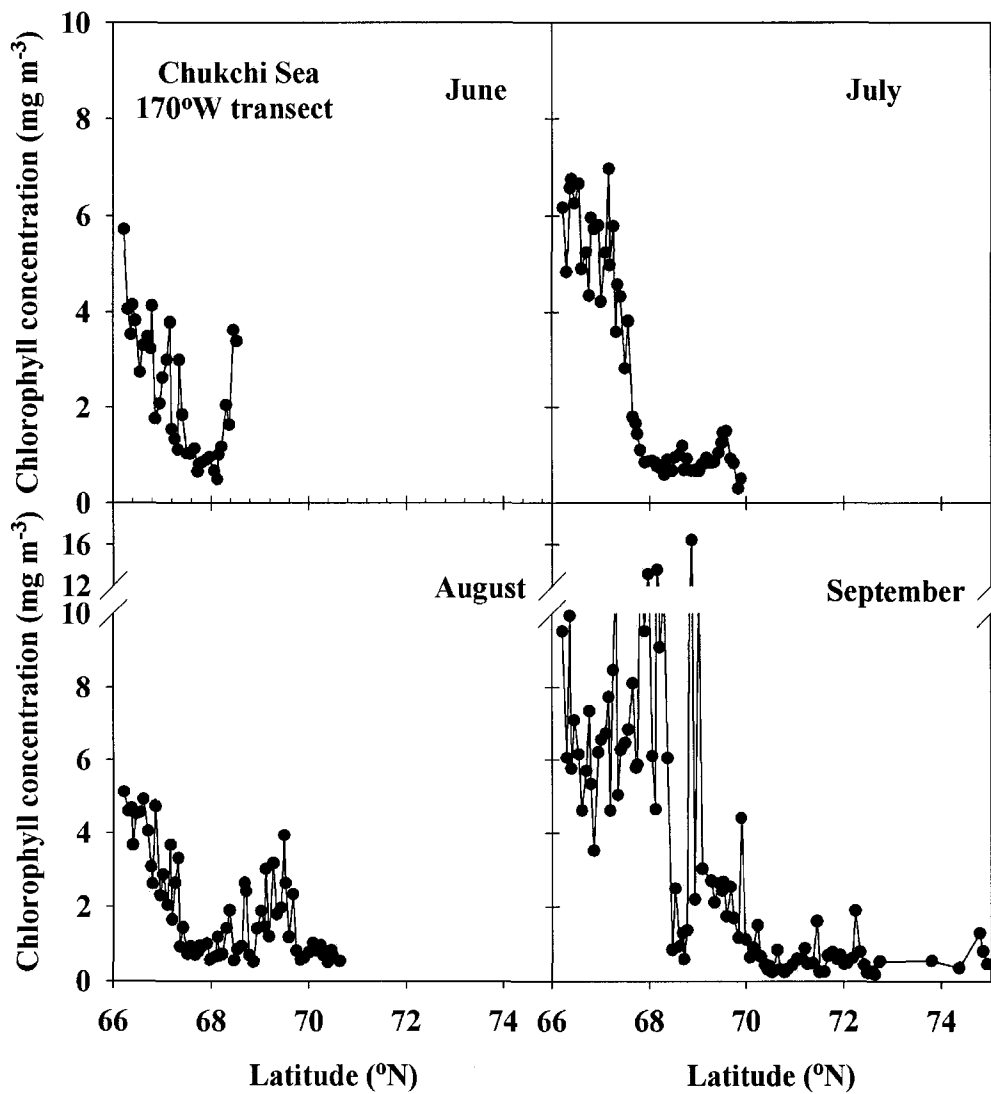


Figure 22. Chlorophyll concentration in June, July, August, and September 1998 along the Chukchi Sea 170°W transect.

*Horner* [1984] found that there was no real evidence for a major spring bloom in the Beaufort Sea. The satellite predicted high chlorophyll concentrations close to the coast (Figure 20 and 21) may be associated with riverine CDOM and resuspended sediments in shallower waters.

Blooms with chlorophyll concentration higher than  $1 \text{ mg m}^{-3}$  are found from June to September along the  $170^\circ\text{W}$  transect across the Chukchi Sea shelf (Figure 22). Compared to the western Beaufort Sea, ocean color data in the Chukchi Sea are available two months earlier when the edge ice starts to retreat. Chlorophyll biomass also shows a pattern of decreasing northward, which shows that blooms are generally restricted to retreating ice edges and the nutrient-rich open waters in the southwestern part of Chukchi Sea close to the Bering Strait. Some elevated chlorophyll values at the northern part of the transect (Figure 22) may be due to ice edge blooms.

The near-surface distributions of phytoplankton vary with surface forcing. The phytoplankton distributional patterns are controlled by competing biological and physical processes [*Steele*, 1978] such that phytoplankton growth enhances the existing patterns and turbulent diffusion breaks down the surface patchiness. Recent studies have shown that in dynamic areas such as coastal upwelling zones, the spatial patterns produced by growth, death, and sinking of phytoplankton cannot persist through the dispersion of mesoscale turbulent motion [*Denman and Abbott*, 1994]. The large-scale patterns of bloom evolution in the western Arctic are revealed by monthly climatologies, as in Figure 20. However, the mesoscale patterns are better resolved with weekly data [*Denman and Abbott*, 1988].

### 3.2 Seasonal variability

Monthly climatologies of ocean color (Figure 20) from SeaWiFS help resolve the seasonal evolution of phytoplankton distributions. The Beaufort and Chukchi Seas are strongly affected by pack ice seasonally. This region was largely ice-covered from April to May in 1998, with only small open water area in the eastern Beaufort shelf. In June, phytoplankton blooms tracked the reduction of ice cover with increased irradiance. Increases in phytoplankton biomass closely followed the onset of breakup. The dominant species are normally centric diatoms, which is characteristic of phytoplankton blooms in this region [Booth and Horner, 1997; Horner and Schrader, 1982]. As ice receded during spring and summer, phytoplankton blooms extended farther north in the Chukchi Sea. Biomass continues to increase until September (Figure 22).

The weekly mean of chlorophyll, ice concentration, and surface temperature for the Beaufort Sea and the Chukchi Sea are shown in Figure 23 and 24, respectively. Mean chlorophyll concentration for both regions displays high variability. Nevertheless, a seasonal trend shows that chlorophyll concentration reaches a maximum value between May and June, but the timing of the vernal bloom tracks the decrease in the ice cover (Figure 23A and 23B; Figure 24A and 24B). While the seasonal variations differ yearly, the single chlorophyll maximum in late spring or early summer is typical in the Arctic regions [Longhurst, 1995]. The seasonal cycles of chlorophyll are associated with environmental factors which influence phytoplankton growth. Among them, light and nutrients are the two main factors. *Sverdrup's* model [1953] links the stability of surface water layer to light to explain the variations of phytoplankton growth. The stable surface prevents phytoplankton being transported to deeper layers with insufficient light, but also

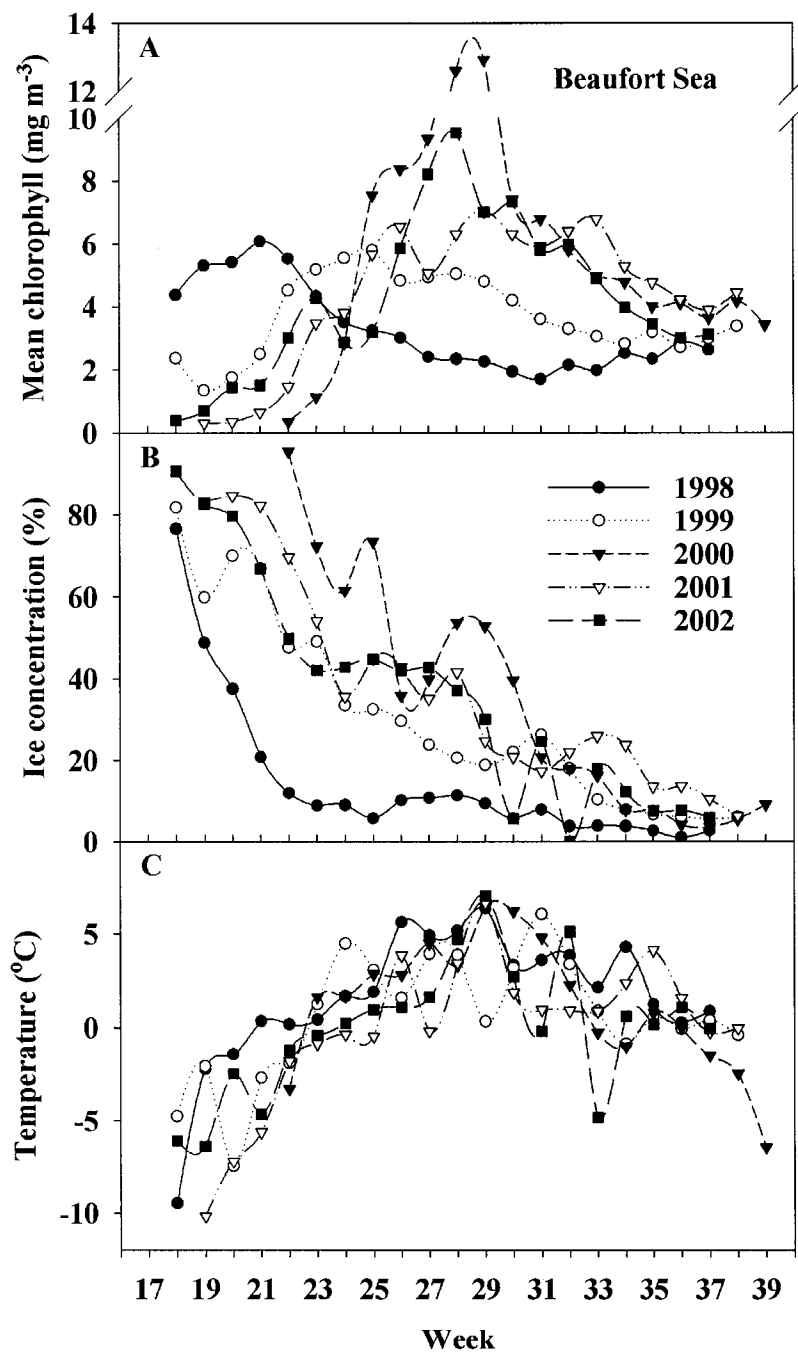


Figure 23. Weekly averages of chlorophyll concentration (A), ice concentration (B), and surface temperature (C) for 1998, 1999, 2000, 2001, and 2002 for the Beaufort Sea.

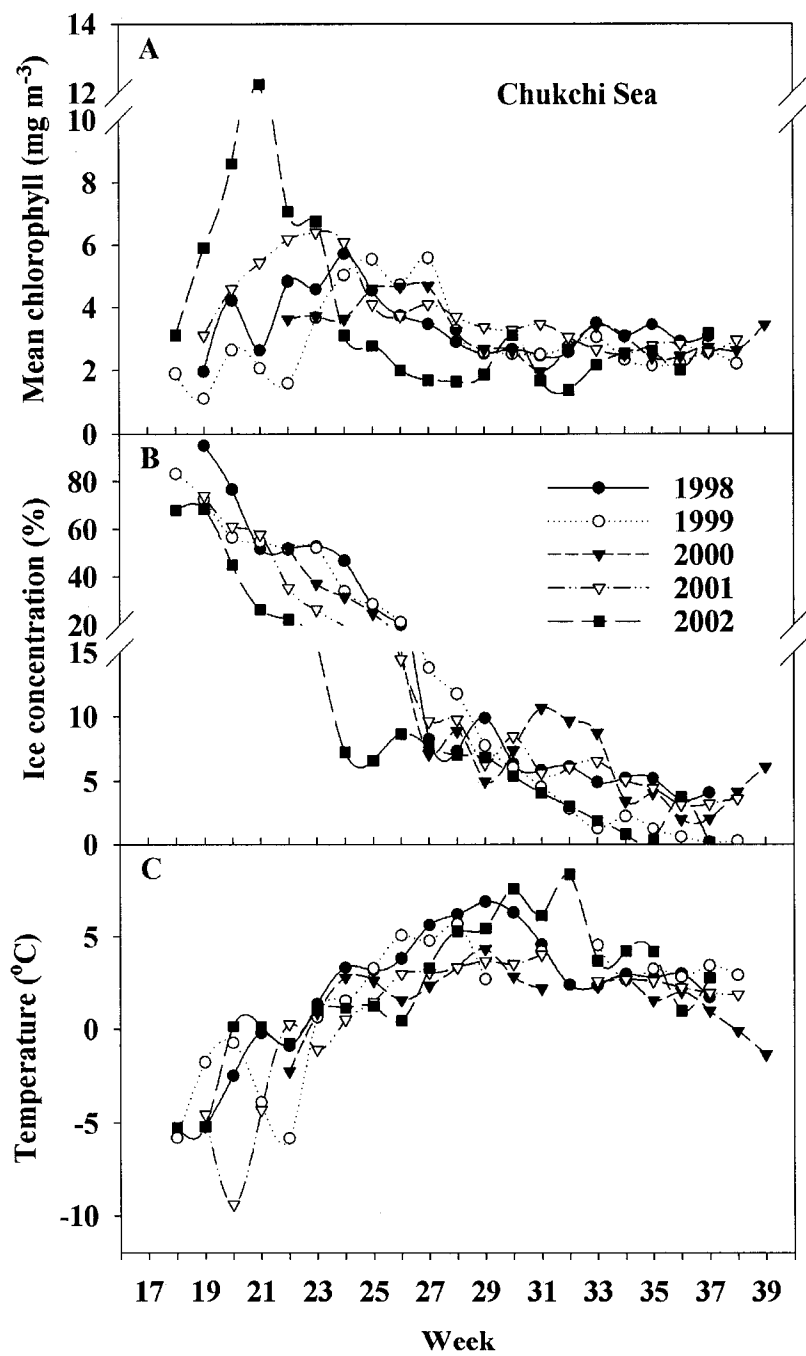


Figure 24. Weekly averages of chlorophyll concentration (A), ice concentration (B), and surface temperature (C) for 1998, 1999, 2000, 2001, and 2002 for the Chukchi Sea.

reduces vertical mixing of nutrients. In the Arctic, it is common that algal cells remain in this surface layer and grow until nutrients become limited.

The retreat of sea ice is a defining seasonal event for phytoplankton development. Seasonal changes in solar radiation and oceanic heat transport can cause major changes in the extent of ice cover. The average extent of sea ice in the Arctic varies from  $8 \times 10^6$  km<sup>2</sup> in late August or early September to  $15 \times 10^6$  km<sup>2</sup> in late February or March [*Walsh and Johnson, 1979*]. The perennial pack ice is mostly confined to the deep basins of the Arctic Ocean in summer. In the Beaufort and Chukchi Seas, mean ice concentration decreases from about 80% in April to less than 10% in September (Figure 23B and 24B) for all five years (1998-2002). The increase in irradiance and a stable surface layer caused by melting ice enhance phytoplankton growth behind the retreating ice edge [*Sakshaug, 1989*].

The weekly mean of surface temperature for the Beaufort and Chukchi Seas are plotted in Figure 23C and 24C, respectively. Surface temperature increases dramatically from ice cover in spring to open water in summer. Data from all five years consistently show July as the warmest month following the seasonal peak in solar radiation. There is about a two-month lag between maximal surface temperature and open water area, because ice continues to melt through September with surface temperature above the freezing point.

### **3.3 Interannual variability**

Interannual environmental variability in the Beaufort and Chukchi Seas can be marked, and phytoplankton respond to it. In 1998 phytoplankton biomass increased much earlier in the Beaufort Sea, when ice concentration declined early (Figure 23A and

23B). For the Chukchi Sea, phytoplankton blooms occurred earliest in 2002 (Figure 24A). The yearly fluctuations of chlorophyll concentration (Figure 23A) show that biomass can peak up to two months later in cold years with more extensive ice cover. Overall, surface temperature and ice cover indicate that 1998 was the warmest among the five years while 2001 was the coldest year.

The evolution of phytoplankton biomass from April to September 2001 in a cold year is illustrated in Figure 25. Compared to a warm year in 1998 (Figure 20), the seasonal differences are apparent. The Beaufort Sea remained largely ice-covered in 2001 until late July, while in 1998 large open water areas were observed in May. *Comiso et al.* [2003] found that the areal extent of open water region in the Beaufort Sea was unusually high in 1998. Their results showed that the retreat of sea ice during 1998 was coherent with warming in both atmosphere and the ocean in the region and with changing wind.

To illustrate the interannual variability more quantitatively, the chlorophyll concentration, open water area, surface temperature, cloud statistics, and albedo for 1998 and 2001 for the Beaufort Sea and the Chukchi Sea are compared in Figure 26 and 27, respectively. This summary provides a quick assessment of interannual variability of multiple parameters. For the Beaufort Sea, mean chlorophyll concentration reached a maximum value in May 1998, showing that phytoplankton peaked a month earlier in 1998 than in 2001 (Figure 26A & 26B). Most areas were ice covered until July in 2001. The open water area of the Beaufort Sea at the end of growth season was about  $1.7 \times 10^5$  km<sup>2</sup> in 2001 versus  $2.8 \times 10^5$  km<sup>2</sup> in 1998. The cumulative chlorophyll concentration in

open water area was twice the normal in 1998. For each of the six months from April to

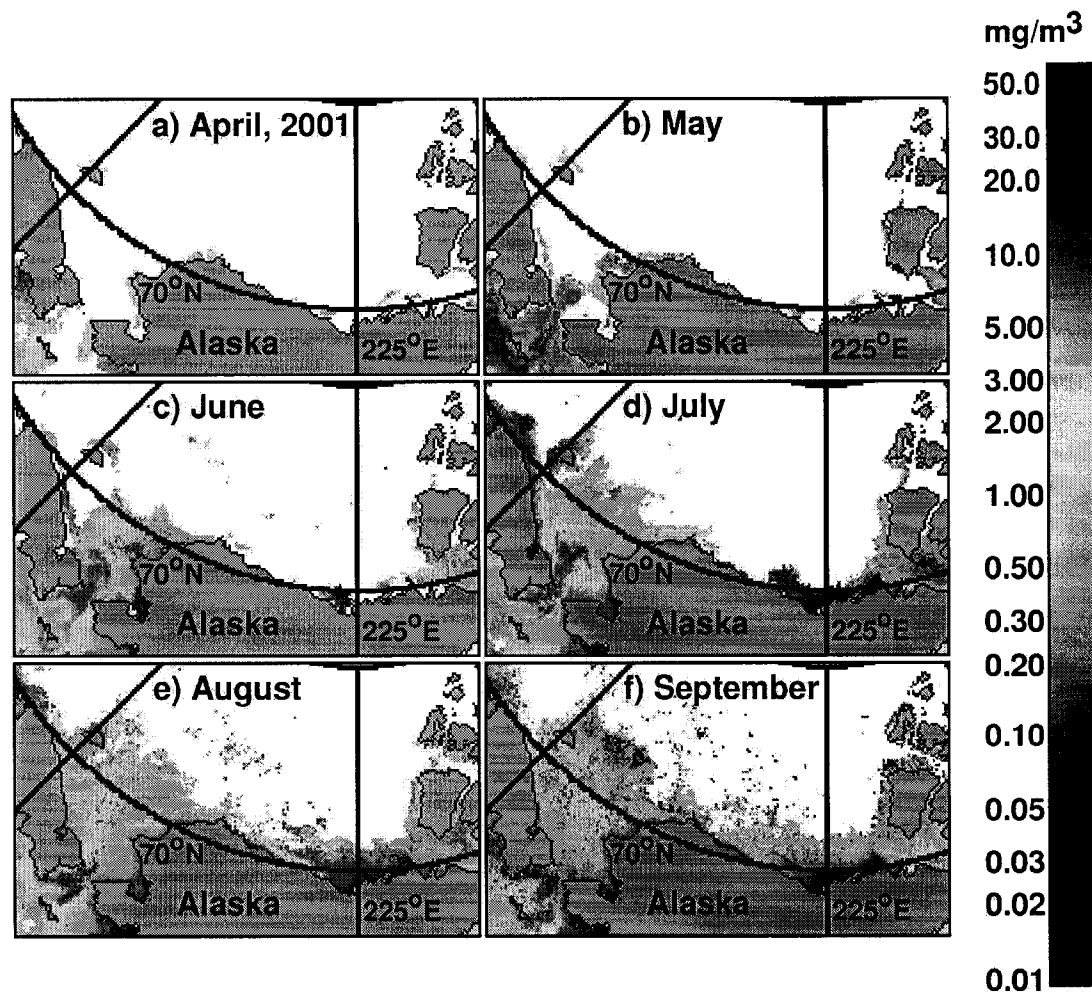


Figure 25. Monthly maps of chlorophyll concentration in April, May, June, July, August, and September 2001.

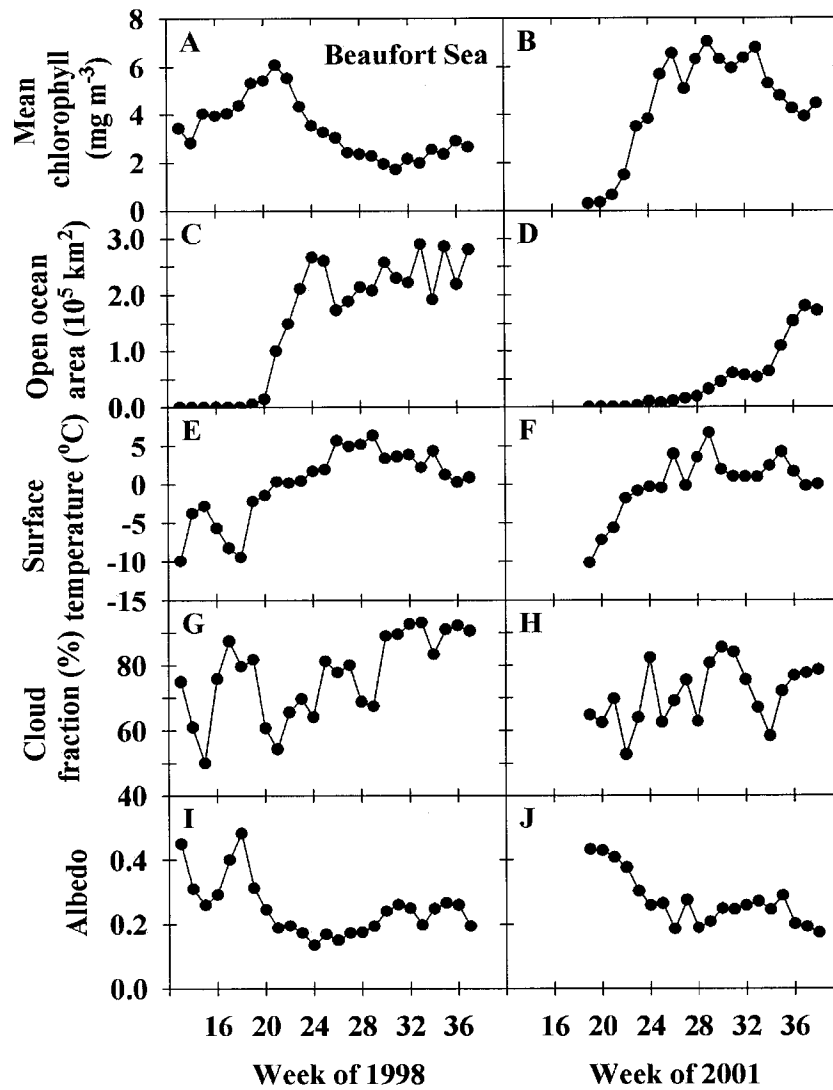


Figure 26. Comparison of weekly averages of chlorophyll concentration (A & B), open water area(C & D), surface temperature (E & F), cloud cover (G & H), and albedo (I & J) in 1998 and 2001 for the Beaufort Sea.

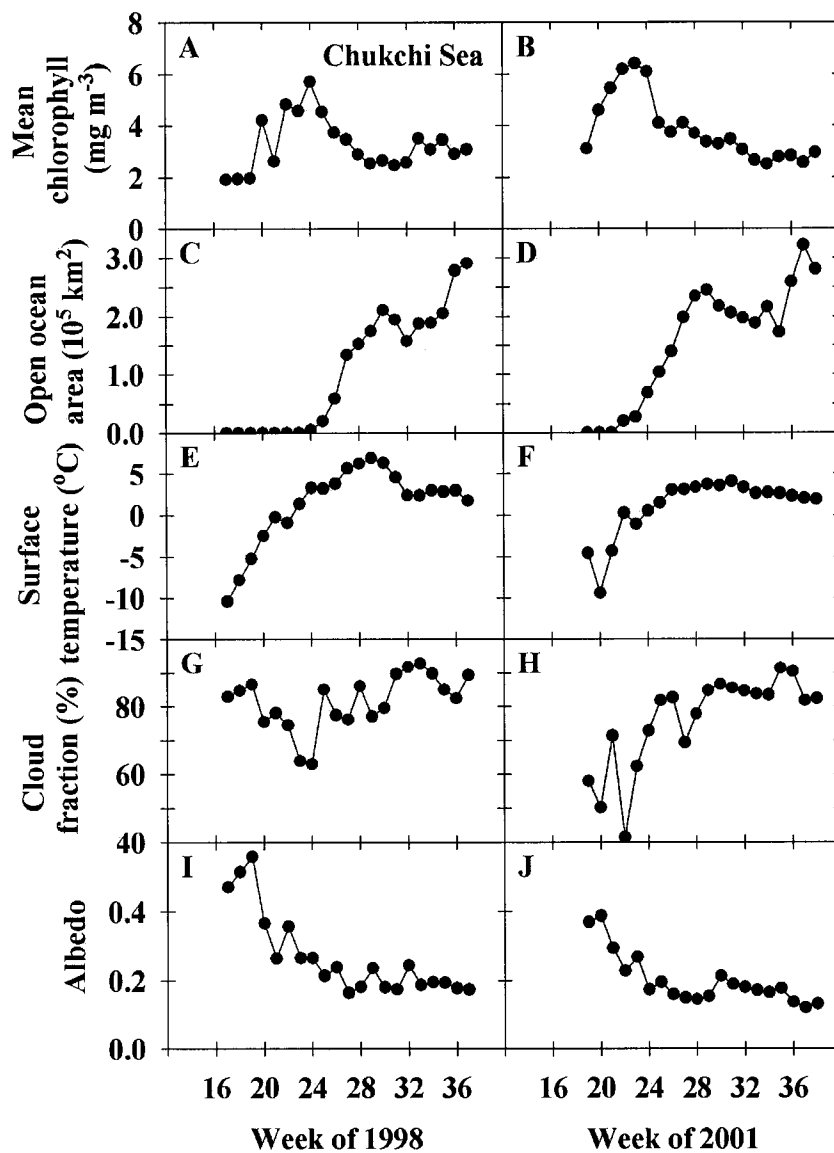


Figure 27. Comparison of weekly averages of chlorophyll concentration (A & B), open water area (C & D), surface temperature (E & F), cloud cover (G & H), and albedo (I & J) in 1998 and 2001 for the Chukchi Sea.

September, surface temperature in 1998 was higher than in 2001, as shown in Figure 26E and 26F. Note that surface temperature in April and May 2001 was well below the freezing point, consistent with more extensive ice cover during that period. In Figure 26G and 26H, the cloud fraction increases from spring to summer, which confirms that higher cloud fraction usually corresponds to increased open water area. Compared to 2001, the surface albedo in spring of 1998 was lower (Figure 26I and 26J). Reduction of ice cover decreases the surface reflectivity and albedo. That the surface albedo reached minimum after June or July is consistent with the minimal ice cover in summer. Similar trends were also observed for the Chukchi Sea. Phytoplankton biomass also increased earlier in 1998 than in 2001 (Figure 27A and 27B). The open water area was about  $3.0 \times 10^5 \text{ km}^2$  for both years (Figure 27C and 27D). Temperature was higher in 1998 than in 2001 for the same time period (Figure 27E and 27F). Clouds showed a general seasonal increase corresponding to more open water area (Figure 27G and 27H), while albedo decreased from April to September (Figure 27I and 27J).

The interannual variability of ice concentration is further demonstrated in Figure 28 and 29. In 1998, it was mostly ice free along the  $150^\circ\text{W}$  in the Beaufort Sea. By contrast, ice concentration was higher than 40% along this transect in August 2001. Only the southern part of the transect was ice free in September 2001 (Figure 28). However, similar observation along the  $170^\circ\text{W}$  transect was complicated by the cloud cover, as illustrated in Figure 29. In July 1998, the  $170^\circ\text{W}$  transect from  $66^\circ$  to  $69^\circ\text{N}$  was already ice free. Therefore, the clusters of ice cover data near Bering Strait in August and September appear suspicious (see Figure 29). The problem is presumably related to the cloud calibration of satellite sensors. It is often difficult for passive satellite sensors to

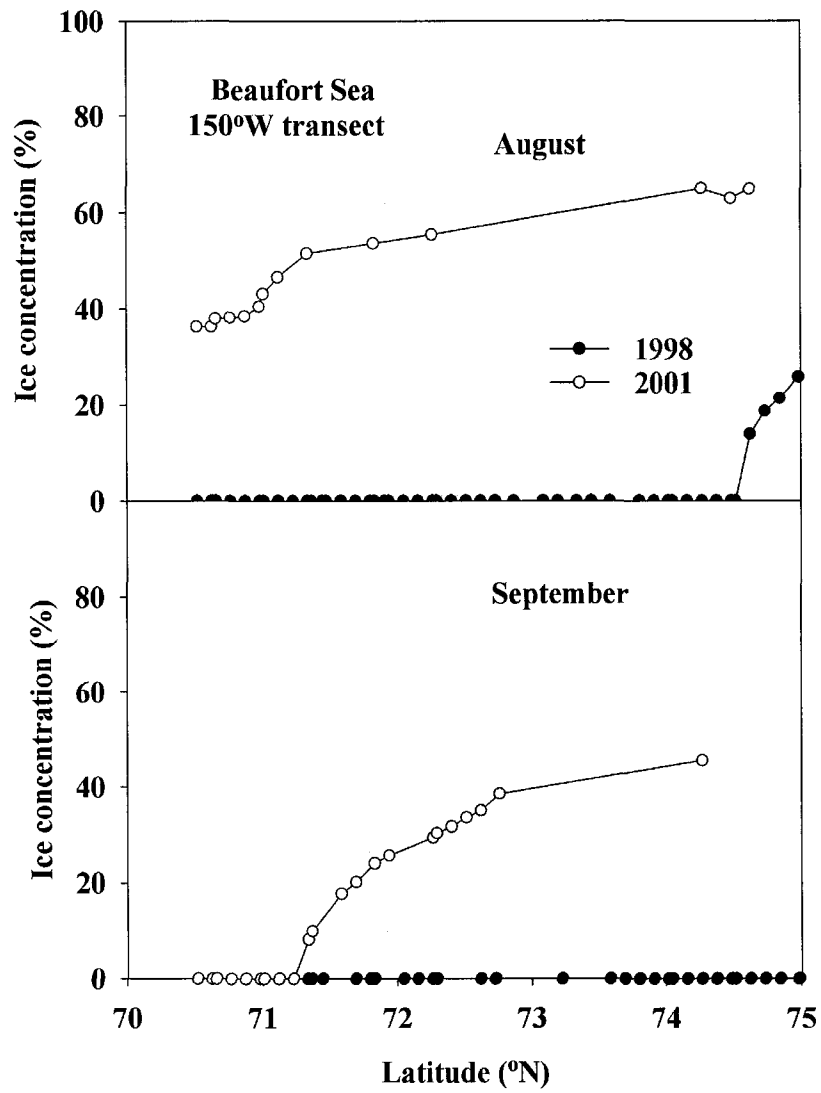


Figure 28. Ice concentration in August and September 1998 (filled circle) and 2001 (unfilled circle) along the Beaufort Sea 150°W transect.

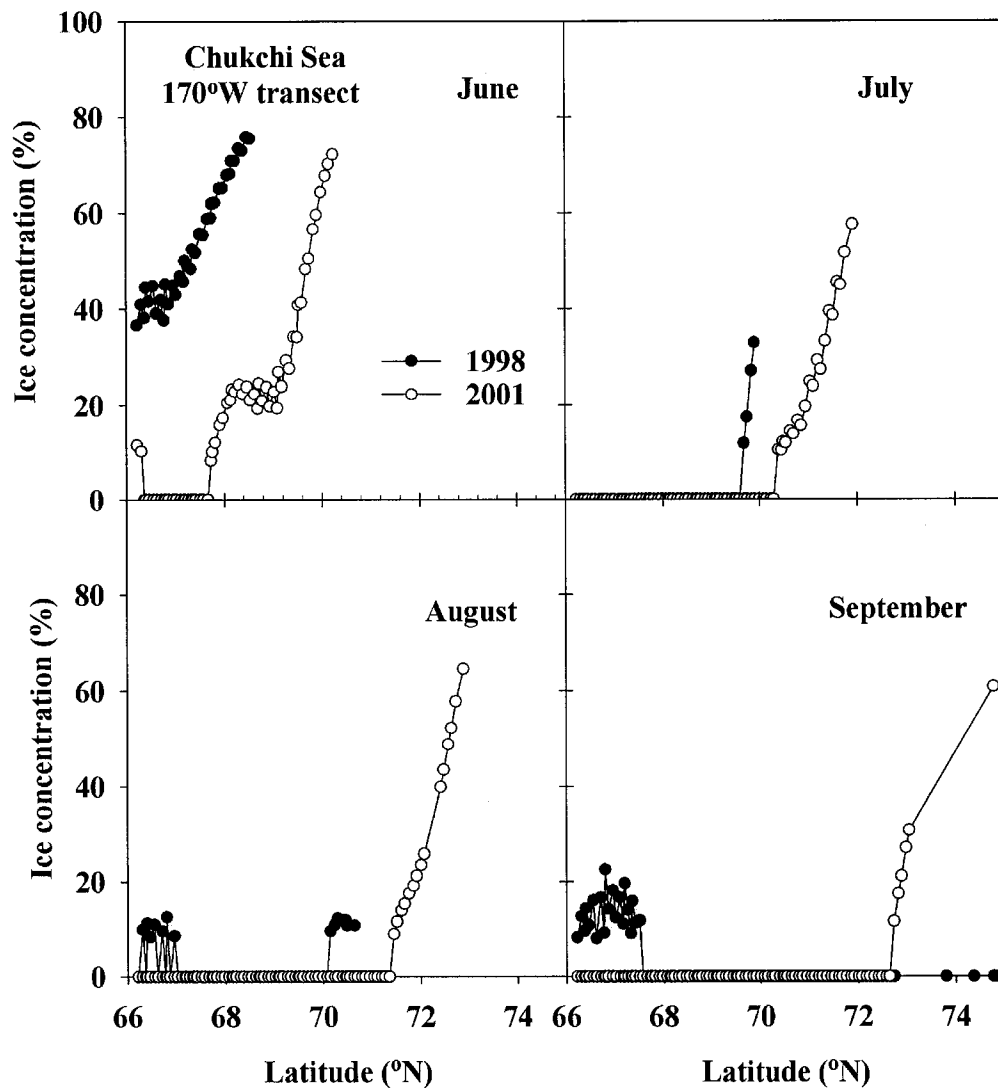


Figure 29. Ice concentration in June, July, August, and September 1998 (filled circle) and 2001 (unfilled circle) along the Chukchi Sea 170°W transect.

distinguish cloud from ice, and cloud cover can be very persistent in the Arctic region. Since the nearby area was ice free in July, the ice observed was not likely due to export of ice floe. The two clusters of data may be contaminated by clouds instead of ice concentration. Nevertheless, the pattern of northward propagation of open water area is clearly shown in Figure 29.

The climate in the Arctic is changing, and the Arctic Oscillation (AO) index has shown an upward trend in recent years [Thompson and Wallace, 1998]. The Arctic Oscillation describes the spatial pattern of sea-level pressure centered over the Arctic, and is highly correlated with the North Atlantic Oscillation (NAO). The AO index is closely related to the variations of mean annual temperature in the Arctic [Overpeck *et al.*, 1997]. Interannual variability of chlorophyll concentration, ice cover, and surface temperature in the Beaufort and Chukchi Seas can be at least partly explained by local responses to such climate oscillations.

### **3.4 Correlation analysis**

The correlation analyses between chlorophyll concentration and ice cover and surface temperature were performed to examine the spatial relationships of these geophysical parameters to the phytoplankton biomass. While the simple linear correlation involving two variables at a time does not provide a complete description of the variability, general trends can certainly be revealed. Since seasonal variations of chlorophyll are evident, the correlation analyses were performed for each month using data from all five years to study the seasonality and the correlation coefficients  $R$  are summarized in Table 9.

Table 9. Results of correlation analyses between two variables for each month from April to September (Chl is chlorophyll concentration and ST is surface temperature).

Correlation	April	May	June	July	August	September
R(Chl, Ice)	-0.180	-0.451	-0.039	0.130	-0.007	-0.097
R(Chl, ST)	0.290	0.211	0.383	0.245	0.186	0.281
R(Ice, Clouds)	0.314	-0.141	-0.589	-0.677	-0.786	-0.730
R(Ice, Albedo)	0.828	0.804	0.874	0.832	0.747	0.657
R(Ice, ST)	-0.788	-0.458	-0.140	-0.456	-0.557	-0.506

Correlations between chlorophyll and ice concentration are strongest in spring with R values of -0.18 and -0.451 in April and May, respectively (Table 9). The coherence of these two variables in spring is due to blooms tracking ice retreat in the Beaufort and Chukchi Seas. Breakup and ice melt trigger phytoplankton bloom as increasing light level, abundant nutrients, and low grazing pressure all favor phytoplankton growth. The retreating ice is the dominant factor in determining the spatial variability of phytoplankton distribution in spring. In later months, the correlation is relatively weak with R values approaching zero in August and September (Table 9) when the whole region is almost ice free. Such low correlations are not unexpected because ice concentration is no longer the dominant forcing. Later in the year other factors including limited nutrients, wind, currents, and mixed layer depth may all have important effects on phytoplankton.

The correlation between chlorophyll concentration and surface temperature is generally positive for all six months (Table 9). *Comiso et al.* [1993] found negative correlation between chlorophyll and surface temperature in the Southern Ocean. They suggested conditions in winter were more favorable to blooming than in summer because phytoplankton in that region were better adapted to low temperatures, but iron depletion may play a larger role. For the Arctic and subarctic regions, *Comiso et al.* [2004] described a maximum temperature about 3-4°C beyond which phytoplankton biomass declined. This was attributed to nutrient drawdown, not a direct temperature effect on phytoplankton growth. Our results imply that the surface temperature is within the normal range for phytoplankton growth in the Beaufort and Chukchi Seas, and phytoplankton are acclimated to ambient temperature.

Since ice concentration plays a very important role in determining the spatial and temporal variability of phytoplankton distribution, especially in spring, the correlation of ice concentration with surface temperature, cloud cover, and albedo were also analyzed to study the relationships between geophysical parameters. Correlation results are also summarized in Table 9. The correlation between ice cover and surface temperature is clearly negative because the surface temperature is lower in regions with higher ice concentration. Negative correlation also exists between ice concentration and cloud cover, with the only exception in April probably because the region is almost all ice covered at that time. Strong positive correlations are present between ice concentration and albedo because higher ice cover markedly increases the surface reflectivity. This represents an important feedback mechanism for regulating the climate in the Arctic. The robust correlation between ice concentration and the three geophysical parameters corroborates the observations, and helps explain spatial and temporal variability of phytoplankton distributions.

#### **4. Conclusions**

Five years of ocean color data from SeaWiFS in conjunction with ancillary data including ice concentration, surface temperature, cloud statistics, and albedo were analyzed to study and quantify the large scale spatial and temporal variability of phytoplankton distributions in the Beaufort and Chukchi Seas. Much of the northern part of this region is largely ice covered the year around. Only data in spring and summer growth season from April to September were used. Strong seasonality in this region was observed. Blooms were more pronounced in the southwestern part of the Chukchi Sea where Pacific waters continually import nutrients through the Bering Strait. There is a

progression of ice edge blooms following seasonal ice retreat. There is large interannual variability, which is at least partly driven by atmospheric forcing such as the Arctic Oscillation and the North Atlantic Oscillation [*Thompson and Wallace, 1998; Moritz et al., 2002*]. The warmest year was 1998, while 2001 was the coldest with more extensive and persist ice cover.

In the ocean, phytoplankton dynamics are forced by physical processes. Simple linear correlation analyses were performed to investigate the effects of the physical forcing. There was strong inverse correlation between phytoplankton biomass and ice concentration in spring. Significant correlation between ice concentration and surface temperature, cloud cover, and albedo were also noted. The relationships between chlorophyll and some environmental factors are far from linear. While the simple correlation does not offer complete information of the relationships between variables, it provides some insight and sensitivity of these relationships. There are other physical factors impacting the phytoplankton distribution including currents and bathymetry. Their effects are beyond the scope of this paper.

This study is the first to investigate the large-scale spatial and temporal variability of phytoplankton distributions in the Beaufort and Chukchi Seas. However, using monthly climatologies is difficult to resolve mesoscale patterns [*Denman and Abbott, 1988*]. Future work will involve in depth analysis of weekly data to study finer spatial and temporal patterns.

## References

- Aagaard, K., L. K. Coachman, and E. C. Carmack, On the halocline of the Arctic Ocean, *Deep-Sea Res.*, 28, 529-545, 1981.
- Aagaard, K., The Beaufort undercurrent, in *The Alaskan Beaufort Sea: Ecosystem and Environments*, edited by P. W. Barnes, D. M. Shell, and E. Reimnitz, pp.47-71, Academic, San Diego, Calif., 1984.
- Aagaard, K., J. H. Swift, and E. C. Carmack, Thermohaline circulation in the Arctic Mediterranean seas, *J. Geophys. Res.*, 90, 4833-4846, 1985.
- Arrigo, K. R., D. H. Robinson, D. L. Worthen, B. Schieber, and M. P. Lizotte, Bio-optical properties of the southwestern Ross Sea, *J. Geophys. Res.*, 103, 21,683-21,695, 1998.
- Austin, R. W., Inherent spectral radiance signatures of the ocean surface, in *Ocean Color Analysis*, pp.2.1-2.20, Scripps Institute of Oceanography, San Diego, CA, 1974.
- Barnard, A. H., W. S. Pegau, and J. R. Zaneveld, Global relationships of the inherent optical properties of the oceans, *J. Geophys. Res.*, 103, 24,955-24,968, 1998.
- Booth, B. C., and R. A. Horner, Microalgae on the Arctic Ocean Section, 1994: species abundance and biomass, *Deep-Sea Res. (Part II, Topical Studies in Oceanography)*, 44, 1607-1622, 1997.
- Bricaud, A., A. Morel, and L. Prieur, Absorption by dissolved organic matter of the sea (yellow substance) in the UV and visible domains, *Limnol. Oceanogr.*, 26, 43-53, 1981.

- Bricaud, A., A. L. Bedhomme, and A. Morel, Optical properties of diverse phytoplankton species: Experimental results and theoretical interpretation, *J. Plankton Res.*, *10*, 851-873, 1988.
- Bricaud, A., M. Babin, A. Morel, and H. Claustre, Variability in the chlorophyll-specific absorption coefficients of natural phytoplankton: Analysis and parameterization, *J. Geophys. Res.*, *100*, 13,321-13,332, 1995.
- Bricaud, A., A. Morel, M. Babin, K. Allali, and H. Claustre, Variations of light absorption by suspended particles with chlorophyll *a* concentration in oceanic (case 1) waters: Analysis and implications for bio-optical models, *J. Geophys. Res.*, *103*, 31,033-31,044, 1998.
- Carder, K. L., R. G. Steward, G. R. Harvey, and G. A. Ortner, Marine humic and fulvic acids: Their effects on remote sensing of ocean chlorophyll, *Limnol. Oceanogr.*, *34*, 68-81, 1989.
- Carder, K. L., F. R. Chen, Z. P. Lee, and S. K. Hawes, Semianalytic Moderate-Resolution Imaging Spectrometer algorithms for chlorophyll *a* and absorption with bio-optical domains based on nitrate-depletion temperatures, *J. Geophys. Res.*, *104*, 5403-5421, 1999.
- Cleveland, J. S., Regional models for phytoplankton absorption as a function of chlorophyll *a* concentration, *J. Geophys. Res.*, *100*, 13,333-13,344, 1995.
- Coachman, L. K., K. Aagaard., and R. B. Tripp, *Bering Strait: The Regional Physical Oceanography*, 172, Univ. of Wash., Press, Seattle, 1975.
- Comiso, J. C., Satellite remote sensing of the Polar Oceans, *J. Mar. Sys.*, *2*, 395-434, 1991.

- Comiso, J. C., C. McClain, C. Sullivan, J. Ryan, and C. L. Leonard, CZCS pigment concentrations in the Southern Ocean and their relationships to some geophysical parameters, *J. Geophys. Res.*, *98*, 2419-2451, 1993.
- Comiso, J. C., D. Cavalier, C. Parkinson, and P. Gloersen, Passive microwave algorithms for sea ice concentrations, *Remote Sens. Environ.*, *60*(3), 357-384, 1997.
- Comiso, J. C., Satellite observed variability and trend in sea ice extent, surface temperature, albedo, and clouds in the Arctic, *Ann. Glaciol.*, *33*, 457-473, 2001.
- Comiso, J. C., J. Yang, S. Honjo, and R. Krishfield, The detection of change in the Arctic using satellite and in situ data, *J. Geophys. Res.*, submitted, 2003.
- Comiso, J. C., and G. F. Cota, Large scale variability of phytoplankton blooms in the Arctic and peripheral seas: Relationships with sea ice, temperature, clouds, and wind, *J. Geophys. Res.*, in revision, 2004.
- Cota, G. F., L. R. Pomeroy, W. G. Harrison, E. P. Jones, F. Peters, W. M. Sheldon, and T. R. Weingartner, Nutrients, primary production and microbial heterotrophy in the southeastern Chukchi Sea: Arctic summer nutrient depletion and heterotrophy, *Mar. Ecol. Prog. Ser.*, *135*, 247-258, 1996.
- Cota, G. F., W. G. Harrison, T. Platt, S. Sathyendranath and V. Stuart, Bio-optical properties of the Labrador Sea, *J. Geophys. Res.*, *108* (C7), 3228, doi:10.1029/2000JC000597, 2003.
- Cota, G. F., J. Wang, and J. Comiso, Transformation of global satellite chlorophyll retrievals with a regionally tuned algorithm, *Remote Sens. Environ.*, *90*, 373-377, 2004.

- DeGrandpre M. D., A. Vodacek, R. K. Nelson, E. J. Bruce, and N. V. Blough, Seasonal seawater optical properties of the U.S. Middle Atlantic Bight, *J. Geophys. Res.*, *101*, 22,727-22,736, 1996.
- Denman, K. L., and M. R. Abbott, Time evolution of surface chlorophyll patterns from cross-spectrum analysis of satellite color images, *J. Geophys. Res.*, *93*, 6789-6798, 1988.
- Denman, K. L., and M. R. Abbott, Time scales of pattern evolution from cross-spectrum analysis of advanced very high resolution radiometer and coastal zone color scanner imagery, *J. Geophys. Res.*, *99*, 7433-7442, 1994.
- Gardeev, V. V., J. M. Martin, I. S. Sidorov, and M. V. Sidorova, A reassessment of the Eurasian river input of water sediment, major elements, and nutrients to the Arctic Ocean, *Amr. J. Sci.*, *296*, 664-691, 1996.
- Garver, S. A., and D. A. Siegel, Inherent optical property inversion of ocean color spectra and its biogeochemical interpretation 1. Time series from the Sargasso Sea, *J. Geophys. Res.*, *102*, 18,607-18,625, 1997.
- Gordon, H. R., O. B. Brown, R. H. Evans, J. W. Brown, R. C. Smith, K. S. Baker, and D. K. Clark, A semi-analytic model of ocean color, *J. Geophys. Res.*, *93*, 10,909-10,924, 1988.
- Gould R. W., R. A. Arnone, P. M. Martinolich, Spectral dependence of the scattering coefficient in case 1 and case 2 waters, *Appl. Opt.*, *38*, 2377-2383, 1999.
- Gregg, W. W., and M. E. Conkright, Global seasonal climatologies of ocean chlorophyll: blending *in situ* and satellite data for the CZCS era. *J. Geophys. Res.*, *106*, 2499-2515, 2001.

- Horner, R., and G. C. Schrader, Relative contributions of ice algae, phytoplankton, and benthic microalgae to primary production in nearshore regions of the Beaufort Sea, *Arctic*, 35, no.4, 485-503, 1982.
- Horner, R., Phytoplankton abundance, chlorophyll *a*, and primary productivity in the western Beaufort Sea, edited by P. W. Barnes, D. M. Shell, and E. Reimnitz, *The Alaskan Beaufort Sea*, pp.295-310, Academic, San Diego, Calif., 1984.
- Hill V., G. F. Cota, D. Stockwell, Seasonal succession of phytoplankton in the Chukchi and Beaufort Seas, *Deep-Sea Res.*, submitted, 2004.
- Johnsen, G., O. Samset, L. Granskog, and E. Sakshaug, In vivo absorption characteristics in 10 classes of bloom-forming phytoplankton: Taxonomic characteristics and responses to photoadaptation by means of discriminant and HPLC analysis, *Mar. Ecol. Prog. Ser.*, 105, 149-157, 1994.
- Jones, E. P., and L. G. Anderson, On the origin of the chemical properties of the Arctic Ocean halocline, *J. Geophys. Res.*, 91, 10,759-10,767, 1986.
- Kirk, J. T. O., Dependence of relationship of between inherent and apparent optical properties of water on solar altitude, *Limnol. Oceanogr.*, 29, 350-356, 1984.
- Kirk, J. T. O., *Light and Photosynthesis in Aquatic Ecosystems*, pp. 254-258, Cambridge Univ. Press, New York, 1994.
- Kishino, M., M. Takahashi, N. Okami, and S. Ichimura, Estimation of the spectral absorption coefficients of phytoplankton in the sea, *Bull. Mar. Sci.*, 37, 634-642, 1985.
- Lee, Z. P., K. L. Carder, S. H. Hawes, R.G. Steward, T. G. Peacock, and C. O. Davis, A model for interpretation of hyperspectral remote-sensing reflectance, *Appl. Opt.*, 33, 5721-5732, 1994.

- Lee, Z. P., K. L. Carder, R. F. Chen, and T. G. Peacock, Properties of the water column and bottom derived from Airborne Visible Infrared Imaging Spectrometer (AVIRIS) data, *J. Geophys. Res.*, *106*, 11,639-11,651, 2001.
- Loisel, H., and A. Morel, Light scattering and chlorophyll concentration in case I waters: A reexamination, *Limnol. Oceanogr.*, *43*, 847-858, 1998.
- Longhurst, A., Seasonal cycles of pelagic production and consumption, *Prog. Oceanogr.*, *36*, 77-167, 1995.
- Macdonald, R. W., and C. S. Wong, The distribution of nutrients in the Southeastern Beaufort Sea: Implications for water circulation and primary production, *J. Geophys. Res.*, *92*, 2939-2952, 1987.
- Maritorena, S., D. A. Siegel, and A. R. Peterson, Optimization of a semi-analytical ocean color model for global scale applications, *Appl. Opt.*, *41*, 2705-2714, 2001.
- Mitchell, B. G., Algorithms for determining the absorption coefficient of aquatic particles using quantitative filter technique (QFT), Ocean Optics 10, *Proc. SPIE Int. Soc. Opt. Eng.*, *1302*, 137-148, 1990.
- Mitchell, B. G., E. Brody, E. N. Yeh, C. McClain, J. C. Comiso, and N. C. Maynard, Meridional zonation of the Barents Sea ecosystem inferred from satellite remote sensing and in-situ Bio-optical observations, Pro Mare Symposium, *Polar Res.*, *10(1)*, 147-162, 1991.
- Mitchell, B. G., and O. Holm-Hansen, Bio-optical properties of Antarctic Peninsula waters: differentiation from temperate ocean models, *Deep-Sea Res.*, *38*, 1009-1028, 1991.

- Mitchell, B. G., Predictive bio-optical relationships for polar oceans and marginal ice zones, *J. Mar. Sys.*, 3, 91-105, 1992.
- Mobley, C. D., *Light and Water: Radiative Transfer in Natural Waters*, pp. 60-61, Academic Press, San Diego, Calif., 1994.
- Mobley, C. D., and D. Stramski, Origins of variability in Remote-sensing reflectance, final report, (Sequoia Scientific, Inc., Redmond, Wash.), 1997.
- Mobley, C. D., L. K. Sundman, and E. Boss, Phase function effects on oceanic light fields, *Appl. Opt.*, 41, 1035-1050, 2002.
- Moisan, T. A., and B. G. Mitchell, Photophysiological acclimation of *Phaeocystis antarctica* Karsten under light limitation, *Limnol. Oceanogr.*, 44, 247-258, 1999.
- Morel, A., Optical modeling of the upper ocean in relation to its biogenous matter content (case 1 waters), *J. Geophys. Res.*, 93, 10,749-10,768, 1988.
- Morel, A., and Y.-H. Ahn, Optics of heterotrophic nanoflagellates and ciliates: a tentative assessment of their scattering role in oceanic waters compared to those of bacteria and algal cells, *J. Mar. Res.*, 49, 177-202, 1991.
- Morel, A., and B. Gentili, Diffuse reflectance of oceanic waters: Its dependence on Sun angle as influenced by molecular scattering contribution, *Appl. Opt.*, 30, 4427-4438, 1991.
- Morel, A., and B. Gentili, Diffuse reflectance of oceanic waters, II, Bi-directional aspects, *Appl. Opt.*, 32, 6864-6879, 1993.
- Morel, A., and L. Prieur, Analysis of variations in ocean color, *Limnol. Oceanogr.*, 22, 709-722, 1977.

- Moritz, R. E., C. M. Bitz, and E. J. Steig, Dynamics of recent climate change in the Arctic, *Science*, 297, 1497-1502, 2002.
- Mueller, J. L., and R. W. Austin, "Ocean optics protocols for SeaWiFS validation, revision 1," *NASA Tech. Memo.*, 25(104566), pp.67 , 1995.
- Nelson, N. B., D. A. Siegel, and A. F. Michaels, Seasonal dynamics of colored dissolved material in the Sargasso Sea, *Deep-Sea Res., I*, 45, 931-957, 1998.
- Onstott, R. G., and R. A. Shuchman, Remote sensing of the Polar Ocean, in *Polar Oceanography*, ed. by W. O. Smith, Jr., Academic Press, Inc., San Diego, CA, 123-169, 1990.
- O'Reilly, J. E., S. Maritorena, B. G. Mitchell, D. A. Siegel, K. L. Carder, S.A. Garver, M. Kahru, and C. McClain, Ocean color chlorophyll algorithms for SeaWiFS, *J. Geophys. Res.*, 103, 24,937-24,953, 1998.
- O'Reilly, J. E., S. Maritorena, M. C. O'Brien, D. A. Siegel, D. Toole, D. Menzies, R. C. Smith, J.L. Mueller, B. G. Mitchell, M. Kahru, R. P. Charvez, P. Strutton, G. F. Cota, S. B. Hooker, C. R. McClain, K. L. Carder, F. Mueller-Karger, L. Harding, A. Magnuson, D. Phynney, G. F. Moore, J. Aiken, K. R. Arrigo, R. Letelier, and M. Culver, 2000: Ocean color Chlorophyll a Algorithms for SeaWiFS, OC2 and OC4: Version 4, *NASA Tech. Memo.*, 2000-206892, Vol. 11, 2000.
- Overpeck, J., K. Hughen, D. Hardy, R. Bradley, R. Case, M. Douglas, B. Finney, K. Gajewski, G. Jacoby, A. Jennings, S. Lamoureux, A. Lasca, G. MacDonald, J. Moore, M. Retelle, S. Smith, A. Wolfe, and G. Zielinski, Arctic environmental change of the last four centuries, *Science*, 278, 1251-1256, 1997.

- Pegau, S., J. S. Cleveland, W. Doss, C. D. Kennedy, R. A. Maffione, J. L. Mueller, C. C. Trees, A. D. Weidemann, W. H. Wells, and J. R. V. Zaneveld, A comparison of methods for the measurements of the absorption coefficient in the nature waters, *J. Geophys. Res.*, *100*, 13,201-13,220, 1995.
- Pegau, W. S., D. Gray, and J. R. V. Zaneveld, Absorption of visible and near-infrared light in water: The dependence on temperature and salinity, *Appl. Opt.*, *36*, 6035-6046, 1997.
- Pegau, W. S., Inherent optical properties of the central Arctic surface waters, *J. Geophys. Res.*, *107*(C10), 8035, doi:10.1029/2000JC000382, 2002.
- Peterson, B. J., R. M. Holmes, J. W. McClelland, C. J. Vorosmarty, R. B. Lammers, A. L. Shiklomanov, I. A. Shiklomanov, and S. Rahmstorf, Increasing river discharge to the Arctic Ocean, *Science*, *298*, 2171-2173, 2002.
- Reynolds, R. A., D. Stramski, and B. G. Mitchell, A chlorophyll-dependent semianalytical reflectance model derived from field measurements of absorption and backscattering coefficients within the Southern Ocean, *J. Geophys. Res.*, *106*, 7125-7138, 2001.
- Risović, D., Effect of suspended particulate-size distribution on the backscattering ratio in the remote sensing of seawater, *Appl. Opt.*, *41*, 7092-7101, 2003.
- Sakshaug, E., The physiological ecology of polar phytoplankton, Rey, L. and Alexander, V., eds., 61-89. Leiden, E. J. Brill, *Proceedings of the sixth conference of the comite arctique international*, 1989.
- Sathyendranath, S., L. Lazzara, and L. Prieur, Variations in the spectral values of specific absorption of phytoplankton, *Limnol. Oceanogr.*, *32*, 403-415, 1987.

- Sathyendranath, S., G. Cota, V. Stuart, H. Maass, and T. Platt, Remote sensing of phytoplankton pigments: a comparison of empirical and theoretical approaches, *Int. J. Remote Sensing*, 22, 249-273, 2001.
- Springer, A. M., and C. P. McRoy, The paradox of pelagic food webs in the northern Bering-III. Patterns of primary production, *Cont. Shelf Res.*, 13, 575-599, 1993.
- Steele, J. H. (Ed.), *Spatial patterns in Plankton Communities*, pp.470, Plenum, New York, 1978.
- Strickland, J. D., and T. R. Parsons, Pigment analysis, in *A Practical Handbook of Seawater analysis*, pp.185-196, Fisheries Research Board of Canada, Ottawa, Ont., 1972.
- Stramski, D., and D. A. Kiefer, Light scattering by microorganisms in the open ocean, *Prog. Oceanogr.*, 28, 343-383, 1991.
- Sverdrup, H. U., On the conditions for vernal blooming of the phytoplankton, *Journal du Conseil Permanente Internationale pour l'Exploration de la Mer*, 18, 287-295, 1953.
- Thompson, D. W., and J. M. Wallace, The Arctic oscillation signature in the wintertime geopotential height and temperature field, *Geophys. Res. Lett.*, 25, 1297-1300, 1998.
- Toole, D. A., D. A. Siegel, D. W. Menzies, M. J. Neumann, and R. C. Smith, Remote-sensing reflectance determinations in the coastal ocean environment: Impact of instrumental characteristics and environmental variability, *Appl. Opt.*, 39, 456-469, 2000.
- Toole, D. A., and D. A. Siegel, Modes and mechanisms of ocean color variability in the Santa Barbara Channel, *J. Geophys. Res.*, 106, 26,985-27,000, 2001.

- Ulloa, O., S. Sathyendranath, and T. Platt, Effect of the particle-size distribution on the backscattering ratio in seawater, *Appl. Opt.*, *33*, 7070-7077, 1994.
- Walsh, J. E., and C. M. Johnson, An analysis of Arctic sea ice fluctuations, 1957-77, *J. Phys. Oceanogr.*, *9*, 580-591, 1979.
- Walsh, J. J., C. P. McRoy, L. K. Coachman, J. J. Goering, J. J. Nihoul, T. E. Whitledge, T. H. Blackburn, P. L. Parker, C. D. Wirick, P. G. Shuert, J. M. Grebmeier, A. M. Springer, R. D. Tripp, D. A. Hansell, S. Djenidi, E. Deleersnijder, K. Henriksen, B. A. Lund, P. Andersen, F. E. Muller-Karger, and K. Dean, Carbon and nitrogen cycling within the Bering/Chukchi Seas: Source regions for organic matter affecting AOU demands of the Arctic Ocean, *Prog. Oceanogr.*, *22*, 279-361, 1989.
- Wang, J., and G. F. Cota, Remote-sensing reflectance in the Beaufort and Chukchi Seas: observations and models, *Appl. Opt.*, *44*, 2754-2765, 2003.
- Wang, J., G. F. Cota, and D. Ruble, Absorption and backscattering in the Beaufort and Chukchi Seas, *J. Geophys. Res.*, in press, 2004.
- Weingartner, T. J., D. J. Cavalieri, K. Aagaard, and Y. Sasaki, Circulation, dense water formation, and outflow on the northeast Chukchi shelf, *J. Geophys. Res.*, *103*, 7647-7661, 1998.
- Yoder, J. A., C. R. McClain, G. C. Feldman, and W. Esaias, Annual cycles of phytoplankton chlorophyll concentrations in the global ocean: a satellite view. *Global Biogeochemical Cycles*, *7*, 181-193, 1993.

## VITA

### **Jian Wang**

Date of birth: April 24, 1974 in Nanjing, China

Center for Coastal Physical Oceanography  
Department of Ocean, Earth and Atmospheric Science  
Old Dominion University  
Norfolk, Virginia 23508

### **Education**

B.S., Biology, Nanjing University, 1995

Ph. D., Oceanography, Old Dominion University, 2004

### **Research Interests**

Bio-optics and satellite remote sensing. Modeling involving inherent optical properties (IOPs) and apparent optical properties (AOPs). Development of chlorophyll retrieval algorithms from satellite data.

### **Publications**

Wang, J., and G. F. Cota, Remote-sensing reflectance in the Beaufort and Chukchi Seas: observations and models, *Appl. Opt.*, 42, 2754-2765, 2003.

Wang, J., G. F. Cota, and D. Ruble, Absorption and backscattering in the Beaufort and Chukchi Seas, *J. Geophys. Res.*, accepted, 2004.

Wang, J., G. F. Cota, and J. C. Comiso, Phytoplankton in the Beaufort and Chukchi Seas: Distribution, dynamics, and environmental forcing, *Deep-Sea Res.*, submitted, 2004.

Cota, G. F., J. Wang, and J. C. Comiso, Transformation of global satellite chlorophyll retrievals with a regionally tuned algorithm, *Remote Sens. Environ.*, in press, 2004.